ISSN 2738-2656

2023-4

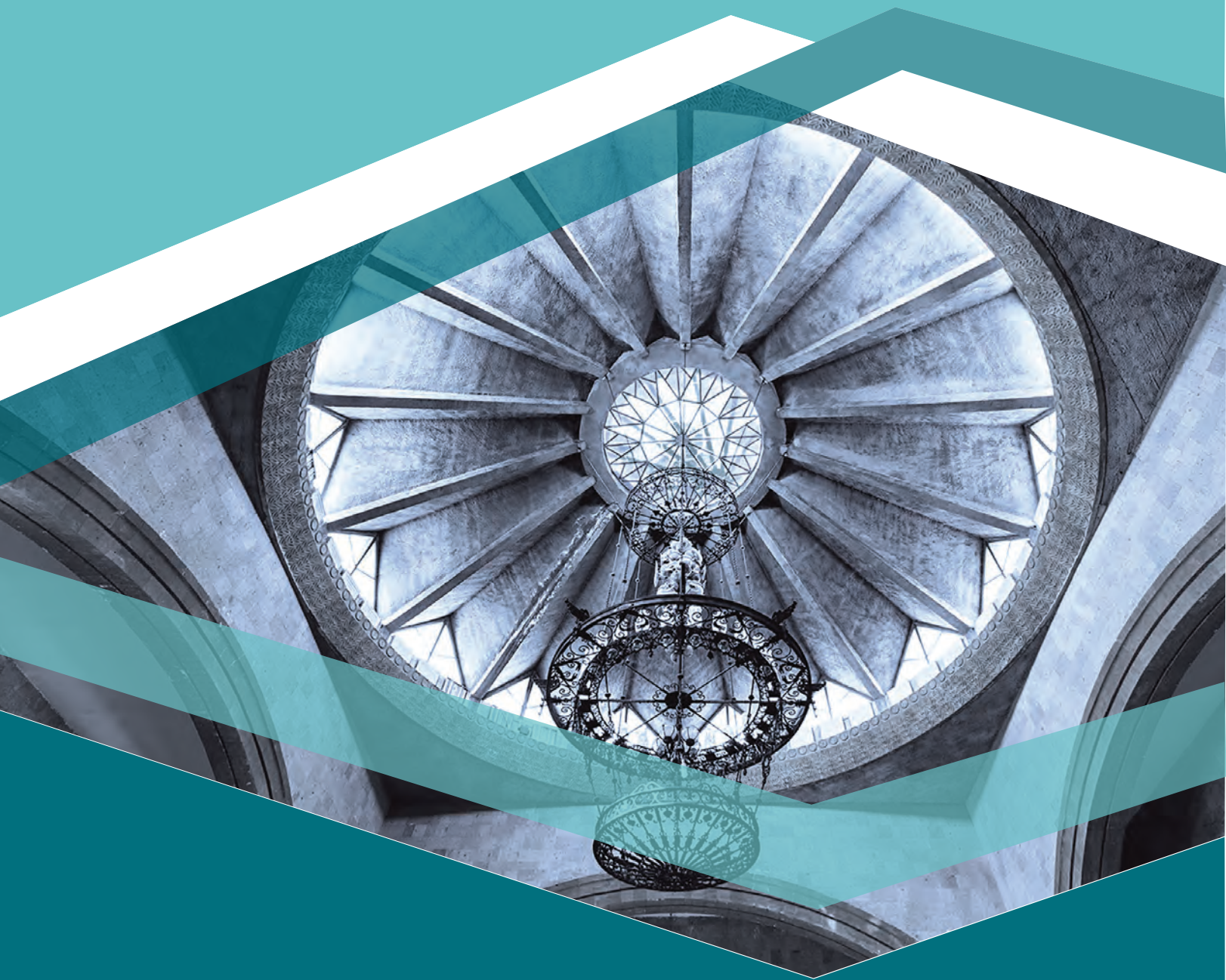

JOURNAL OF ARCHITECTURAL AND ENGINEERING RESEARCH

National University of Architecture and Constraction of Armenia approve the journal for publication
Scientific Council

THE MINISTRY OF EDUCATION, SCIENCE, CULTURE AND SPORTS OF THE REPUBLIC OF ARMENIA

JOURNAL OF ARCHITECTURAL AND ENGINEERING RESEARCH

2 0 2 3 - 4

YEREVAN 2023

CONTENT

AN ENGINEERING COMMENT FOR SIMPLY ACCELERATING SEISMIC RESPONSE HISTORY ANALYSIS OF MID-RISE STEEL-STRUCTURE BUILDINGS

Aram Soroushian[1]*, Abdolreza S. Moghadam[1], Ahmad Sabzei[1], Saeed Amiri[2], Aram Saaed[1], Ali Yahyapour[1]

[1]*International Institute of Earthquake Engineering and Seismology, Tehran, Iran*

[2] *Polytechnique Montreal, Department of Civil, Geological and Mining Engineering, Montreal, Canada*

Abstract: *Response history analysis using a time integration method is a powerful versatile tool in accessing structures seismic behaviours. To reduce the analysis run-time, a technique was proposed in 2008 for time integration with steps larger than the steps of ground motions. The technique has been implemented in seismic assessment of frames, buildings, bridges, silos, etc., leading to considerable reductions in the analysis run-time, without notable effect on the response accuracy. The technique has recently been named as the SEB THAAT (Step-Enlargement-Based Time-History-Analysis-Acceleration-Technique). To use the SEB THAAT, the smallest dominant period of the response needs to be available prior to the analysis. In this paper, concentrating on 5-20-floor steel-structure buildings, a simple engineering comment is proposed that eliminates this need. As a result, in response history analysis of mid-rise steel-structure buildings subjected to ground motion, by using the proposed comment, we may reduce the analysis run-time, significantly, without any initial information about the response. The reduction is 50% for the linear analyses.*

Keywords: *response history analysis, ground motion, mid-rise steel-structure buildings, the SEB THAAT, integration step, excitation step, run-time, accuracy.*

Aram Soroushian*

E-mail: a.soroushian@iiees.ac.ir

Received: 11.01.2023
Revised: 30.01.2023
Accepted: 20.02.2023

Introduction

Response history analysis using a time integration method is a powerful versatile tool, for analysing structures subjected to ground motions, irreplaceable in important analyses [1-3]. After discretization in space, the initial value problem, representing the behaviour of the structural system, is expressible as [4-7]:

$$\mathbf{M}\ddot{\mathbf{u}}\,(t) + \mathbf{f}_{\text{int}}(t) = \left(\mathbf{M}\Gamma\,\ddot{u}_{\text{g}}(t)\right) \qquad 0 \le t \le \text{t}_{\text{end}}$$

$$\text{Initial Conditions: } \begin{vmatrix} \mathbf{u}(t=0) = \mathbf{u_0} \\ \dot{\mathbf{u}}(t=0) = \dot{\mathbf{u}}_0 \\ \mathbf{f}_{\text{int}}(t=0) = \mathbf{f}_{\text{int}_0} \end{vmatrix} . \qquad (1)$$

$$\text{Additional Constraints: } \mathbf{Q}$$

In Eq. (1), t and t_{end} imply the time and the analysis time interval; $\mathbf{M}$ is the mass matrix; $\mathbf{f}_{\text{int}}$ is the vector of the internal force (in linear problems, generally $\mathbf{f}_{\text{int}} = \mathbf{Ku} + \mathbf{C}\dot{\mathbf{u}}$, where $\mathbf{K}$ and $\mathbf{C}$ stand for the matrices of stiffness and viscous damping, respectively); $\ddot{u}_{\text{g}}(t)$ implies the single-component ground acceleration, and Γ is a vector with the size of the degrees of freedom, needed for matrix multiplication and considering spatial changes of $\ddot{u}_{\text{g}}(t)$; $\mathbf{u}(t)$; $\dot{\mathbf{u}}(t)$, and $\ddot{\mathbf{u}}(t)$, denote the vectors of displacement, velocity, and acceleration, relative to the ground; $\mathbf{u}_0$, $\dot{\mathbf{u}}_0$, and $\mathbf{f}_{\text{int}_0}$, define the initial status (generally all zero), and $\mathbf{Q}$ implies the limiting conditions due to nonlinearity. (When the ground motion is multi-component, Γ and $\ddot{u}_{\text{g}}(t)$ will change to a matrix and a vector, respectively). The core of response history analysis is an approximate step-by-step computation, widely known as direct time integration (see Fig. 1 and [1,3,6]). The resulting

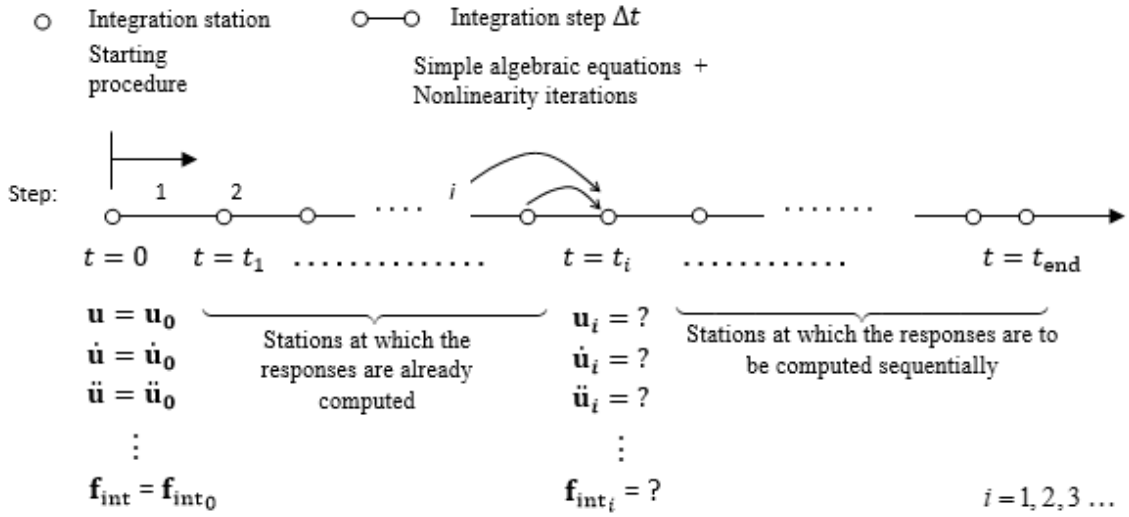

Fig. 1. ***A pictorial review of direct time integration analysis of Eq. (1) [3]***

responses are inexact, and the analysis run-times are generally considerable [3,6]. The integration step is the analysis parameter, with adverse effects on the run-time and the accuracy [3]. Accordingly, a regulation for assigning an appropriate value to Δt is essential. A simple comment, broadly accepted in practice, is as follows [2,3,8]:

$$\Delta t \cong\leq \text{Min}\left(\frac{T}{X},\ h,\ {}_f\Delta t\right). \tag{2}$$

In Eq. (2), T is the smallest dominant period in the time history of the response, h implies the largest integration step preserving numerical stability and consistency, ${}_f\Delta t$ denotes the step, by which, the ground motion is digitized, and X equals 10 for linear systems, 100 for nonlinear systems not involved in impact, and 1000 for systems involved in impact. When, the dominant term in the right hand side of Eq. (2) is ${}_f\Delta t$, the difference between ${}_f\Delta t$ and the next smallest term in the right hand side of Eq. (2) implies the effort required mainly to account for all the excitation data. In order to eliminate or lessen this effort, in 2008, a technique was proposed [3,9,10], that replaces the earthquake record with a record digitized in larger steps. The technique, which is recently named "the SEB THAAT (Step-Enlargement-Based Time-History-Analysis-Acceleration-Technique)" [10], is formulated such that to prevent any negative effect because of the record replacement on the convergence of the computed response to the exact response. Considering that convergence is the main essentiality of approximate computations [11,12], the expectation from the SEB THAAT is to reduce the computational effort with negligible effect on the response accuracy. In view of the studies carried out since 2008, the SEB THAAT has been successful, in earthquake engineering and beyond; see Table 1 [3,10] and [13]. Nevertheless, to set the scaling value of the record's step (i.e. how much to enlarge the step), some information about the response is needed, prior to the analysis [3,10]. The objective in this paper is to eliminate this need for a special class of analyses. In view of the number and social importance of buildings with 5-20 floors, hereafter referred to as mid-rise buildings, seismic response history analysis of steel-structure mid-rise buildings is considered as the special class of the analyses. Accordingly, by achieving the objective, the computational effort needed for a large number of response history analyses will be simply reduced. The simplicity in increasing the efficiency and the amount of the increase can encourage engineers to use response history analysis in practice, as well. For achieving the objective, the main attention is paid to Eq. (2), the current design and analysis practice, and the trends of the future advancements. A brief review on the SEB THAAT is presented first. An engineering comment for selecting the enlargement scale is introduced next. The effectiveness of the comment is tested afterwards, and finally, the paper is concluded with a discussion on practical issues, as well as an overview of the achievements.

Table 1. Some past tests on the SEB THAAT with regard to seismic response history analysis

System	Reduction in run-time (%)
A thirty-storey building	50
3-component earthquakes	66
Silo	77
Water tanks and Silos	66
Bridges	45-80
Residential buildings	50-87
An earth dam	< 80
Milad telecommunication tower	50-70
Different lifelines	50-90

A brief look at the SEB THAAT

An overview of the SEB THAAT, its formulation, limitations, challenges, and future prospects, is recently presented in [10]. Therefore, for brevity, only application of the SEB THAAT to direct time integration analysis is referred to in Fig. 2, and the most important features are reviewed as follows:

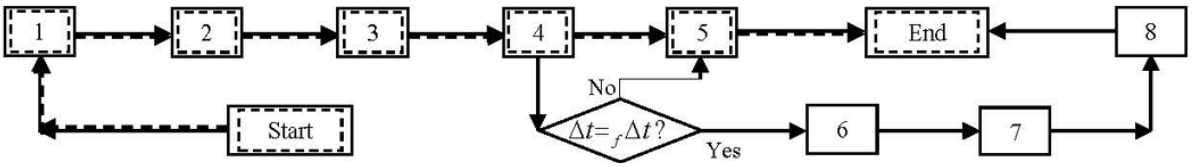

1. Define the structural model and the excitation (the excitation digitization step equals ${}_f\Delta t$)
2. Select the integration method
3. Select the details of the nonlinear solution (if needed)
4. Select the integration step Δt, regardless of the SEB THAAT
5. Step-by-step direct time integration using Δt as the integration step
6. Assign a value to the enlargement scale n
7. Use the SEB THAAT to change the excitation to an excitation digitized at step $n\,{}_f\Delta t$
8. Step-by-step direct time integration using $n\,{}_f\Delta t$ as the integration step

Direct time integration

Direct time integration after applying the SEB THAAT

Fig. 2. *Application of the SEB THAAT to arbitrary direct time integration analysis*

1. The SEB THAAT has a mathematical basis, with the aim and formulation to preserve the responses' convergence, without necessarily avoiding changes in characteristics of the earthquake record (see [9]).
2. Considering Eq. (2) as a basis for selection of the integration step, the SEB THAAT is to be applied, only when ${}_f\Delta t$ dominates the right hand side of Eq. (2), i.e.

$$ {}_f\Delta t \le \mathrm{Min}\left(\frac{T}{X},\ h\right). \tag{3}$$

   It should however be noted that Eq. (2) is not rigorous [2,3,8,14], and hence, the SEB THAAT may be successful, even when Eq. (3) is invalid; see for instance [15].
3. The formulation of the SEB THAAT enables consideration of arbitrary real number greater than one as the step enlargement scale [16].
4. With appropriate details of nonlinear solution and sufficient computational facility, the SEB THAAT can be as successful in application to nonlinear analyses, as it is in application to linear analyses; see [17].
5. While in linear analyses application of the SEB THAAT causes reduction in the analysis run-time, R, obtainable from

$$ R = 100\frac{n-1}{n}\ \% \tag{4}$$

   (n is the step enlargement scale), in nonlinear analyses, the reductions are not necessarily obtainable from Eq. (4) [3].

6. With a basis on convergence of the computed results, the SEB THAAT may be successfully applicable in fields different from structural dynamics and earthquake engineering [13].
7. Compared to the SEB THAAT, direct down sampling [18] is less effective, i.e. the accuracy of the target response obtained from the analysis when using the SEB THAAT is more than when using direct down sampling instead of the SEB THAAT [19].

It is also worth noting that, the future of the SEB THAAT is promising, due to its simplicity, remarkable effectiveness, and everyday more availability of different data as digitized records with smaller digitization steps.

A new engineering comment

For the SEB THAAT to reduce the computational effort, a positive value larger than one should be assigned to the step enlargement scale, n; see also [3,10]. Besides, the greater the n, the more will be the reduction in the run-time, especially for linear analyses [3,9,10]; see Eq. (4). Accordingly and in view of Eq. (2), for the analysis most efficiency and good accuracy of the response, the excitation step $n_{\,f}\Delta t$ should govern the right hand side of Eq. (2). Accordingly, when $h \to \infty$ (broadly recommended [3,4,6,20,21]):

$$n \cong \frac{T}{X_{\,f}\Delta t}, \tag{5}$$

which is effective, when the resulting n is greater than one. (The reason of using an approximation sign in Eq. (5) is that, different from h and ${}_f\Delta t$, the T/X in Eq. (2), the definition of T, the values of X, and the form of Eq. (2), are not rigorous (see [3,14])).

The existing seismological instrumentations provide the capability of recording ground motions, in steps, as small as 0.004 sec [22]. These instrumentations are in continuous progress, towards smaller digitization steps; see [23]. Considering this, along with the about largest digitization steps currently in use [24], we can conclude that:

$${}_f\Delta t \le 0.02\ \text{sec}, \tag{6}$$

and,

$$\frac{T}{X_{\,f}\Delta t} \ge \frac{50}{X}T. \tag{7}$$

Therefore, considering that smaller values of n will be more reliable from the standpoint of response accuracy, it is practically acceptable to replace Eq. (5), with

$$n \cong \frac{50\,T}{X}. \tag{8}$$

Accordingly, if for a class of structural analyses there exists a minimum for T (see Eq. (2)), i.e. $T_{\min}$, such that:

$$n \cong \frac{50\,T_{\min}}{X} > 1, \tag{9}$$

the n is suitable in application of the SEB THAAT in that class without any information about the response.

Taking into account 5-20-floor steel-structure buildings, designed according to the Iranian codes[1,2], and in agreement with the International code[3] and [25,26], the least dominant periods of the displacements linear oscillations, because of ground motions, satisfy (displacements, velocities, and accelerations, are the unknowns generally being computed first in time integration analysis):

$$T_{\min} \cong \ge 0.38 - 0.40\ \text{sec}. \tag{10}$$

[1] BHRC (Building and Housing Research Centre), Standard No. 2800-05, Iranian Code of Practice for Seismic Resistant Design, Iran, 2007 (in Persian).
[2] INBR (Iranian National Building Regulations), Iranian National Building Code, Part 10-Steel Structures, Iran, 1993 (in Persian).
[3] ICC (International Code Council), IBC - International Building Code, Club Hills, USA, 2003.

Besides, nowadays the technology of buildings construction proceeds towards lighter designs, and generally less stiff structural systems and larger values of $T_{\min}$ [27]. Considering these, in application of the SEB THAAT to analysis of 5-20-floor steel-structure buildings, the following comment is reasonable:

$$n = 2\,. \tag{11}$$

It is worth noting that Eq. (11) is in agreement with the experiences on the SEB THAAT's application, reviewed in [10]; see also Table 1. Equation (11) implies an engineering comment, for implementation of the SEB THAAT [9] which, is considered above for linear analyses, and simply reduces the analysis run-time for about 50%. Nonlinearity because of inelastic behaviour is inherent to structures subjected to severe earthquakes [1], and generally causes increase of both $T_{\min}$ and X. Besides, the T/X in Eq. (2), the definition of T, the form of Eq. (2), and especially the values of X are not rigorous [14]. Furthermore, seismic standards mostly permit linear analyses for ordinary building structures[4,5,6,7,8,9,10], and the only seismic standard, with a procedure for nonlinear response history analysis, i.e. NZS 1170.5:2004[11], also proposes a regulation to check the accuracy of the response. Accordingly, it is reasonable to use Eq. (11) in application of the SEB THAAT to analysis of 5-20-floor steel-structure buildings inelastic behaviours, as well. Nevertheless, because of the iterative nonlinear solutions [7,28,29], using Eq. (11) will not lead to twice faster analysis when the behaviour is inelastic. Consequently, we can use Eq. (11) in application of the SEB THAAT to seismic response history analysis of 5-20-floor steel-structure buildings, and reduce the analysis run-time, without prior information about the response. This claim is tested in the next section, considering quiescent condition at $t = 0$ and S.I. system of units for all computations.

Numerical study

Simple test on a six-floor steel shear frame

Consider response history analysis of the system defined in Fig. 3 (g stands for the acceleration of gravity) and Table 2, by the C-H method [30] ($\rho_\infty = 0.8$). The top displacement is set as the target response. The suitability of using Eq. (11) is tested via analysis with the integration step $\Delta t = {}_f\Delta t$ and a second analysis using $\Delta t = 2\,{}_f\Delta t$. The sufficient accuracy of the response and the validity of Eqs. (3) and (10) are displayed in Figs. 3 and 4, while the numbers of integration steps (37500 and 18750, for Figs. 4(a) and 4(b), respectively) imply 50% reduction in the analysis run-time.

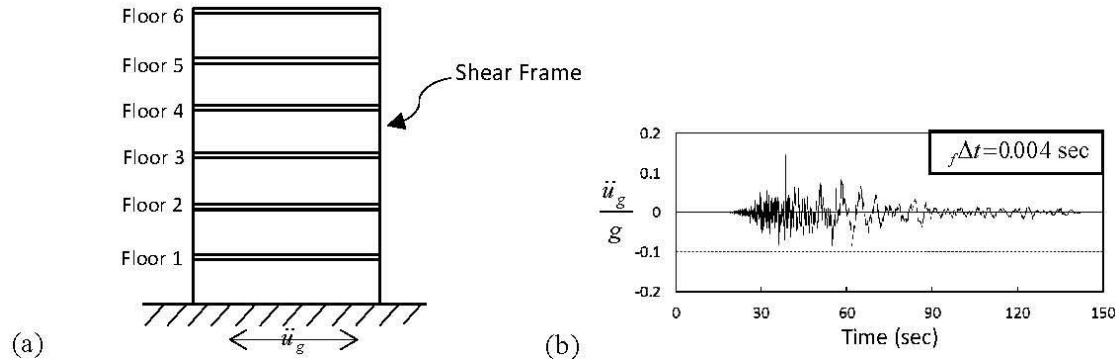

Fig. 3. *Pictorial introduction to the first example: (a) Structural model, (b) Ground motion*

[4] NZS (New Zealand Standards), NZS 1170.5: 2004 Structural Design Actions, Part 5: Earthquake actions, New Zealand, 2004.
[5] BHRC (Building and Housing Research Centre), Standard No. 2800-05, Iranian Code of Practice for Seismic Resistant Design, Iran, 2007 (in Persian).
[6] INBR (Iranian National Building Regulations), Iranian National Building Code, Part 10-Steel Structures, Iran, 1993 (in Persian).
[7] ICC (International Code Council), IBC - International Building Code, Club Hills, USA, 2003.
[8] BCJ (Building Centre of Japan), Structural Provisions for Building Structures, Tokyo, Japan, 2001.
[9] EAK, Greek Code for Seismic Resistant Structures, Athens, Greece, 2000.
[10] NRCC (National Research Council Canada), National Building Code of Canada, Canada, 2005.
[11] NZS (New Zealand Standards), NZS 1170.5: 2004 Structural Design Actions, Part 5: Earthquake actions, New Zealand, 2004.

Table 2. Main properties of the structural model in the first example

Property	Floor (*i*) / Mode (*i*)					
	1	2	3	4	5	6
Mass (m_i)×10^{-9}	1.8	1.8	1.8	1.8	0.6	0.6
Stiffness (k_i)×10^{-11}	1.20	1.20	1.20	1.20	0.20	0.20
Natural period (T_i)	2.7191	1.4919	0.7695	0.6544	0.4973	0.4088
Damping	Classical damping [2], considering 2% damping for the 1st and 3rd natural modes					

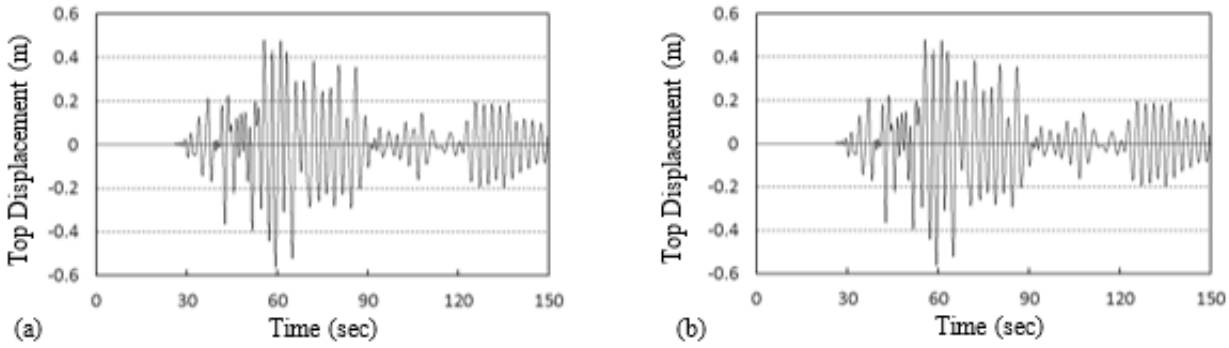

Fig. 4. *Target response computed for the first example by the C-H time integration method ($\rho_\infty = 0.8$) using an integration step equal to: (a) $_f\Delta t$, (b) $2\ _f\Delta t$ (by means of the SEB THAAT)*

A fifteen-floor steel-structure building

Consider the 15-floor steel-structure building displayed in Fig. 5. There are two identical axes of symmetry in the plan; the lengths of the spans are four meters; the bracings are placed at the last spans of the surrounding frames; the structural system is dual[12], and the other basic details are reviewed in Table 3. The structure is designed in a previous study [31], based on the Iranian standards[13,14], for the lowest total cost of construction using a fully constrained optimal criterion [31,32]. The members' cross-sections are as reported in Table 4.

Four two-component records, of the historically most devastating earthquakes in Iran, are considered, as the ground motion records (see Fig. 6) (for the first earthquake, the two components are identical). The structure is modelled as a three dimensional shear frame [2,24]. The translational natural periods are in the interval (0.035 sec 0.8 sec). The seismic response history analyses are carried out using the average acceleration time integration method [33], twice, for each two-component record; once, ordinarily, and once, after application of the SEB THAAT [9,10], considering Eq. (11). The acceleration at top, the mid-height displacement, and the base shear, are considered as the target responses. The computed histories are depicted in Figs. 7-10, where, for further clarity, the mid-sections of the time histories are not displayed in Figs. 8-10. These figures show that Eq. (11) may present an adequate comment for assigning a value to n in application of the SEB THAAT in response history analysis of mid-rise steel-structure buildings.

[12] BHRC (Building and Housing Research Centre), Standard No. 2800-05, Iranian Code of Practice for Seismic Resistant Design, Iran, 2007 (in Persian).
[13] Ibid.
[14] INBR (Iranian National Building Regulations), Iranian National Building Code, Part 10-Steel Structures, Iran, 1993 (in Persian).

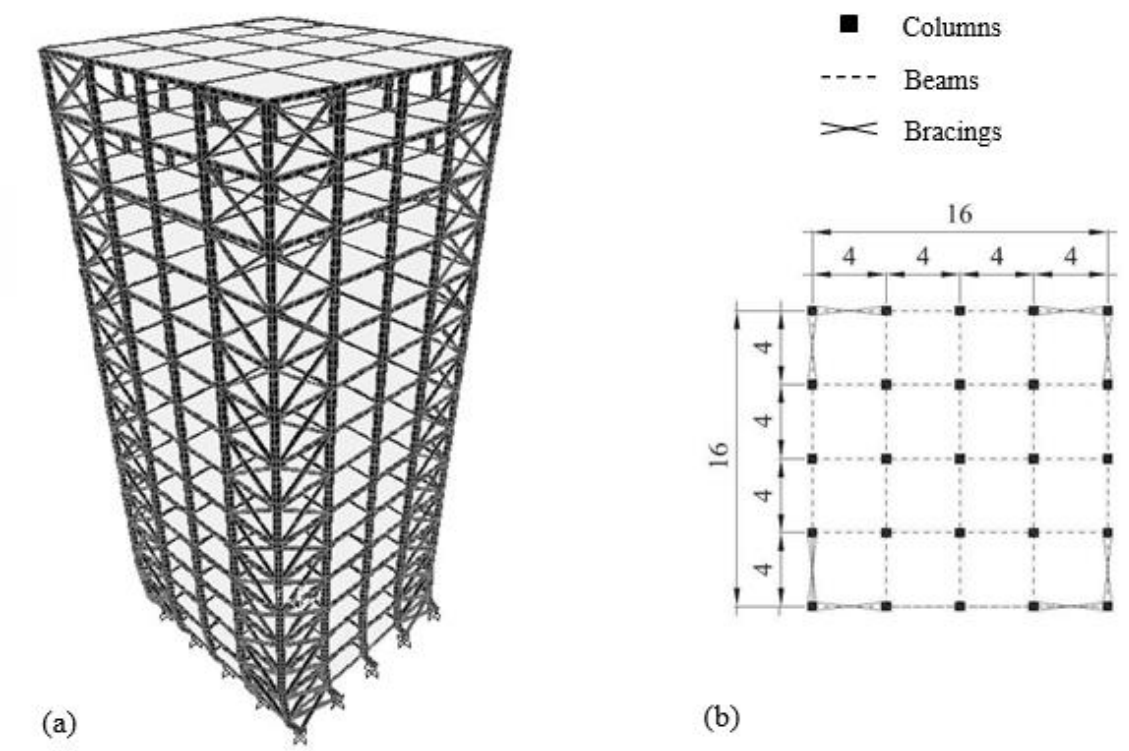

Fig. 5. *The building structure in the second example: (a) Schematic view, (b) Top view*

Table 3. Basic details for the structural systems in the second and third examples

Material	Steel (ST-37)
Occupancy	Residential (in Shiraz, Iran; mass: 175000 and 200000 Kg for the roof and other floors respectively)
Seismic zone factor	0.35[15]
Soil type	II ($375\,\text{m/s} \le \overline{V}s \le 750\,\text{m/s}$)[16] [a]
Floor height	3 meters
Bracing	X
Damping	Negligible (considered zero in the analyses)

[a] $\overline{V}_S$ is the velocity of shear waves.

Table 4. Members' cross-sections for the structural system introduced in Fig. 5 and Table 3

Floor (from ground)	Inner columns	Peripheral columns	Corner columns	Inner beams	Peripheral beams	Bracings
1	IPB400 [a]	Box400*12.5	Box360*10	IPE 300	2IPE160	2L130*12
2-3	IPB400 [a]	Box400*12.5	Box360*10	PL200*10 + 2PL240*20	2IPE200	2L130*12
4-5	Box320*10	Box400*16	Box360*10	2IPB200	2IPE200	L180*16
6-7	Box320*10	Box360*16	Box320*10	PL200*10 + 2PL240*20	2IPE200	2L110*10
8-11	Box320*10	Box360*12.5	Box320*10	PL200*10 + 2PL240*20	INP240	2L110*10
12-15	Box320*12.5	Box320*10	Box280*8	PL150*10 + 2PL180*15	PL220*6 + 2PL120*10	L130*12

[a] For construction problems, the properties in the weaker direction of the cross-section are considered as the properties in both directions.

[15] BHRC (Building and Housing Research Centre), Standard No. 2800-05, Iranian Code of Practice for Seismic Resistant Design, Iran, 2007 (in Persian).
[16] Ibid.

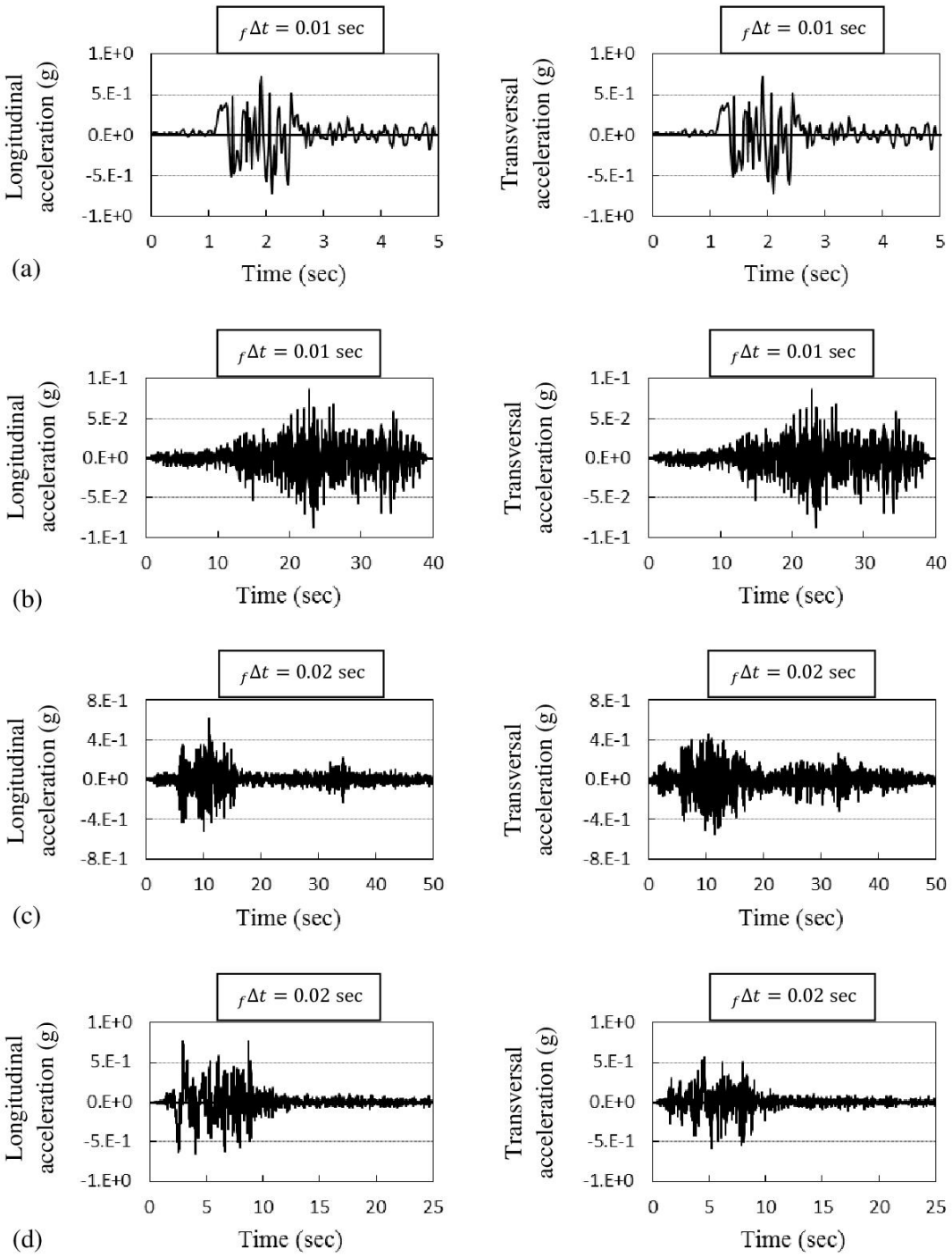

Fig. 6. *Two-component records of the four most devastating earthquakes in Iran, as the ground motion records in the second example: (a) Naghan (1977), (b) Tabas (1978), (c) Abbar (1990), (d) Bam (2003)*

Sixty-five 10-20-floor steel-structure buildings

In this section, the adequacy of Eq. (11) is studied, in view of 25 ten-, 25 fifteen-, and 15 twenty-story steel-structure buildings, each with two identical axes of symmetry, X bracings with the configuration displayed in Fig. 11, and span lengths constant throughout the structure, equal to either of the followings (see also [31]):

$$s = 4,\ 5,\ 6\ \text{(meters)}\,. \tag{12}$$

Two two-component ground motions, selected, based on the soil type and shear wave speed, are applied, at the ground level, in the principle directions of the structures (see also Fig. 12 and Tables 3, 5, 6). The response

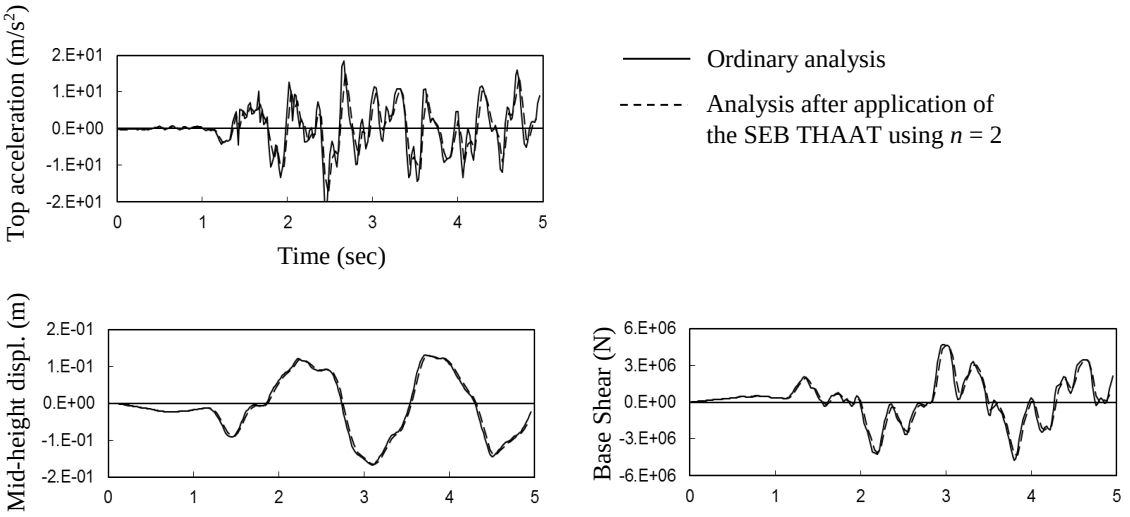

Fig. 7. *Target responses computed for the second example when subjected to the records in Fig. 6(a)*

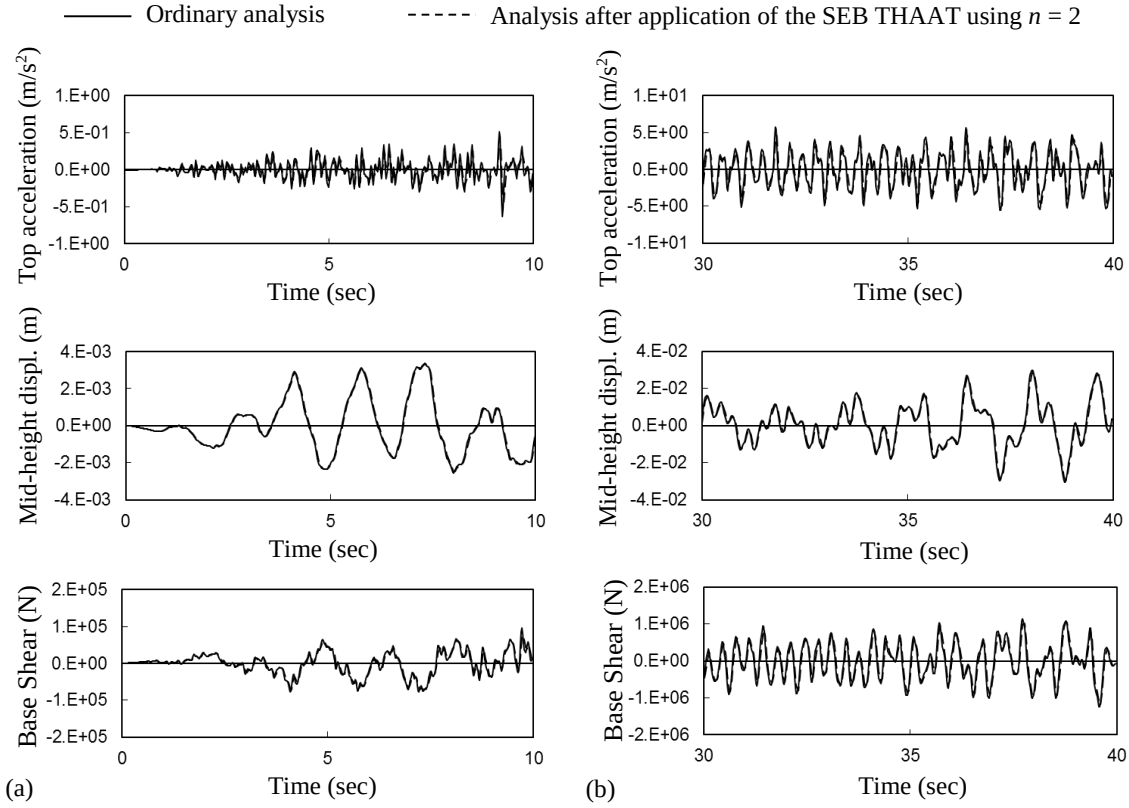

Fig. 8. *Target responses computed for the second example when subjected to the records in Fig. 6(b): (a) The starting ten seconds, (b) The ending ten seconds*

history analyses are carried out using the average acceleration method [33], once with the step $\Delta t = {}_f\Delta t$, and then with the step $\Delta t = 2\,{}_f\Delta t$ (after applying the SEB THAAT considering Eq. (11)). The maximum relative difference between the two responses in the L_∞ norm [34] is reported in Tables 7-9. Smallness of the reported values, that the ordinarily computed responses are not exact [2-4,6,35], and the 50% reduction in the analysis run-time, imply the good performance of the SEB THAAT when using Eq. (11).

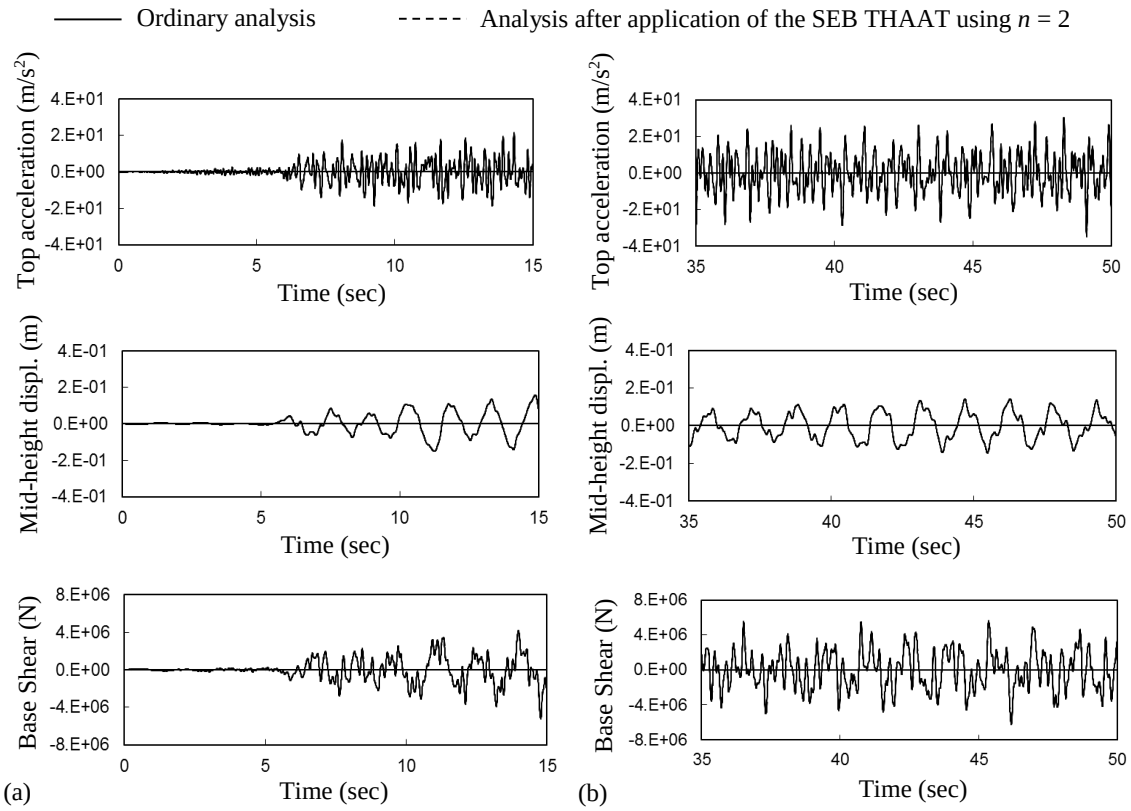

Fig. 9. *Target responses computed for the second example when subjected to the records in Fig. 6(c): (a) The starting fifteen seconds, (b) The ending fifteen seconds*

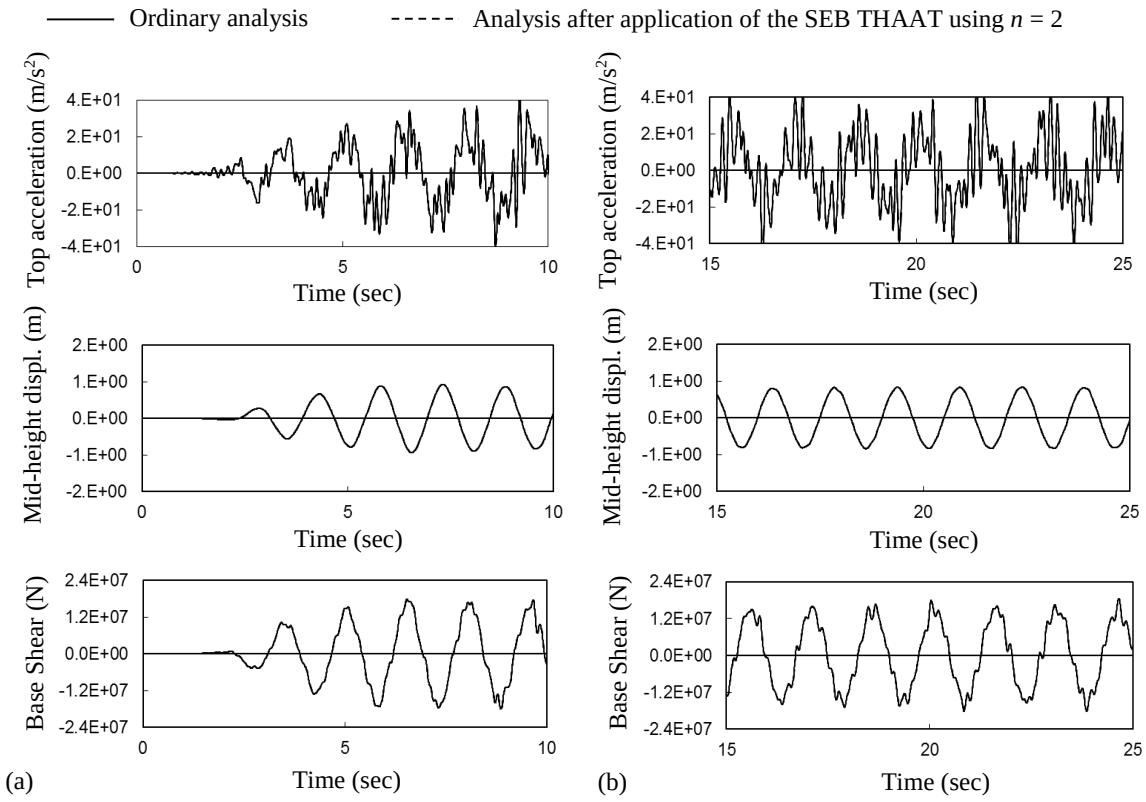

Fig. 10. *Target responses computed for the second example when subjected to the records in Fig. 6(d): (a) The starting ten seconds, (b) The ending ten seconds*

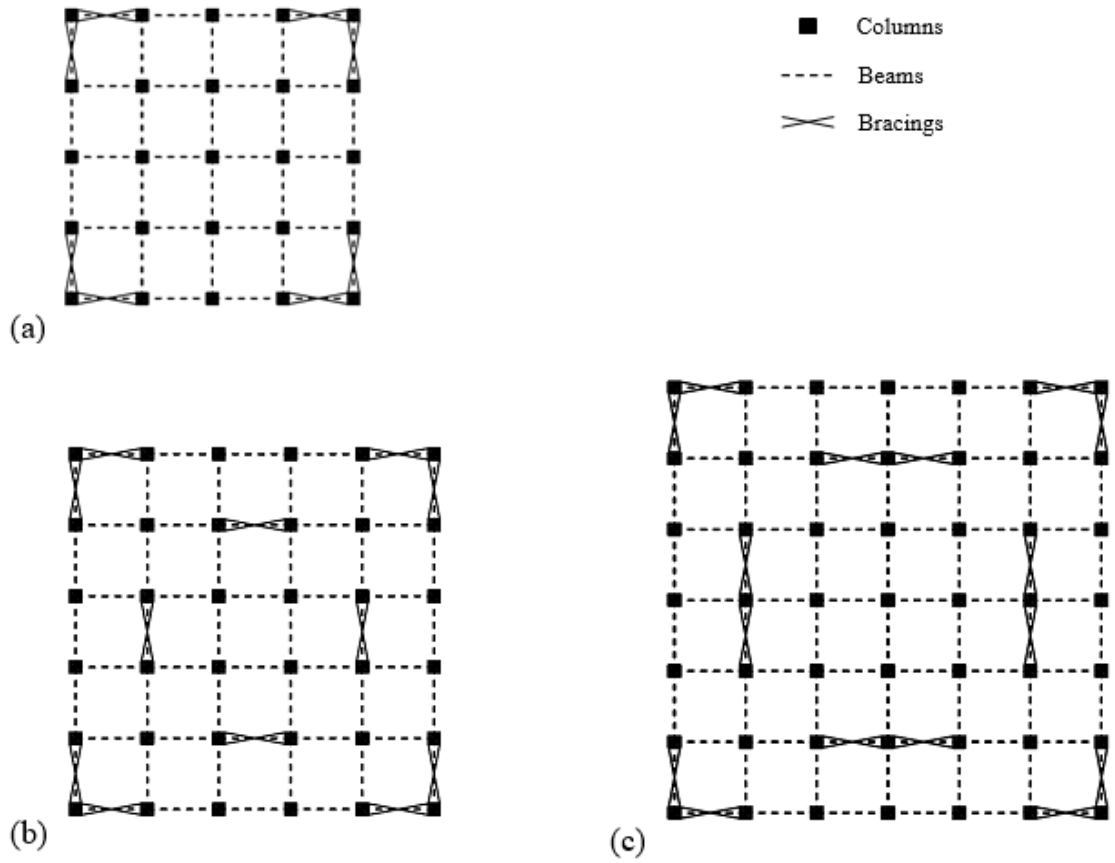

Fig. 11. *Structural plans in the third example:*
(a) Plans with four spans, (b) Plans with five spans, (c) Plans with six spans

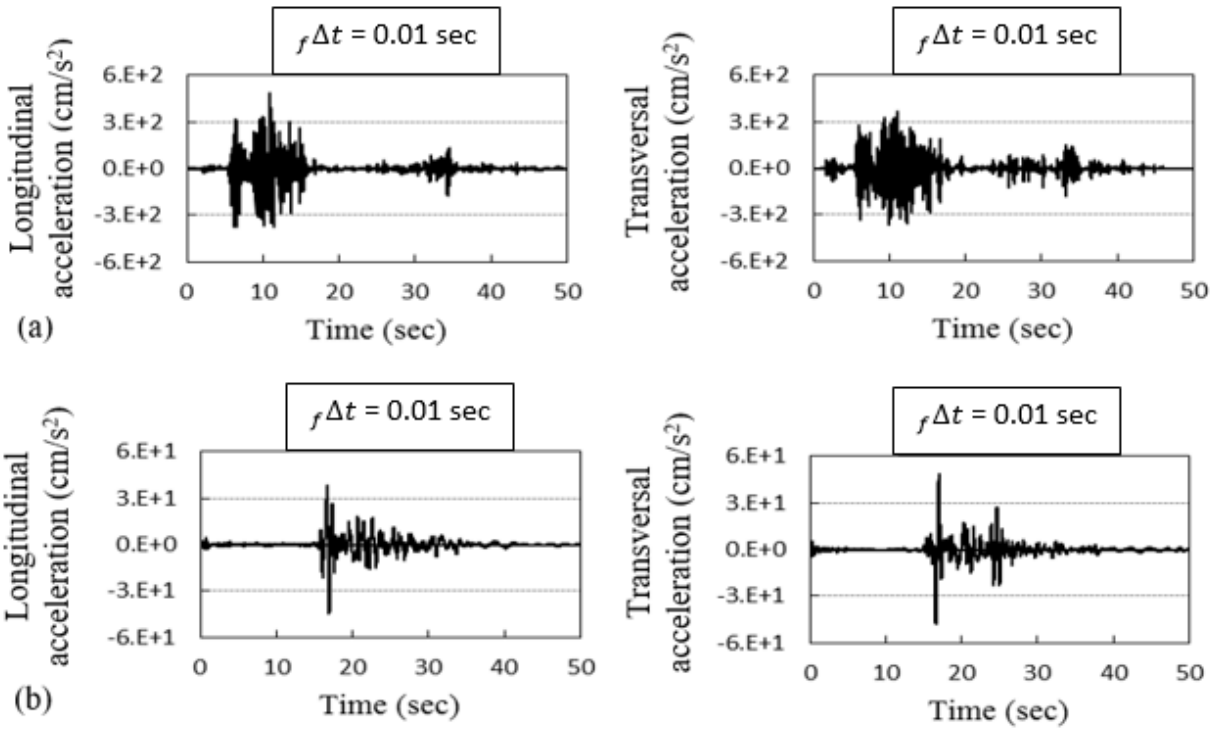

Fig. 12. *Records of the ground motions in the third example: (a) Manjil (1990), (b) Koujoor (2004)*

Table 5. Systems of the buildings structures in the third example according to the Iranian codes[17,18] [a]

System	10-floors	15-floors	20-floors
Dual consisted of special moment frames and concentrically braced frames	+	+	+
Special moment frames	+	+	+
Dual consisted of intermediate moment frames and concentrically braced frames	+	+	+
Intermediate moment frames	+	+	-
Ordinary concentrically braced frames	+	+	-

a "+" and "-" imply being and not being considered in the design code (and in this paper), respectively

Table 6. Groups of identical structural members in the sixty-five buildings in the third example

Buildings	Floors with identical structural members [a, b]
10-floor buildings	1-2-(3, 4)-(5, 6)-(7, 8, 9, 10)
15-floor buildings	1-(2, 3)-(4, 5)-(6, 7)-(8, 9, 10, 11)-(12, 13, 14, 15)
20-floor buildings	1-2-(3, 4)-(5, 6)-(7, 8)-(9, 10, 11, 12)-(13, 14, 15, 16)-(17, 18, 19, 20)

a The numbers in each "( )" address the floors' numbers with identical structural members (groups in height)

b The seven groups with identical structural members in plan are: internal columns, side columns, corner columns, internal beams, peripheral beams, internal bracings (only for cases in Figs. 11(b) and 11(c)) and side bracings

Table 7. Differences in the L_∞ norm, between the responses obtained when using the SEB THAAT and Eq. (11) and the responses computed using $\Delta t = {}_f\Delta t$, for the 10-floor buildings in the third example (%)

Structural system	Top acceleration	Mid-height displacement	Base shear
Dual consisted of special moment frames and concentrically braced frames	≤ 5.39	≤ 0.83	≤ 1.79
Special moment frames	≤ 5.92	≤ 0.89	≤ 0.72
Dual consisted of intermediate moment frames and concentrically braced frames	≤ 5.46	≤ 0.66	≤ 1.91
Intermediate moment frames	≤ 5.77	≤ 0.83	≤ 1.17
Ordinary concentrically braced frames	≤ 6.20	≤ 0.89	≤ 2.55

Table 8. Differences in the L_∞ norm, between the responses obtained when using the SEB THAAT and Eq. (11) and the responses computed using $\Delta t = {}_f\Delta t$, for the 15-floor buildings in the third example (%)

Structural system	Top acceleration	Mid-height displacement	Base shear
Dual consisted of special moment frames and concentrically braced frames	≤ 0.53	≤ 1.67	≤ 5.98
Special moment frames	≤ 0.15	≤ 0.57	≤ 5.43
Dual consisted of intermediate moment frames and concentrically braced frames	≤ 0.60	≤ 1.80	≤ 5.96
Intermediate moment frames	≤ 0.13	≤ 0.59	≤ 5.90
Ordinary concentrically braced frames	≤ 0.62	≤ 1.46	≤ 5.58

Table 9. Differences in the L_∞ norm, between the responses obtained when using the SEB THAAT and Eq. (11) and the responses computed using $\Delta t = {}_f\Delta t$, for the 20-floor buildings in the third example (%)

Structural system	Top acceleration	Mid-height displacement	Base shear
Dual consisted of special moment frames and concentrically braced frames	≤ 0.23	≤ 0.79	≤ 5.38
Special moment frames	≤ 0.14	≤ 0.98	≤ 5.63
Dual consisted of intermediate moment frames and concentrically braced frames	≤ 0.28	≤ 1.15	≤ 5.13

[17] BHRC (Building and Housing Research Centre), Standard No. 2800-05, Iranian Code of Practice for Seismic Resistant Design, Iran, 2007 (in Persian).

[18] INBR (Iranian National Building Regulations), Iranian National Building Code, Part 10-Steel Structures, Iran, 1993 (in Persian).

A 15-floor steel-structure building with nonlinear behaviour and non-classical damping

A 15-floor steel-structure building model is under study for the top displacement and base shear; see Fig. 13 and Table 10. The behaviour is nonlinear, with attention to Fig. 14, with regard to which, for the top displacement, $T \cong 1.0 > 0.40$ sec; see also Eq. (10). This is also in agreement with the fact that the first seven natural periods of the system are greater than 0.4 sec (see the mode shape in Fig. 15), nonlinear behaviour can

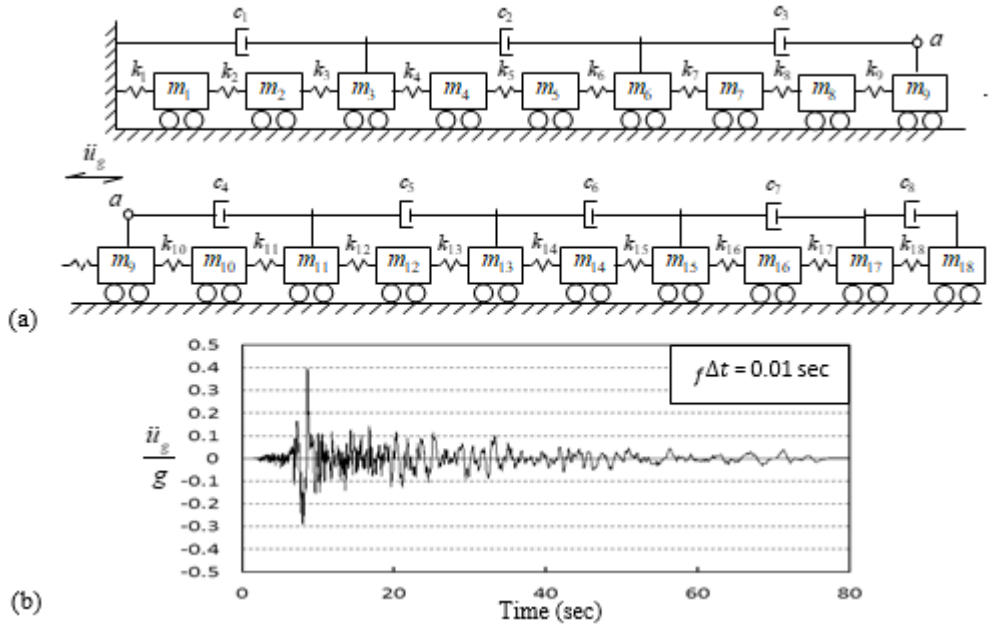

Fig. 13. *Pictorial introduction to the fourth example: (a) Structural model, (b) Ground motion*

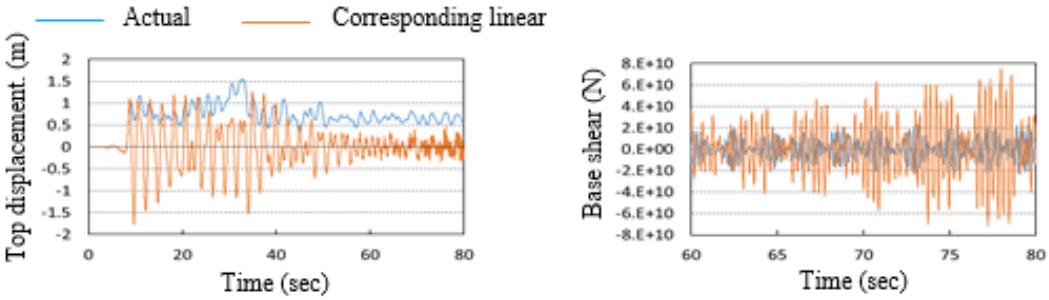

Fig. 14. *Exact responses of the fourth example*

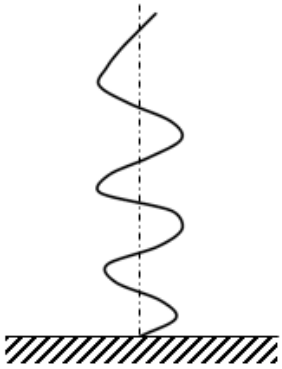

Fig. 15. *Shape of the seventh natural mode ($T_7 = 0.42$ sec), for the linear system corresponding to the nonlinear system introduced in Fig. 13(a) and Table 10*

Table 10. Main properties of the structural model in the fourth example

Property	i																	
	1	2	3	4	5	6	7	8	9	10	11	12	13	14	15	16	17	18
$10^{-9} \times m_i$	3	3	3	3	3	3	3	3	1.5	1.5	1.5	1.5	1.5	1.5	0.5	0.5	0.5	0.5
$10^{-12} \times k_i$	2	2	2	2	1.2	1.2	1.2	1.2	0.6	0.6	0.6	0.6	0.6	0.6	0.1	0.1	0.1	0.1
$10^{-8} \times c_i$	12	8	6	2.5	2.5	1.5	0.5	0.2										
$10^{2} \times u_{y_i}$	8	8	8	8	8	8	5	5	5	5	5	5	5	5	3	3	3	3

be considered an extension of linear behaviour, the first few natural modes play the main role in the structural behaviour, and that the linear response is a combination of the responses in different natural modes. (In view of Fig. 14, for the base shear, $T \cong 0.1$ sec.) Consequently, we can expect the good performance of the SEB THAAT and Eq. (11) when applied to the response history analysis of the structure, especially for the top displacement. It is meanwhile worth noting that, different from the previous examples, where the damping was classical viscous (in the first example) and zero (in the second and third examples), in view of Fig. 13(a) and Table 10, the damping is non-zero and non-classical viscous in this example [2,36,37].

The model is analysed twice using the average acceleration method [33], and twice using the Wilson-θ [38,39] ($\theta = 1.4$) method. In the first analyses by either method, the integration step is set to ${}_f\Delta t$ (obtained from Eq. (2) for the first target response). The analyses are then repeated using $\Delta t = 2\,{}_f\Delta t$, after implementation of the SEB THAAT. The fractional time stepping method [40,41] is used for nonlinearity solution, and the nonlinearity tolerance and the maximum number of iterations are considered equal to 1E-6 and 5, respectively (see [17,40,41]). The results are displayed in Fig. 16, and are evaluated, taking into account that the responses of nonlinear dynamic analyses may be inaccurate even significantly regardless of the SEB THAAT [1,3,7,28,42-46]. For the first target response, i.e. the top displacement, the responses obtained with or without application of the SEB THAAT coincide, when analysing with either integration method. For the base shear, the two responses are close, in analysis with the average acceleration method [33]. In analysis with the Wilson-θ [38,39] ($\theta = 1.4$) method, however, the computed two base shears are evidently different. To better study the difference between the two base shears, obtained from the Wilson-θ [38,39] ($\theta = 1.4$) method (see Fig. 16(b)), the results of analysis with very small steps is displayed in Fig.16(c). In view of this figure, both of the base shears computed by the Wilson-θ [38,39] ($\theta = 1.4$) method (when applying and not applying the SEB THAAT) differ significantly from the exact base shear (displayed in Fig. 16(c)). In more detail, the two differences (between the two base shears in Fig. 16(b) and the exact base shear in Fig. 16(c)) are much larger than the difference between the two base shears in Fig. 16(b). Therefore, the accuracy of the base shears in Fig. 16(b), is acceptable, in the sense that replacing the base shear obtained using $\Delta t = {}_f\Delta t$ with the base shear obtained using $\Delta t = 2\,{}_f\Delta t$ (both displayed in Fig. 16(b)) does not imply meaningful change in the response accuracy. Even more, returning to the origin of the Wilson-θ method [38], one of the main purposes of the Wilson-θ method is to filter high mode responses out of the response [47]. This filtering, which is broadly known as numerical damping of time integration methods [3,4,6,20,21,48,49], is essential, when we are seeking the responses of the structural model before the discretization resulting in Eq. (1). The discretization, replaces the structural model (with infinite number of degrees of freedom) with the mathematical model in Eq. (1) (with finite number of degrees of freedom), in the price of spurious high frequency oscillations in the response, which can be eliminated by numerical damping [3,6,49]. (Numerical damping can also eliminate real high modes with small contribution in the response, but computed erroneously because of largeness of the $\Delta t/T$ [3,6,47-49]). Considering this, when using the Wilson-θ method [38], the purpose of the analysis may be different from achieving good accuracy compared to the exact response reported in Fig. 16(c). As a result, because of "selection" of the integration method, the base shears in Figs. 16(a) and 16(b) not only show the good performance of SEB THAAT when using Eq. (11), but can also be considered sufficiently accurate.

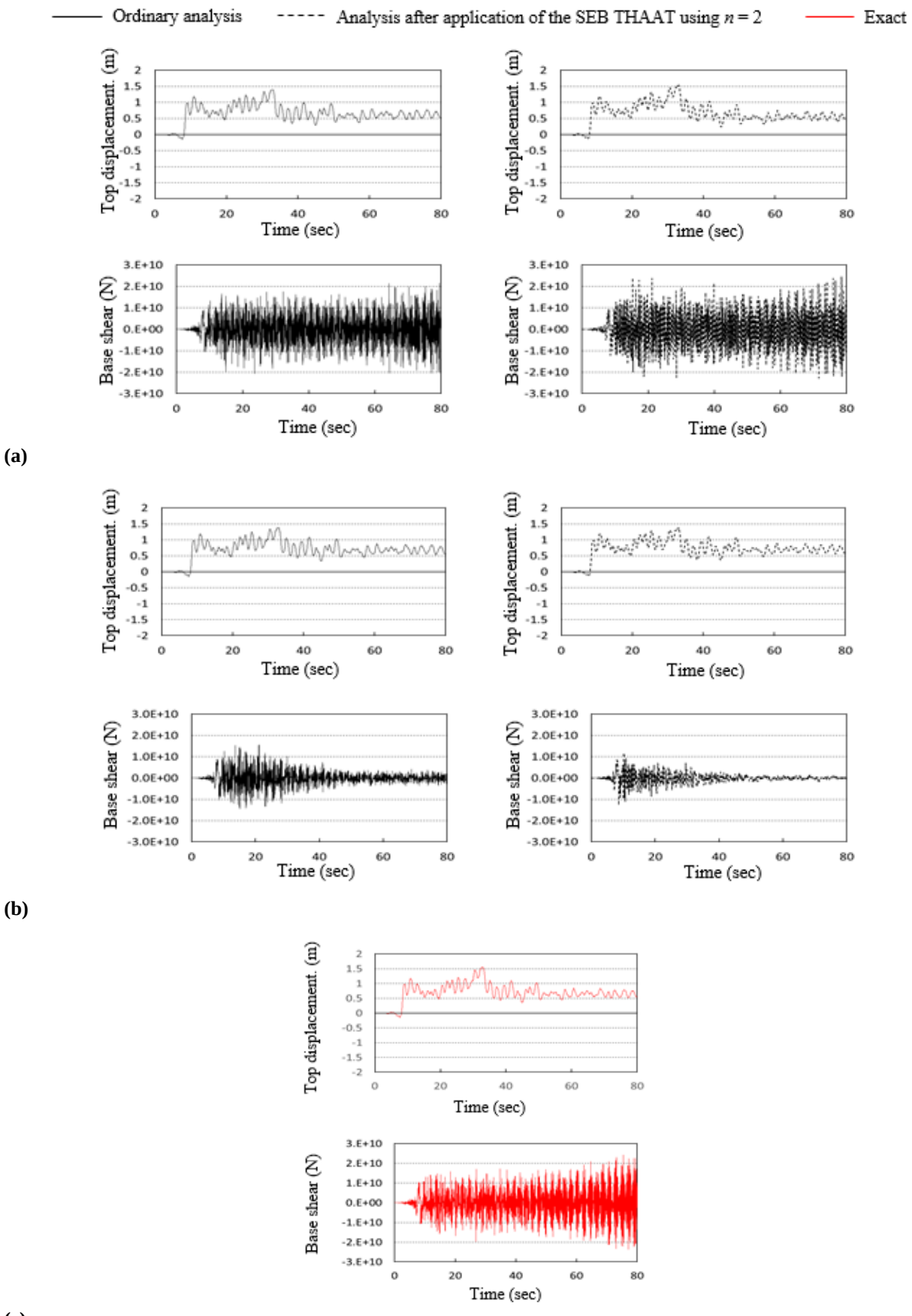

Fig. 16. *Target responses of the fourth example: (a) Computed using the average acceleration method, (b) Computed using the Wilson-θ (θ =1.4) method, (c) Exact*

For further clarity, the following two questions are to be answered, as well:

(a) What is the reason of the different performances of the SEB THAAT using Eq. (11), in Figs. 16(a) and 16(b)? Meanwhile, why are the base shears in Figs. 16(a) (and Fig. 16(c)) and 16(b) such different that while in Fig. 16(a) (and Fig. 16(c)) the base shear increases with time, in Fig. 16(b), the base shear decreases with time?

(b) What is the reason of the negligible difference between the top displacements in Fig 16(b), while the difference between the two base shears in Fig. 16(b) is recognizable?

The answer to Question (a) lies in the fact that Eq. (2) is not rigorous; besides other ambiguities, it is not clear why the integration method does not affect the selection of the integration step. More specifically, the numerical damping referred to in the previous discussion is very different in the average acceleration and Wilson-θ methods, with no influence on Eq. (2). The *difference* is evident in Fig. 17, for problems with classical viscous damping [50], and is yet unstudied for problems with non-classical viscous damping. (In Fig. 17, ρ and $\bar{T}$ imply the spectral radius [6,20,48-50] and the oscillations period, respectively, and the difference of spectral radius from one at large value of $\Delta t/\bar{T}$ represents the capability of eliminating the oscillations with period $\bar{T}$ in analysis with step Δt.) Despite the latter, there are experiences in the literature (e.g. see [51]), for extending the discussions on classical viscous damping to non-classical viscous damping, using complex variables [52], such that the classical case can be considered as a special case of the whole discussion. Therefore, it is reasonable to consider significant difference between the numerical damping of average acceleration and Wilson-θ methods, when the viscous damping is non-classical, as well. This explains the considerable difference between the base shears in Figs. 16(a) and 16(b). The numerical details however cannot be presented, because the figure corresponding to Fig. 17 is yet unavailable for problems with non-classical viscous damping (the case in this example). Only, as a simple rough study, the mid-parts of the base shears in Figs. 16(b) and 16(c) are compared in Fig. 18. Accordingly, the change of the base shear (versus time),

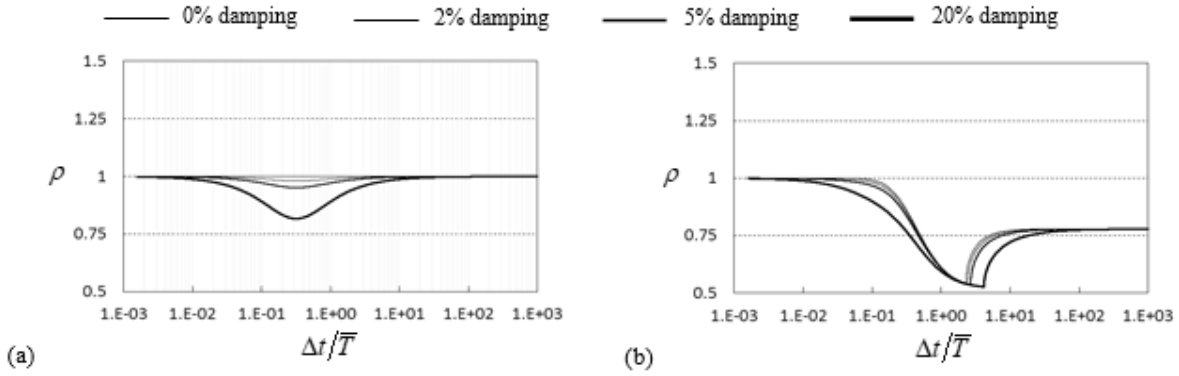

Fig. 17. *Changes of spectral radius (ρ) with respect to $\Delta t/\bar{T}$ for the (a) average acceleration method [33], (b) Wilson-θ (θ =1.4) [38,39]*

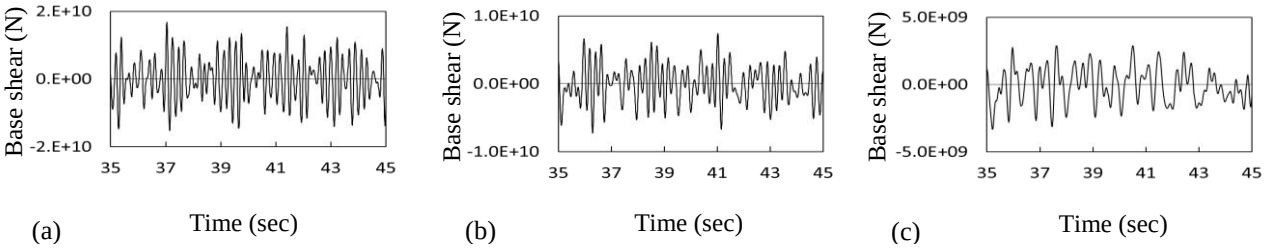

Fig. 18. *A simple rough comparison between the base shears in Figs. 16(b) and 16(c): (a) Middle ten seconds of Fig. 16(c), (b) Middle ten seconds of Fig. 16(b) (the left figure), (c) Middle ten seconds of Fig. 16(b) (the right figure)*

including the change of base shear increase (in Fig. 16(c)) to the base shear decrease (in Fig. 16(b)), occurs along with further removal of high frequency oscillations, in analysis with larger integration steps.

In answer to Question (b), if we compare the exact top displacement and the exact base shear in Fig. 16(c) (or even in Figs. 16(a) and 16(b)), the value of T is much larger for the top displacement. As a result, the value of $\Delta t/T$ and accordingly the value of $\Delta t/\overline{T}$ is much smaller for the top displacement, compared to the base shear. From the other side of view, because of the essentiality of convergence for time integration methods [3,4,6,11,12,20,21], the difference between the spectral radii of different time integration methods disappears for sufficiently small values of $\Delta t/\overline{T}$. (This is evident for problems with classical viscous damping in Fig. 17, as well as in the extended study considering many integration methods reported in [50].) Consequently, the effect of the numerical damping of Wilson-θ method on the top displacement is much less than the effect on the base shear. In other words, the integration has removed the high frequency oscillations from the response, and since the high frequency oscillations have negligible contribution to the top displacement (see Fig. 16(c)), the two top displacements in Fig. 16(b) are different negligibly. Due to a similar reason, the difference between the two base shears in Fig. 16(b) is noteworthy. This plus the role of T in Eq. (2) (though not rigorous) completes the answer to Question (b).

Finally, the reductions in analysis run-time, due to the SEB THAAT using Eq. (11), are equal to 29.32% and 22.34%, when using the Wilson-θ ($\theta = 1.4$) and average acceleration methods, respectively. The difference of these values with 50% is because of the nonlinearity of the problem, explained previously in this paper.

Complementary discussion

In the previous sections, it was demonstrated that, in seismic response history analysis of mid-rise steel-structure buildings, by using Eq. (11), the SEB THAAT can reduce the analysis run-time, leading to sufficiently accurate responses, without prior knowledge about the response. Besides, in practice, buildings are subjected not only to ground motions, but also to gravity loads. As a result, the effect of using the SEB THAAT and Eq. (11) on the real analyses is even better than that discussed in the previous sections. This enhances the importance of the simplicity obtained from Eq. (11). Further discussion on some ambiguities and limitations is however essential.

The first ambiguity is whether the good performance observed in the presented examples relates to the seismic design code. In other words, is the observed good performance limited to the analysis of structures designed using the Iranian seismic standards? By using different design codes, the results of response history analysis with/without using the SEB THAAT will change. The simplicity and good performance of using the SEB THAAT and Eq. (11) will however not change, because of two main reasons. First, the scientific bases of seismic codes are close, and hence for a similar seismicity, the designs obtained from using different codes generally differ slightly. As a result, the effect of the change of the code on the performance of the SEB THAAT taking into account Eq. (11) would be reasonably tolerable. The second reason is that the codes used in the presented examples were the standards of Iran, and the seismicity of Iran is higher than many other regions of the world [53]. Therefore, when changing the design codes, the resulting T in Eqs. (2), (3), and (5) will probably increase. This implies even more suitability for Eq. (11) and more accuracy for the computed responses, when using seismic codes different from the codes of Iran.

In view of the presented examples (see Figs. 5 and 11), the second ambiguity is whether the SEB THAAT's performance is acceptable when the structural system is irregular in height or plan. In two separate studies [54,55], attention was paid to the performance of the SEB THAAT when applied to analysis of buildings' structures with irregularity in height or plan. In both studies, Eq. (11) provided an appropriate selection for n. A similar observation was made in a slightly different study on the SEB THAAT [56], as well. Accordingly, applying the SEB THAAT to seismic response history analysis of mid-rise steel-structure buildings with

irregularity in height or plan may be successful, for values of n equal to or greater than two. Irregularities simultaneous in both height and plan are yet not tested for the performance of the SEB THAAT. Considering this and for the sake of brevity, none of the tests on irregular structures is reported here. Therefore, the claims in this paper are limited to mid-rise steel-structure buildings categorized regular by the seismic codes. This limitation is however practically unimportant, because, it is decades that buildings' designers mostly prefer to design the structures to be regular according to the seismic codes[19,20,21,22,23,24] ; see also [25,26,57].

In view of the presented discussions, it is notable to add that few successful tests are reported on taller buildings [58] and buildings with concrete structure [56], as well. Besides, in view of the presented discussions and examples, and the more studied examples, not reported here for the sake of brevity, no limitation seems existing on the time integration method. Further investigation is essential.

Considering the limitations addressed above, the social importance and large number of mid-rise buildings, the simplicity of Eq. (11), the everyday smaller values of digitization steps, the generally time-consuming nature of response history analyses, and the considerable reductions in run-time reported in the presented examples, the achievements are significant. Therefore, the future of the presented research is promising, at least until Eq. (11) can be replaced with a better comment or computational procedure (see also [10]).

Conclusion

The SEB THAAT is a technique for accelerating different analyses of structural systems. In this paper, an engineering comment for applying the SEB THAAT in seismic response history analysis of mid-rise steel-structure buildings without any details about the response is proposed. The engineering comment implies obtaining the step enlargement scale n, in application of the SEB THAAT to response history analysis of mid-rise steel-structure buildings, from Eq. (11). By implementation of this comment, without notable effects on the response accuracy:

(a) The SEB THAAT can be applied to response history analysis of mid-rise steel-structure buildings, in a much simpler way (Step 6 in Fig. 2 is considerably simplified).
(b) The analysis run-times can be significantly reduced (50% for linear analyses).

This is a significant achievement, which, as a secondary achievement, can encourage structural analysts of mid-rise steel-structure buildings to use response history analysis in real projects.

Limitations exist for the proposed comment. In addition to those implied in the expression "mid-rise steel-structure buildings", the most important limitation is that the building structure must be "regular" according to the seismic code. This is however not a severe limitation, in view of the results of some recent researches, and the current practice of buildings structural design. Besides, the accuracy of the obtained responses need to be interpreted considering the numerical damping of the integration method. Other minor limitations exist, as well.

The future of the proposed comment is promising, with attention to its simplicity and effectiveness, and the fact that digitization steps are in every day decrease. Finally, extending the application of the proposed comment from response history analysis of mid-rise steel-structure buildings to other classes of analyses, and improvement of this comment are two areas for further research.

[19] BHRC (Building and Housing Research Centre), Standard No. 2800-05, Iranian Code of Practice for Seismic Resistant Design, Iran, 2007 (in Persian).
[20] INBR (Iranian National Building Regulations), Iranian National Building Code, Part 10-Steel Structures, Iran, 1993 (in Persian).
[21] ICC (International Code Council), IBC - International Building Code, Club Hills, USA, 2003.
[22] BCJ (Building Centre of Japan), Structural Provisions for Building Structures, Tokyo, Japan, 2001.
[23] EAK, Greek Code for Seismic Resistant Structures, Athens, Greece, 2000.
[24] NRCC (National Research Council Canada), National Building Code of Canada, Canada, 2005.

Acknowledgments

The authors are grateful for the reviewers' comments, which have caused significant improvements in the paper. The role of the editorial team in quickly reviewing the paper and editing it very well is also sincerely appreciated. Finally, the first author acknowledges the financial support of the International Institute of Earthquake Engineering and Seismology (IIEES) in relation to the Projects 7510, 7528, and 7537.

References

[1]. P. Fajfar, Analysis in Seismic Provisions for Buildings: Past, Present and Future. Bulletin of Earthquake Engineering, 16 (7), 2018, 2567–2608. Doi: https://doi.org/10.1007/s10518-017-0290-8
[2]. R.W. Clough, J. Penzien, Dynamics of Structures. McGraw-Hill, Singapore, 1993.
[3]. A. Soroushian, Integration Step Size and Its Adequate Selection in Analysis of Structural Systems Against Earthquakes, in: M. Papadrakakis, V. Plevris, N.D. Lagaros (eds.), Computational Methods in Earthquake Engineering. Springer, 3, 2017, 285-329. Doi: https://doi.org/10.1007/978-3-319-47798-5_10
[4]. K.J. Bathe, Finite Element Procedures. Prentice-Hall, USA, 1996.
[5]. J. Henrych, Finite Models and Methods of Dynamics in Structures. Elsevier, Amsterdam, 1990.
[6]. T. Belytschko, T.J.R. Hughes, Computational Methods for Transient Analysis. Elsevier, Amsterdam, 1983.
[7]. T. Belytschko, W.K. Liu, B. Moran, Non-linear Finite Elements for Continua and Structures. Wiley-Intersciences, Chichester, 2000.
[8]. J.F. McNamara, Solution Schemes for Problems of Nonlinear Structural Dynamics. Journal of Pressure Vessels, 96 (2), 1974, 147-155. Doi: https://doi.org/10.1115/1.3454158
[9]. A. Soroushian, A Technique for Time Integration with Steps Larger than the Excitation Steps. Communications in Numerical Methods in Engineering, 24 (12), 2008, 2087-2111. Doi: https://doi.org/10.1002/cnm.1097
[10]. A. Soroushian, A Technique for Time Integration with Steps Larger than the Excitation Steps: Review of the Past Addressing the Existing Challenges and a Perspective of the Future. Proceedings of 8th ECCOMAS Thematic Conference on Computational Methods in Structural Dynamics and Earthquake Engineering (COMPDYN 2021), Athens, Greece, June 28-31, 2021, 1476-1491. Doi: https://doi.org/10.7712/120121.8574.19609
[11]. P. Henrici, Discrete Variable Methods in Ordinary Differential Equations. Prentice-Hall, USA, 1962.
[12]. J.C. Strikwerda, Finite Difference Schemes and Partial Differential Equations. Wadsworth & Books/Cole, USA, 1989.
[13]. A. Soroushian, E.M. Farahani, Efficient Static Analysis of Assemblies of Beam-Columns Subjected to Continuous Loadings Available as Digitized Records. Frontiers in Built Environment, 4, 2019, 215-229. Doi: https://doi.org/10.3389/fbuil.2018.00083
[14]. A. Soroushian, Assessment of the Sufficiency and Necessity of the Conventionally Accepted Proposed Time Step for Nonlinear Structural Dynamic Analysis. Report No. 7528. International Institute of Earthquake Engineering and Structural Dynamics (IIEES), Tehran, Iran, 2022 (in Persian).
[15]. A. Sabzei, On the performance of a recent technique for seismic analyses computational cost reduction when applied to buildings structural systems: MSc thesis, International Institute of Earthquake Engineering and Seismology (IIEES), Tehran, Iran, 2013 (in Persian).
[16]. A. Soroushian, Y. Zarabimanesh, K. Soleymani, S.M. Khalkhali, A New Technique for Fractional Enlargement of Integration Steps in Transient Analysis against Digitized Excitations. Proceedings of International Conference on Structural Engineering Dynamics (ICEDyn 2017*)*, Ericeira, Portugal, July 3-5, 2017.
[17]. A. Soroushian, On the Performance of a Recent Technique for More Efficient Time Integration in Severe Seismic Conditions. Proceedings of 1st International Conference on Advances in Structural Engineering and Mechanics (ASEM'11), Seoul, South Korea, September 18-23, 2011, 6077-6095.
[18]. A.V. Oppenheim, R.W. Schafer, Discrete-time Signal Processing. 3-rd Ed. Prentice-Hall, Upper Saddle River, 2009.
[19]. A. Soroushian, P. Farshadmanesh, S. Azad. On the Essentiality of Techniques to Enlarge Integration Steps in Transient Analysis Against Digitized Excitations. Journal of Seismology and Earthquake Engineering, 17, 2015, 43-60.
[20]. W.L. Wood, Practical Time Stepping Schemes. Oxford, USA, 1990.

[21]. T.J.R. Hughes, The Finite Element Method: Linear Static and Dynamic Finite Element Analysis. Prentice-Hall, Upper Saddle River, 1987.
[22]. A. Taghinia, Development of seismic fragility functions for integral concrete bridges in Iran: PhD thesis, International Institute of Earthquake Engineering and Seismology (IIEES), Tehran, Iran, 2021 (in Persian).
[23]. J. Havskov, G. Alguacil, Instrumentation in Earthquake Seismology. Springer, The Netherlands, 2016.
[24]. A.K. Chopra, Dynamics of Structures: Theory and Application to Earthquake Engineering. Prentice-Hall, USA, 2012.
[25]. W. Schueller, The Vertical Building Structure. Van Nostrand Reinhold, USA, 1990.
[26]. B. Stafford Smith, A. Coull, Tall Building Structures: Analysis and Design. Wiley, USA, 1991.
[27]. V. Plevris, C.C. Mitropoulou, N.D. Lagaros, Structural Seismic Design Optimization and Earthquake Engineering: Formulations and Applications. IGA Global, USA, 2012.
[28]. P. Wriggers, Nonlinear Finite Element Methods. Springer, Berlin, 2008.
[29]. E.L. Allgower, K. Georg, Numerical Continuation Methods, An Introduction. Springer, Berlin, 1990.
[30]. J. Chung, G.M. Hulbert, A Time Integration Algorithm for Structural Dynamics with Improved Numerical Dissipation: The Generalized-a Method. Journal of Applied Mechanics, 60 (2), 1993, 371-375. Doi: https://doi.org/10.1115/1.2900803
[31]. A. Soroushian, Optimization of geometry and structural system of residential complexes: MSc thesis, Shiraz University, Shiraz, Iran, 1995 (in Persian).
[32]. R.T. Haftka, Z. Gurdal, Elements of Structural Optimization. Kluwer, The Netherlands, 1991.
[33]. N.M. Newmark, A Method of Computation for Structural Dynamics, Journal of the Engineering Mechanics Division, 85 (3), 1959, 67-94. Doi: https://doi.org/10.1061/JMCEA3.0000098
[34]. B. Noble, J.W. Daniel, Applied Linear Algebra. Prentice-Hall, Upper Saddle River, 1977.
[35]. A.F. D'Souza, V.K. Garg, Advanced Dynamics Modeling and Analysis. Prentice-Hall, Englewood Cliffs, 1984.
[36]. A. Soroushian, Performance of a Time Integration Acceleration Technique Applied to Seismic Analysis of Non-Classically Damped Structural Dynamics. Iranian Journal of Science and Technology, Transactions of Civil Engineering, 46 (2), 2022, 1281-1300.
Doi: https://doi.org/10.1007/s40996-021-00666-z
[37]. B.J. Lazan, Damping of Materials and Members in Structural Mechanics. Pergamon, London, 1968.
[38]. E.L. Wilson, A Computer Program for the Dynamic Stress Analysis of Underground Structures, SESM Report 68-1, Department of Civil Engineering, University of California, Berkeley, USA, 1968.
[39]. A. Soroushian, J. Farjoodi, K. Bargi, M. Rajabi, A. Saaed, M. Arghavani, M.M. Sharifpour, Two Versions of the Wilson-θ Time Integration Method. Proceedings of 10th International Conference on Vibration Problems, ICOVP, Prague, Czech Republic, 2011, 229-234.
[40]. J.M. Nau. Computation of Inelastic Response Spectra. Journal of Engineering Mechanics, 109 (1), 1983, 279 -288. Doi: https://doi.org/10.1061/(ASCE)0733-9399(1983)109:1(279)
[41]. S.A. Mahin, J. Lin, Construction of Inelastic Response Spectra for Single Degree-of-Freedom Systems, Technical Report No. UCB/EERC-83/17. Earthquake Engineering Research Center (EERC), University of California, CA, USA, 1983.
[42]. Y.M. Xie, G.P. Steven, Instability, Chaos, and Growth and Decay of Energy of Time-Stepping Schemes for Non-linear Dynamic Equations. Communications in Numerical Methods in Engineering, 10 (5), 1994, 393-401. Doi: https://doi.org/10.1002/cnm.1640100505
[43]. S. Rashidi, M.A. Saadeghvaziri, Seismic Modeling of Multi-span Simply-supported Bridges Using ADINA. Computers and Structures, 64 (5-6), 1997, 1025-1039.
Doi: https://doi.org/10.1016/S0045-7949(97)00016-3
[44]. W.L. Wood, M.E. Oduor, Stability Properties of Some Algorithms for the Solution of Nonlinear Dynamic Vibration Equation. Communications in Applied Numerical Methods, 4 (2), 1988, 205–212.
Doi: https://doi.org/10.1002/cnm.1630040211
[45]. P.B. Bornemann, U. Galvanetto, M.A. Crisfield, Some Remarks on the Numerical Time Integration of Non-linear Dynamical Systems. Journal of Sound and Vibration, 252 (5), 2002, 935–944.
Doi: https://doi.org/10.1006/jsvi.2001.4044
[46]. D. Soares Jr, G. Großeholz, Nonlinear Structural Dynamic Analysis by a Stabilized Central Difference Method. Engineering Structures, 173, 2018, 383-392.
Doi: https://doi.org/10.1016/j.engstruct.2018.06.115

[47]. K.J. Bathe, E.L. Wilson, Stability and Accuracy Analysis of Direct Integration Methods. Earthquake Engineering & Structural Dynamics, 1 (3), 1972, 283-291. Doi: https://doi.org/10.1002/eqe.4290010308
[48]. P. Paultre, Dynamics of Structures. John Wiley & Sons, UK, 2013.
[49]. H. Kardestuncer, Finite Element Handbook. McGraw Hill, USA, 1987.
[50]. A. Soroushian, A General Rule for the Influence of Physical Damping on the Numerical Stability of Time Integration Analysis. Journal of Applied and Computational Mechanics, 4 (5), 2018, 467-481. Doi: https://doi.org/10.22055/JACM.2018.25161.1235
[51]. L. Meirovitch, Fundamentals of Vibration. McGraw Hill, Singapore, 2001.
[52]. J.W. Brown, R.V. Churchill, Complex Variables and Applications. McGraw Hill, USA, 2014.
[53]. M. Barazangi, J. Dorman, World Seismicity Maps Compiled from ESSA, Coast and Geodetic Survey, Epicenter Data, 1961-1967. Bulletin of the Seismological Society of America, 59 (1), 1969, 369-380. Doi: https://doi.org/10.1785/BSSA0590010369
[54]. A.A. Hadad, Reducing computational costs in time integration analyses of buildings with irregularities in height because of mass: MSc thesis, International Institute of Earthquake Engineering and Seismology (IIEES), Tehran, Iran, 2015 (in Persian).
[55]. A. Baiani, On the possibility to accelerate time history analysis of buildings with irregularities in plan because of mass distribution: MSc thesis, University of Pooyandegan Danesh, Chalus, Iran, 2018 (in press, in Persian).
[56]. M.H. Ghondaghsaz, A study on a recent technique for more efficient seismic analysis applied to concrete and steel buildings: MSc thesis, Islamic Azad University West Tehran Branch, Tehran, Iran, 2017 (in Persian).
[57]. F. Naeim, S. Zhongzhi, The Seismic Design Handbook. Kluwer, USA, 2001.
[58]. A. Soroushian, A. Aziminejad, More Efficient Seismic Analysis of Tall Buildings by Implementing a Recently Proposed Technique. Proceedings of the 6th International Conference on Seismology and Earthquake Engineering (SEE6), Tehran, Iran, 16-18 May, 2011.

Aram Soroushian, Doctor of Philosophy (PhD) in Civil Engineering, Assistant Professor *(Iran, Tehran) - International Institute of Earthquake Engineering and Seismology (IIEES), Faculty member of Structural Engineering Research Centre, a.soroushian@iiees.ac.ir*

Abdolreza S. Moghadam, Doctor of Philosophy (PhD) in Earthquake Engineering, Associate Professor *(Iran, Tehran) - International Institute of Earthquake Engineering and Seismology (IIEES), Faculty member of Structural Engineering Research Centre, moghadam@iiees.ac.ir*

Ahmad Sabzei, Doctor of Philosophy (PhD) in Earthquake Engineering *(Iran, Tehran) - International Institute of Earthquake Engineering and Seismology (IIEES), Research Assistant of Structural Engineering Research Centre, ahmad.sabzei64@gmail.com*

Saeed Amiri, Master of Science (MS) in Civil Engineering, PhD Candidate *(Canada, QC, Montreal) - Department of Civil, Geological and Mining Engineering, Polytechnique Montreal, saeed.amiri@polymtl.ca*

Aram Saaed, Master of Science (MS) in Civil Engineering, PhD Candidate *(Iran, Tehran) - Structural Engineering Research Centre, International Institute of Earthquake Engineering and Seismology (IIEES), a.saaed@iiees.ac.ir*

Ali Yahyapour, Master of Science (MS) in Civil Engineering *(Iran, Tehran) - Structural Engineering Research Centre, International Institute of Earthquake Engineering and Seismology (IIEES), Research Assistant of Structural Engineering Research Centre, aliyahyapour7@gmail.com*

WATER SUPPLY NETWORK ZONING PROCEDURE DEVELOPMENT CONSIDERING LOCAL CONDITIONS

Aram Sahakyan

National University of Architecture and Construction of Armenia, Yerevan, RA

Abstract: *The methods of performing zoning implemented in the water supply networks of various settlements in RA have been continuously improved over the past years and are currently carried out by a procedure developed by us, which has increased the efficiency of the water supply system operation.We have implemented this to increase the efficiency of the water supply system. There are several principles for the zoning of the water supply network's concepts in the literature, but using the current techniques only reduces the volume of water provided to the zone by 8 to 10 percent and the time of supply by a fixed amount (not around the clock). Additional investigation led to finding the causes of zoning's poor effectiveness, the shortcomings of the design, insufficient level of network research, application of incorrect principles of zoning and pressure management. We developed the methods discussed in this paper to resolve the aforementioned problems. Analyzing the results of multi-year studies and considering the current technical situation of the distribution network, we recommend continuing the zoning of the networks for the current stage until the night-time consumption of the zone is less than half of the daytime consumption.*

Keywords: *water supply network, water supply network zoning, leakage, night water consumption, network zero pressure test.*

Aram Sahakyan
E-mail: sahakyan.aram@nuaca.am

Received: 17.01.2023
Revised: 07.02.2023
Accepted: 22.02.2023

Introduction

The requirement for zoning of the distribution network arises in mountainous conditions when there is a significant difference in levels within the boundaries of the settlement. Both gravity and pressing systems (reverse zoning) may require zoning [1,2].

When high-rise multi-residential buildings are constructed in areas where low-rise buildings are already present or when the high-rise buildings' absolute height exceeds that of the low-rise buildings within the water supply zone's boundaries, zoning becomes crucial. Therefore, to increase the controllability of the distribution network, it is necessary to implement effective zoning of the network, i.e., to transform the network into hydraulically separated zones that are isolated from one another. Isolation must be implemented by installing existing or new valves, which will be closed during the regular operation of the water supply network, but can be opened if necessary. In mountainous areas, it is advisable to use vertical zoning in a sequential or parallel scheme.

Many automatic network zoning approaches have recently become widely used with specifically created computer programs (hybrid approaches for the automatic partitioning of a water distribution network, spatial analysis zoning approach, semi-supervised method etc.). However, the application of these techniques is unworkable with an existing network that is worn out, elementally constructed and reconstructed, or fragmented. Our original research showed that some additional problems arise when creating zones using existing weathered, prefabricated, reconstructed, or fragmented networks. Thus, after zoning Arabkir zone 1, Kievan, Gulbekyan, and Keri streets, it was found that the amount of water supplied to the zone decreased by only 8%–10%, and the 8-hour duration of supply was 12 h instead of the planned round-the-clock.

Because the designed pressure wasn't maintained, accidents happened more frequently. Additional investigation led to finding the causes of zoning's poor effectiveness:

- the shortcomings of the design,
- insufficient level of network research,
- application of incorrect principles of zoning and pressure management.

We developed the methods discussed in this paper to resolve the aforementioned problems.

Because of the analysis of the original research and operation data on the water supply network, as well as the international experience applied in similar conditions and the study of the existing literature, the zoning works carried out in the water supply network of different settlements of RA have been improved and are currently being carried out efficiently according to a procedure developed by us. The principles of water supply network zoning are found in several versions of the literature currently in print. Many automatic network zoning approaches have recently become widely used with specifically created computer programs. However, the application of these techniques is unworkable with an existing network that is worn out, elementally constructed and reconstructed, or fragmented.

Different models have been proposed, based on classic optimization methodologies or on meta-heuristic approaches [3-7].

The optimal design of DMAs as part of a Decision Support System (DSS) for reducing the water losses has been addressed only recently in the literature. Some authors have proposed hybrid approaches for the automatic partitioning of a water distribution network, based on both meta-heuristic algorithms and on applications from the graph theory [8,9].

The proposed models mainly focus on the preservation of the hydraulic reliability of the network, while less control is allowed on the costs of the provided solutions [10].

Sempewo et al. [11] developed a spatial analysis zoning approach based on the METIS graph partitioning tool [12].

The proposed technique follows the analogy with the distributed computing methodology of equally distributing workloads among processors. However, as stated by the same authors, although the method results effective in the demarcation of contiguous districts, the quality of the provided solution degrades when considering multi-objective partitioning, and uncertainties are produced when increasing the number of DMAs.

Herrera et al. [13] proposed a semi-supervised method named multi-agent adaptive boost clustering. This complex technique considers both the WDN features (e.g. node elevations and demands) and the economic issues (edge cut = number of pipes to be intercepted) for the partitioning of the network. Nevertheless, the procedure is only applied to cases in which the number of DMAs is lower than the number of supply nodes.

More recently, [14] have introduced an approach for automatic creation of DMAs based on the hierarchical community structure of the WDN. In this study, the selection of the feeding lines for the DMAs is made through an iterative selection method based on a sensitivity analysis. The methodology was tested on a very large network with reasonable computing times, but the results showed high sensitivity towards the assignment of the input parameters.

A comprehensive description of the possible objective functions for the problem can be found in Gomes et al. [15].

The two-step approach proposed by the authors consists of a preliminary partitioning of the WDN into suitable DMAs through the application of the design criteria and graph theory concepts, i.e. the Floyd-Warshall Algorithm (FWA). Next, Simulated Annealing (SA) is used for the localization of entry points and of boundary valves, but also for planning the reinforcement/replacement of pipes in the network. Although the results have resulted satisfactory, the global optimality of the solution is not ensured by the SA. Hence, despite the newest contributions, further developments seem required about this topic [16].

Among the available approaches for pressure management, the use of District Metered Areas (DMAs) also allows for a more accurate localization of the leakages in the water distribution network, which is achieved by monitoring the input and the output discharges for each district. Nowadays, this approach is widely used in practice, but its application is still largely entrusted to the experience of technicians [10].

According to the proposed principles, to increase the zoning and manageability of the water supply network, it is necessary to create hydraulically isolated zones with up to 3000 subscribers in the settlement. Since the zoning is carried out under the conditions of the existing system, the procedures developed during the design and reconstruction work consider the features of the existing system: difference in characters; dictating characters of the day regulatory reservoirs; location and volumes; diameters of the existing pipes; height of the buildings; population density; etc.

It is suggested to remove the inner rings of the zone by temporarily converting the ring network within the presented zone boundaries into a dead-end network using valves and separate sectors. Magnetic flowmeters and pressure recording sensors should be installed on the feeding pipes. It will allow for assessing the water balance within individual zones, determining the amount of unaccounted water, and discovering its nature and location [17].

These investigations aim to calculate how much water enters each zone and compare it to how much water is received based on the number of subscribers. By creating water supply sectors with one-way flow and an exact number of subscribers, it is possible to estimate the amount of unaccounted water in the presented zone. During the zoning (design and construction) of the existing water supply network, it may be necessary to apply the following procedures: changes of water sources (spring, aqueduct, daily regulating reservoir) in zones or sometimes in entire districts, change of design and/or operating hydraulic regimes of water pipelines, converting the ring network temporarily into dead-end sectors with separate one-way flow, loss detection and elimination, installation of pressure regulators at required points, decommissioning or replacing backyard pumping stations with smaller capacity pumps, as well as a grouping.

Before the implementation, it is crucial to perform studies and designs at a high level through experienced engineering solutions because zonings require financial investments and impact the quality of services offered. However, experience shows that it is almost impossible to have a final zoning project, so during the execution of the works, there is a need to review the scope of the study.

Materials and Methods

Design and implementation of a water supply zone

Before starting the zoning, it is necessary to analyze the problems and data recorded during the operation, define the registration procedure, create a working group, acquire the needed equipment for measuring and control, and eliminate obvious (visible) leakages.

The following sequence of work has been developed for the design of zones and their implementation (construction).

1. The existing water supply distribution network is divided into separate zones through valves on the plan. During this demarcation, it is necessary to consider the possibility of creating optimal pressure regimes in the zones and excluding the dead sections in pipelines.

   Limiting valves should be installed just away following the connections of relatively large volume of water users to prevent the creation of dead-end areas (no flow or small flows), as the valves turn the pressure zone into a dead-end network. Water quality degradation is possible in areas with a low water flow rate [1]. As mentioned above, to ensure the controllability in the pressure zone, it is necessary to create sectors with a smaller number of subscribers. According to the results of the studies, the zone should include 500–3000 subscribers, depending on the level of leakage, the development characteristics of the district,

the applied methods of leakage control, and hydraulic conditions. The water supply zone may serve 3000 customers in densely populated places, as it is in the settlement's city center. However, in these cases, it is challenging to distinguish minor breaks separated from flow data recorded at night, making it more difficult to pinpoint their place. However, by temporarily closing valves, large water supply zones can be divided into sub-sectors of two or smaller sizes. In this situation, extra valves might need to be placed during the water supply zones' design phase.

2. The power source is determined based on the case of providing an uninterrupted water supply to the facility in the most dangerous (critical) conditions of the specified area. In design practice, these zone feeding options are possible:
   1) the zone may have one or two power sources: an aquifer or a reservoir,
   2) zoning work can be carried out sequentially: here, the second zone receives water from the first zone in a transit way (Fig.).

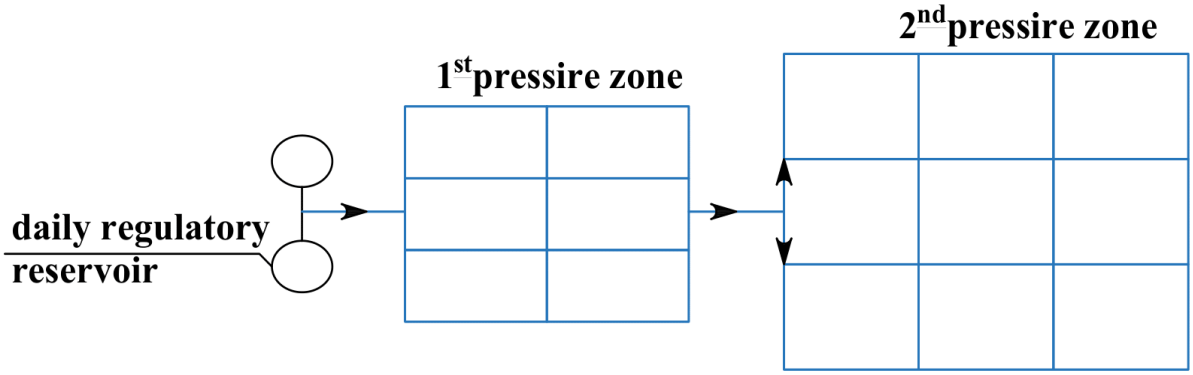

Fig. *Sequential zoning scheme*

3. It is planned to close off the valves on all border feeding lines during the hydraulic isolation of the divided zones, leaving only the targeted feeding line. To guarantee total isolation, sometimes required to install new valves. Small-scale maps of the distribution of water lines, information from operating staff, and existing hydraulic data are employed at this stage of contour limitation of the water supply zone design. In establishing the boundaries of the water supply zones, besides the general design criteria, the following conditions should be considered:
   - make the most of the feed source's power or pressure (day regulating reservoir, aqueduct) position. In this case, area and topography may dictate sequential zoning using existing pipelines.
   - any transit aqueducts or water lines feeding other zones are avoided as much as possible while drawing the boundaries of a zone,
   - if possible, the diameter of the water line supplying the zone should not exceed 300 mm to avoid high financial costs and technical complications associated with the flow measurement unit installation,
   - to ensure that research can take place, the area should have a constant supply of water.
4. "Zero tests" is used to verify the compliance of the design works with the completed reconstruction works. It provides the implementation of the following conditions:
   - inspecting the installed flow meter for accuracy,
   - checking the functioning (hermetic) of the boundary valves,
   - detection of hydraulic connections between neighbouring zones,
   - inspection and assessment of changes in the quality of water supplied to customers in the reconstructed zone and neighboring zones,
   - check for excess pressures.

Zero pressure test procedure

Zero pressure testing is carried out at night, between 1^{00} and 5^{00}. In order to detect hidden connections between zones, data recording devices (loggers) are connected to the cost meters of the lines feeding the tested and neighboring zones.

The tightness of the boundary valves and the existence of any hidden connections are then assessed by closing the boundary valves. For the situation assessment, it is also necessary to temporarily install the automatic pressure recording devices at defined points in the network during testing. After that, the valve supplying the zone is closed, and if there is no significant pressure drop within 5 minutes, any hydrant in the lower part of the network is opened, reducing the pressure to zero. The pressure in the water supply zone must be zero when the hydrant is closed; otherwise, another power source that wasn't considered during the design may exist, or the tightness of any boundary valve that is audibly checked may not be maintained.

The zero pressure tests are a crucial procedure for determining whether the water supply zone is hermetically sealed, so the aforementioned investigations must be continued until the experiment's successful completion is guaranteed. It may take up to a year to get positive results from the zero pressure test, depending on network characteristics (zone size, number of subscribers, population density, and the ratio of private and multi-residential buildings).

The described measures are necessary because proper zoning was not carried out during the design and construction of existing water supply networks. Besides, the circumstance that the drawings created during the construction of the water supply system do not match the actual situation made the design and implementation of the zone more challenging.

Failure detection and elimination are carried out to reduce power losses. For this phase, we determined that the night-time costs of the zone should not exceed 50% of the daytime cost. Finding and eliminating hidden leaks can also take several months.

Day and night flow is recorded after these functions' completion and is necessary for benchmark indicators to evaluate the effectiveness of zoning (redevelopment), which must be monitored and maintained during operation.

The precise estimation of the zone's night flow and its ongoing regulation, as well as data updates, are of particular importance required for the following functions:

- continuous maintenance of the water supply zone's hydraulic isolation. There is often a conflict of interests between the operating units and the zoning group: opening of boundary valves, disturbance of zone boundaries, etc. Such cases must be monitored and prevented until their elimination,
- regularly updating the number of subscribers,
- modernization and improvement of data acquisition methods and technologies,
- leak detection and elimination in a planned manner,
- regular analysis of received data.

Conditions for creating a sector (dead - end network) during the design

Because of the formation of sectors within the borders of a separate zone, the existing ring network turns into a dead-end having a one-way supply. Hydraulic calculations are required to verify the transmittivity and pressure losses of the sections to maintain the water supply of the dead-end network.

For this purpose, a calculation scheme for the dead-end network has been created. It is divided into calculation sections, where the directions of water flow are noted, and the actual outputs in the sections are measured.

In contrast to the well-known method for calculating the dead-end network, during the conducted studies, the outputs obtained through experimental measurements are taken as the calculation output for each section

based on the maximum actual water demand. When choosing the endpoint for constructing pressure lines based on the measured outputs, not only the distance and relief but also the required pressure at that point, considering the height and location of the buildings, are considered.

After measuring the outputs of the designed dead-end network segments, the network transmittivity condition is checked. For this purpose, the pressure losses occurring in the sections are determined by the formula $h_l = SQ^2$, using F.A. from Shevelyov's tables [3], based on which the free pressure lines of the network are built to have the pressure magnitude at all points of the selected calculation direction. Free pressure lines are installed in every direction possible to assess the pressure at the examined network's sites. In the event of a problem providing pressure in the subzone of the designed dead-end network, based on specific conditions, it can be solved by the following options:

- by over-correcting the pressure regulators or opening the compressed valves on the supplying water pipe (if available),
- the excess pressure regulation increased the pressure in the initial part of the considered sub-zone in the neighboring sub-sector,
- to change the power source of the zone that will provide the required pressure or apply another zone scheme,
- pressure losses in the specified sections reveal the significant leaks by finding and fixing leaks in any section or sections. Therefore, it may be found that the cause of the pressure loss is a hidden local resistance (unknown compressed valve, presence of a gasket, or blockage),
- by increasing the diameter of a specific network section if the pressure line in that section has a steep slope,
- by installing local pumps if the pressure is insufficient for a few high-rise buildings.

The last two options are advisable to use in case of economic feasibility. It should be added that when performing zoning, the need to increase the diameter or install a pump arises in rare cases because the diameters of pipelines built in the Soviet era are chosen with a high stockage.

The priority of the implementation of distribution network zoning

Because of the zoning processes' financial and technical requirements, it is impossible to carry out operations simultaneously in all planned zones. Instead, priority is given to the zones with the highest leakage levels. Based on the technical condition of the distribution network of the settlement, it is recommended to use the following expression of specific losses of flow:

$$q_{leak} = \left(Q_{night} - Q_{cons.}\right) / L_w \ (1/\text{hour m}), \quad (1)$$

where

q_{leak} - specific loss of flow, l/s m,

Q_{night} - average night flow recorded by the zone flowmeter, l/h

$Q_{cons.}$ - the average consumption of subscribers during the night l/h,

L_w - length of pipelines of the zone, m.

In the sector of own residences, the accepted average consumption per subscriber during the night was 1.7 l/h, while in multi-apartment buildings, it was 0.6 l/h. These numbers are used to calculate the amount of leakage in the systems of European cities where operational circumstances match up with regional water supply systems.

Because customer overnight costs can significantly affect the zone's estimated night loss, they are calculated independently using actual data.

Results and Discussion

Analyzing the results of multi-year studies and considering the current technical situation of the distribution network, it is recommended to continue the accident detection and elimination work for the current phase until the night-time consumption of the zone is less than half of the daytime consumption:

$$Q_{night} \leq Q_{day}/2(l/s), \quad (2)$$

where Q_{night} and Q_{day} are the average water volumes given to the zone during the night (1^{00}-5^{00} period) and daytime.

The mentioned expression was defined after studying the zones with the lowest water losses in RA settlements (Davtashen, South West, and other districts). Thus, let's discuss the study results on the "Arabkir 1" zone, where the average amount of water supplied at night is 102 l/s, and during the day is 133 l/s. Applying the expression (2), we can determine the amount of leakage reduction in the "Arabkir 1" zone to meet the current stage requirements, which should not be greater than 133/2=66.5 l/s. From the data obtained, we can conclude that in the mentioned zone, there is still leakage of 102-66.5=35.5l/s more than the permissible one, which needs to be detected and eliminated.

Conclusion

To increase the efficiency of the aqueduct network, zoning problems were studied, taking into account the technical condition of the system. Scientific calculations were carried out, and a methodology for zoning was developed:

- The analyses showed that the water pipe network should be transformed into hydraulically separated zones while using the current distribution system, taking into consideration the position, placement, and dependence of the site's relief features. It was necessary to create a zone design and implementation that considers the principles of system management, the formation of sub-zones (dead-end networks), the calculation of optimal pressures, the detection and elimination of current losses, etc.
- To increase the level of management of zone distribution networks, the means of automatically transferring the fundamental characteristics of operation: pressure, output, and electricity consumption values are applied, the investment of which in water supply systems will give the desired results.

References

[1]. A.A. Sahakyan, Sectorization and Reconstruction Problems of Yerevan City's Water Supply Network. Bulletin of National University of Architecture and Construction of Armenia, 4 (48), 2015, 3-9 (in Armenian).

[2]. A.A. Sahakyan, Hydraulic Pressure Management of Yerevan City's Water Supply Systems. Journal of Architectural and Engineering Research, 3, 2022, 78-84. Doi: https://doi.org/10.54338/27382656-2022.3-009

[3]. K. Vairavamoorthy, J. Lumbers, Leakage Reduction in Water Distribution Systems: Optimal Valve Control. Journal of Hydraulic Engineering, 124(11), 1998, 1146-1154. Doi: https://doi.org/10.1061/(ASCE)0733-9429(1998)124:11(1146)

[4]. L.S. Araujo, H. Ramos, S.T. Coelho, Pressure Control for Leakage Minimization in Water Distribution systems Management. Water Resources Management, 20, 2006, 133-149. Doi: https://doi.org/10.1007/s11269-006-4635-3

[5]. M.Giugni, N.Fontana, D.Portolano, Energy Saving Policy In Water Distribution Networks. International Conference on Renewable Energies and Power Quality, Valencia, Spain, April 15-17, 2009.

[6]. S.Liberatore, G.M. Sechi, Location and Calibration of Valves in Water Distribution Networks Using a Scatter-Search Meta-heuristic Approach. Water Resources Management, 23, 2009, 1479–1495. Doi: https://doi.org/10.1007/s11269-008-9337-6

[7]. N.Fontana, M.Giugni, D.Portolano, Losses Reduction and Energy Production in Water Distribution Networks. Journal of Water Resources Planning and Management, 138 (3), 2012, 237-244.
[8]. A.Di Nardo, M.Di Natale, A Heuristic Design Support Methodology Based on Graph Theory for District Metering of Water Supply Networks. Engineering Optimization, 43(2), 2011, 193-211.
[9]. S. Alvisi, M. Franchini, Una procedura per la distrettualizzazione delle reti di distribuzione idriche. In Proc. XXXIII Convegno Nazionale di Idraulica e Costruzioni Idrauliche, Brescia, Italy, 2012.
[10]. Francesco De Paola, Nicola Fontana, Enzo Galdiero, Maurizio Giugni, Gianluca Sorgenti degli Uberti, Marcello Vitaletti, Optimal Design of District Metered Areas in Water Distribution Networks. Procedia Engineering, 70, 2014, 449 - 457.
[11]. J. Sempewo, A. Pathirana, K.Vairavamoorthy, Spatial Analysis Tool for Development of Leakage Control Zones from the Analogy of Distributed Computing. Proceedings of the 10th Annual Water Distribution Systems Analysis Conference, Kruger National Park, South Africa, Aug. 17-20, 2008. Doi: https://doi.org/10.1061/41024(340)57
[12]. G.Karypis, V.Kumar, METIS: Unstructured graph partitioning and sparse matrix ordering system. Technical report, University of Minnesota, Department of Computer Science, 1995.
[13]. M. Herrera, J. Izquierdo, R. Pérez-García, I. Montalvo, Multi-Agent Adaptive Boosting on Semi-Supervised Water Supply Clusters. Advances in Engineering Software, 50, 2012, 131-136. Doi: https://doi.org/10.1016/j.advengsoft.2012.02.005
[14]. K. Diao, Y. Zhou, W. Rauch, Automated Creation of District Metered Area Boundaries in Water Distribution Systems. Journal of Water Resources Planning and Management, 139 (2), 2013, 184-190. Doi: https://doi.org/10.1061/(ASCE)WR.1943-5452.0000247
[15]. R.Gomes, A.Sa Marques, J. Sousa, Decision Support System to Divide a Large Network into Suitabledistrict Metered Areas. Water Science & Technology, 65(9), 2012, 1667-1675. Doi: https://doi.org/10.2166/wst.2012.061
[16]. F.A. Shevelev, A.F.Shevelev, Tablitsy dlya gidravlicheskogo raschota vodoprovodnykh trub. Stroyizdat, Moscow, 1984 (in Russian).
[17]. A. Sahakyan, Water Loss Assessment in the Internal Water Supply Networks of Yerevan City Apartment Buildings and Private Houses. Scientific Papers of National University of Architecture and Construction of Armenia, 85 (1), 2023, 132-143. Doi: https://doi.org/10.54338/18294200-2023.1-14

Aram Sahakyan, Doctor of Philosoph (Ph.D) in Engineering *(RA, Yerevan) - National University of Architecture and Construction of Armenia, Dean of the Construction Faculty, sahakyan.aram@nuaca.am*

DETERMINATION OF DEPRECIATION PERIOD OF AUTOMOBILE OPERATION THROUGH PHYSICAL WEAR COEFFICIENT

Yeghiazar Vardanyan [1], ***Valerik Harutyunyan*** [1], ***Vladimir Koichev*** [2], ***Karapet Mosikyan*** [1]*

[1] *National University of Architecture and Construction of Armenia, Yerevan, RA*

[2] *Baltic Fishing Fleet State Academy, Kaliningrad, RA*

Abstract: *The paper touches upon a newly developed methodology for determining the automobile physical wear coefficient, taking into account some technological factors during operation that compose the rolling stock life cycle in the given operating conditions. A concept for determining the operation period of an automobile has been proposed based on maintaining the smooth operation of the rolling stock throughout the life cycle. The quantitative and qualitative indicators of automobile physical wear are determined aimed at solving the problem. The theoretical and scientific experimental research has identified the analytical connections of their interactions and relations. Given the stochastic nature of physical wear coefficient variations, it has been considered as a random value, and the characteristics of its variations pattern have been determined.*

Keywords: physical wear; coefficient; function; linear; automobile; depreciation; operation; rolling stock.

Karapet Mosikyan*

E-mail: karomosikyan@mail.ru

Received: 29.01.2023
Revised: 19.02.2023
Accepted: 07.03.2023

Introduction

Operation practice has shown [1,2] that two automobiles of the same brand have different levels of a residual resource after a particular mileage[1], both in terms of constituent units and the whole automobile [2].

It means that the automobile physical wear coefficient [3] needs to be considered more deeply by analyzing and taking into account some technical and technological factors during the operation, which forms the rolling stock life cycle in the given operating conditions [4]. The proposed concept for determining the automobile depreciation period is based on maintaining the smooth operation of the rolling stock throughout its entire life cycle. Technical disruptions that cause the transport process to stop, result in inefficient downtime as well as material and labour expenses [1]. To avoid accidental and sudden disruptions, the actual coefficient of the automobile's physical wear[2] should characterize the current technical condition of the rolling stock and engine constituents, ensuring the need for repair and maintenance within a given period of millage and time [5,6]. Up to date, the current methods for determining the operating life have been of analytical nature. They do not reveal how the physical wear coefficient of the automobile varies due to the increase in overall mileage, exact operating conditions, and other factors [4,10].

The paper proves the stochastic nature of variations in the automobile's physical wear coefficient, it is considered as a random value. The characteristics of its variations pattern have been determined, allowing the automobile depreciation period to be calculated based on the economic indicator value preferred by the given economic entity.

Materials and Methods

It is necessary to develop qualitative and quantitative indicators for assessing the automobile's physical wear aimed at solving the proposed problem and then discovering the analytical connections of their

[1] GOST R 50779.10-2000

[2] R 03112194-0376-98. Metodika otsenki ostatochnoy stoimosti transportnykh sredstv s uchetom tekhnicheskogo sostoyaniya, 1998 (in Russian).

interactions and relations through theoretical and scientific-experimental research [6]. It is well-known that the resource indicators of automobile units, auto parts, and interchanges have quite different values and are of stochastic nature [7]. A scientific-experimental research has been conducted for a group of minibuses (30 units) performing intra-city passenger transportation to study the variation in the automobile physical wear coefficient and identify the distribution patterns as a random value[3].

The following indicators have been studied during the scientific-experimental research:

The number of automobile disruptions (nd) by years and hence the number of downtime (ndtp) days caused by them,

The average daily mileage of one automobile (ℓd) –per km,

The average annual mileage of one automobile (ℓa), per thousand km,

The total mileage of the automobile group ($\sum \ell$) per thousand km,

The number of annual operation days of one automobile (nw) per day,

The coefficient (α) of technical readiness of the automobile group,

The disruption flow parameter (ω) of the automobile group per-thousand km,

The average mileage of automobile smooth operation (ℓ) per thousand km ℓs,

The physical wear coefficient (K) of the automobile group.

The graphs (Figs. 1, 2) based on the data presented in the Table indicate the variations in the coefficient of the automobile technical readiness, average mileage of smooth operation, number of maintenance downtimes, and physical wear coefficient. According to the presented data, the coefficient of the automobile's technical readiness during the fifth year of operation was 0.73, which is less than the average value of this coefficient (0.8). A similar solution is observed in terms of the average mileage of the smooth operation of automobiles. In case of an average value of 12.8 thousand km, the indicator for the fifth year of operation was 8.87 thousand km or decreased by 3.93 thousand km (30.9%).

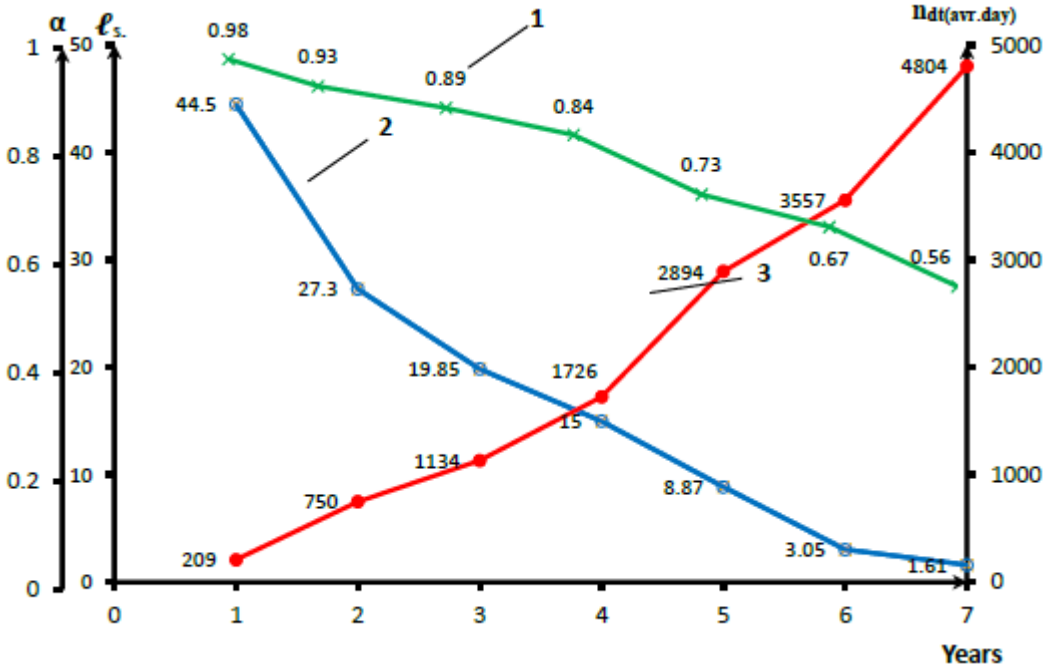

Fig. 1. *Dynamics of quantitative and qualitative variation of automobile operating indicators (α (1), ℓs. (2), ndt. (3)) by years*

[3] GOST R 50779.10-2000

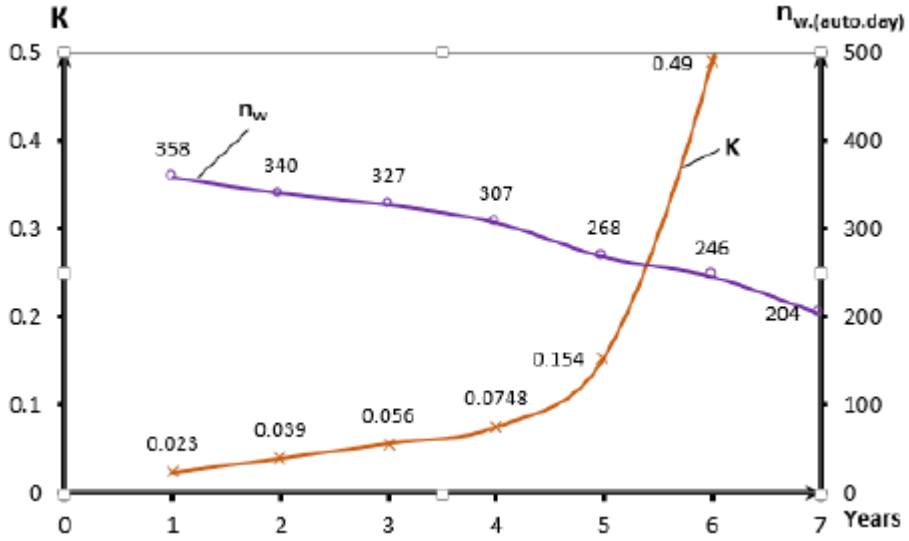

Fig. 2. *Change in the automobile physical wear coefficient (K) and the average number of working days per automobile (nw) according to the years of operation*

Further analysis of the automobile's smooth operation shows that, according to the operation results of the sixth-year, the indicator was 3.03 thousand km. The same dynamics is observed in the operation results seven year. According to the data, the automobile's technical readiness coefficient during the fifth year of operation was 0.73, which is less than the average value of this coefficient (0.8). A similar situation is with the smooth operation of automobiles. In the case of an average value of 12.8 thousand km, the index for the fifth year of operation was 8.87 thousand km or decreased by 3.93 thousand km (30.9%). It indicates the following: if we are to be directed by the dynamics of the change in the average mileage of automobiles, we must decomission the rolling stock at the end of the fifth year of operation or the beginning of the sixth year due to low technical and economic indicators.

Table. Operational indicators of the Automobile group

N	Year of operation / Indicator	1	2	3	4	5	6	7
1.	Number of disruptions n_d	60	78	92	110	148	388	516
2.	Downtime n_{dt} (automobile-per day)	209	750	1134	1726	2894	3557	4804
	TS – 2 (number)	203	164	140	127	101	91	64
	Current repair (number)	6	586	998	1599	2793	3466	4740
3.	Working days, annual average(n_w)	358	340	327	307	268	246	204
	Total	10741	10200	9816	9224	8056	7399	6146
4.	Coefficient of technical readiness, α	0.98	0.93	0.89	0.84	0.73	0.67	0.56
5.	Average daily mileage, ℓ_d (km)	218	210	186	179	163	160	135
6.	Total mileage, $\sum \ell$ (thousand km)	2341.5	2142.0	1825.8	1641.1	1313	1182.9	829.7
7.	Average mileage of smooth operation, ℓ, (thousand km)	44.5	27.3	19.85	15.0	8.87	3.05	1.61
8.	Disruption flow parameter ω(disruption per thousand km)	0.0225	0.036	0.050	0.0666	0.113	0.328	0.578
9.	Physical wear coefficient, K	0.023	0.039	0.056	0.0748	0.154	0.490	1.032

Now the problem should be considered in light of the dynamics of changing the indicator of inefficient downtime of the automobile.

The average indicator of inefficient downtime for a group of automobiles' downtime was 2150 automobiles per day, or 71.67 automobiles per day for one automobile. Moreover, during the fifth year of operation (Table, Fig. 1), the average downtime was 96.5 automobiles per day, which is about 25 automobile per day more than the average value. If we observe the variations in the number of automobiles' operation days over the years, it becomes evident that in the fifth year, there are already 8056 automobiles per day, with an average value of 8799 automobile per day. It equates to 35.9% inefficient automotive downtime in regard to the number of operation days. Naturally, the monthly number of automobiles operating by the order was 74.1%, which is inefficient from an operational standpoint (the accepted efficiency amounts to no less than 80% from a financial and economic standpoint).

Discussion of Results

To assess the efficiency of automobile operation, the physical wear coefficient should be observed on terms of quantitative and qualitative standards, as it is defined by inefficient dowtime spent on recovery and an indicator of recovery duration [3]. This is evidenced by the fact that the calculated physical wear coefficient according to the value of the automobile coefficient of technical readiness amounted to 0.154 in the fifth year, while in the sixth year it grew rapidly, amounting to 0.490. It means (Fig. 2) that the amount of inefficient downtime hasn't increased sharply, but the disruption flow parameter has increased, which has led to a sharp increase in the physical wear coefficient. If we consider the physical wear coefficient with the average millage of inefficient downtime and smooth operation, it turns out that this indicator has not undergone drastic changes.

Based on the above-mentioned analysis results, it can be firmly insisted that the automobile's physical wear coefficient should be assessed from quantitative and qualitative perspectives, firstly - taking into account the quantitative value of the disruption flow parameter[4] and seondly - the amount of ineffective downtime days spent on the recovery from disruptions.

To this end, the automobile physical wear coefficient should be considered as a random function, i.e. according to the millage or years of operation of the rolling stock [6,11].

The automobile physical wear coefficient can be represented as a function of the rolling stock mileage $\boldsymbol{\ell}$, in that case [6]:

$$K = \eta(\ell). \tag{1}$$

At the same time, the automobile mileage is a variable with a probability density function of $\mathbf{f(\ell)}$, which causes variation of **K** parameters. Let use the Laplace transformation (1), which for the normal probability distribution law of random variables is [2]:

$$f(\ell) = \frac{1}{\sigma\sqrt{2\pi}} exp\left[-\frac{(\ell-\overline{\ell})^2}{2\sigma^2}\right], \tag{2}$$

where $\boldsymbol{\sigma}$ is the root-mean-square deviation, km (dispersion), $\boldsymbol{\pi}$ - constant (3,14), $\boldsymbol{\ell}$ - milage, km, $\overline{\boldsymbol{\ell}}$ - milage mean path, km, and has the following form:

$$\varphi(\mathrm{z}) = exp\left[-\ell \cdot \mathrm{Z} + \frac{\sigma^2 Z^2}{2}\right], \tag{3}$$

where $\mathbf{Z}$ is the constant function for normal distribution, $\boldsymbol{\varphi}(\mathbf{z})$ is the function of $\boldsymbol{K}$ value.

It can be assumed that the first two members of the function are the automobile physical wear coefficient **K**, and it is a linear function:

$$K = a_0 + a_1 \cdot \ell\,, \tag{4}$$

[4] GOST R 50779.10-2000

where a_0 is the resource of the new automobile, a_1- is the specific value of automobile resource change per mileage (1000 km).

In this case, the function Laplace transformation (4) for the linear function is as follows:

$$\varphi_{\mathrm{K}}(\mathrm{z}) = \varphi_{\ell}(a_1 \cdot \mathrm{z}) \exp(-a_0 \cdot z)\,, \tag{5}$$

or

$$\varphi_{\mathrm{K}}(\mathrm{z}) = \left\{exp\left[-\overline{\ell} \cdot \mathrm{a}_1 \cdot \mathrm{z} + \frac{\sigma^2 \cdot Z^2 \cdot a_1^2}{2}\right]\right\} \exp[-a \cdot z]\,, \tag{6}$$

Thus:

$$\varphi_{\mathrm{K}} \cdot Z = exp\left\{\left[1 - \left(\overline{\ell} \cdot \mathrm{a}_1 + \mathrm{a}_0\right)z\right] + \frac{(\sigma \cdot \mathrm{a}_1)^2 \cdot Z^2}{2}\right\}. \tag{7}$$

Comparing the expressions (7) and (3), it follows that the expression (7) is also considered a Laplace transformation for a new normal distribution value K, the average value of which is:

$$\overline{K} = a_0 + a_1 \cdot \ell\,, \tag{8}$$

where $\overline{K}$ is the mean physical wear coefficient.

Root-mean square deviation is:

$$\sigma_K = a_1\sigma\,, \tag{9}$$

and the coefficient of variation is

$$V_K = \frac{1}{\frac{a_0}{a_1\sigma} + \frac{1}{V_1}}\,. \tag{10}$$

The coefficient variation for the new random variable is dependent on the coefficient of variation of argument and the intensity of the parameter change, particularly on its increase.

Considering the change in the automobile's physical wear coefficient along with the increase in the total mileage (1), it becomes evident that the dynamics of the change in the physical wear coefficient has increasing nature. It means the probability density function of the automobile physical wear coefficient f (K), taking into account the expression (6) will have the following form:

$$f(K) = \frac{1}{a_1 \cdot \sigma\sqrt{2\pi}} exp\left[1 - \frac{(K - a_0 - a_1 \cdot \ell)^2}{2\sigma^2 \cdot a_1^2}\right]. \tag{11}$$

It is also evident from the graph presented in Fig. 2, which comes to prove along with the automobile's physical wear coefficient (**K**), the number of operation days decreases as the maintenance downtime for the rolling stock repair increases. While solving the practical problems, if the function $\boldsymbol{\eta(\ell)}$ is not linear, but is continuous in the range of $\boldsymbol{\ell_1 - \ell_2}$ millage and is close to being linear, it can be replaced by a linear function [6].

Summarizing the results of the theoretical and experimental research, it becomes evident that the change in the physical wear coefficient under the specific conditions of an automobile operation has a stochastic nature with a normal distribution pattern. Considering the change in physical wear coefficient as a random value and determining the characteristics of its change pattern - mathematical expectation, dispersion, and variation coefficient, allow to determine the depreciation period of the automobile according to the value of the technical and economic indicator preferred by the economic entity.

Conclusion

The research on the changes in the automobile's physical wear coefficient in the actual operating condition allows to identify the pattern of actual change of the coefficient, its mathematical expectation, root-mean-square deviation, and variation coefficient, as well as allows to assess the current value of the indicator in a definitive range. It will be possible if the density of the function f (K) is calculated, which in fact is related to intensity of operation (a_0 *and* a_1), and it is the main and dominant factor in the change of the automobile's physical wear coefficient, and the milestone of the developed methodology.

References

[1]. Ye.S. Kuznetsov, Tekhnicheskaya ekspluatatsiya avtomobiley. Nauka, Moscow, 2001 (in Russian).
[2]. K.H. Mosikyan, V.S. Kochiev, A.M. Jinyan, Operating Experience and Reliability Performance of Internal Combustion Engine when Operating on Compressed Natural Gas. Stavropol State Agrarian University, 2 (14), 2014, 75-78.
[3]. A.V. Yudin, Otsenka stoimasti transportnykh sredstv. Moskovskaya finansovo-promyshlennaya akademiya, Moscow, 2005 (in Russian).
[4]. Y.V. Vardanyan, V.M. Harutyunyan, K.H. Mosikyan, V.S. Kochiev, The Basics of Developing an Alternative Concept for Commercial and Military Vehicle Operation (Random Strategy). Journal of Architectural and Engineering Research, 1 (2), 62-69, 2021.
Doi: https://doi.org/10.54338/27382656-2021.2-4
[5]. I. Bazovsky, Nadezhnost'. Teoriya i praktika. Mir, Moscow, 1965 (in Russian).
[6]. E.S. Wentzel, Teoriya veroyatnostey. Vysshaya shkola, Moscow, 1999 (in Russian).
[7]. B.L.Van der Waerden, Mathematical Statistics. Publishing House of Foreign Literature, Moscow, 1960 (in Russian).
[8]. C. Rohlfs, R. Sullivan, The Cost-Effectiveness of Armored Tactical Wheeled Vehicles for Overseas US Army Operations. Defence and Peace Economics, 24 (4), 2013, 293-316.
Doi: https://dx.doi.org/10.2139/ssrn.1916818
[9]. C.R. Harz, Problems in Army Vehicle Maintenance: Results of a Questionnaire Survey, Rand Corporation, 1981.
[10]. V. Loan, D. Viorel, G. Constantin, Research on Improving the Maintenance Activities for Military Vehicles. International Conference Knowledge - Based Organization, 21 (3), 2015, 896-903.
Doi: https://doi.org/10.1515/kbo-2015-0152
[11]. R. Haider, Al. M. Kakar, S. B. Khattak, S. Rehman, S. Maqsood, M. Ullah, R. Akhtar, A. Sikandar, Development of Optimized Maintenance System for Vehicle Fleet. Journal of Engineering and Applied Sciences, 34 (2), 2015, 21-27.
[12]. V. Mickunaitis, S. Nagurnas, The Improvement of the Technical Exploitation of Automobiles. Transport, 17 (4), 2002, 143-146.
Doi: https://doi.org/10.3846/16483840.2002.10414031

Yeghiazar Vardanyan, Doctor of Science (Engineering) *(RA, Yerevan) - National University of Architecture and Construction of Armenia, Professor at the Chair of Construction Machinery and Organization of Traffic, yeghiazar.vardanyan@gmail.com*

Valerik Harutyunyan, Doctor of Philosophy (PhD) in Engineering *(RA, Yerevan) - National University of Architecture and Construction of Armenia, Associate Professor at the Chair of Construction Machinery and Organization of Traffic, vmh-1961@mail.ru*

Vladimir Sahidovich Koichev, Doctor of Philosophy (PhD) in Engineering *(RF, Kaliningrad) - Baltic Fishing Fleet State Academy, Associate Professor at the Chair of Motor Transport and Car Service, bugakova@bga.gazinter.net*

Karapet Mosikyan, Doctor of Philosophy (PhD) in Engineering *(RA, Yerevan) - National University of Architecture and Construction of Armenia, Associate Professor at the Chair of Construction Machinery and Organization of Traffic, karomosikyan@mail.ru*

EXPLORING THE CAVES OF ARMENIA BY THE FIRST OFFICIAL U.S. CAVING EXPEDITION (2007-2013)[1]

Charles Chavdarian[1], Smbat Davtyan [2], Samvel Shahinyan[3]*

[1]*AstraZeneca, Cambridge, United Kingdom*

[2]*Brusov State University, Yerevan, RA*

[3]*National University of Architecture and Construction of Armenia, Yerevan, RA*

Abstract: *The first U.S. caving expedition to Armenia, the South Caucasus, by NSS cavers took place in August 2007. Subsequent expeditions took place in 2010, 2011, and 2013, with additional trips planned for the future. The goal is the exploration and photo-documentation of the caves of Armenia, and to increase awareness of its underground realms. Although, in the past, there had been a few known caving expeditions to Armenia, overall little information existed. In addition, Armenia's local caving community is small in number. As a result, this topic was studied and the first official US caving expedition to Armenia was organized in 2007. During the first expedition, four of Armenia's significant natural caves were explored in the province of Vayots Dzor: Mozrov Cave, Arjeri Cave (Cave of the Bears), Mageli Cave, and Karmir Cave (Red Cave). Man-made caves were also visited. Subsequent trips to Armenia in 2010, 2011, and 2013 included (1) further exploration of Mozrov, Arjeri, and Mageli caves, (2) a cave trip to the neighboring independent Armenian Republic of Nagorno-Karabagh to explore Azokh Cave, and (3) the exploration of several caves in the northeast Armenian provinces of Tavush and Lori. Natural caves consisting of limestone, conglomerate, and lava were explored during these expeditions. Also, a number of man-made caves were visited, some of which were used as churches in centuries past. This article summarizes the four expeditions and discusses both the natural and man-made caves of Armenia. I beleive the article will be interesting to builders, gas pipelines and road engineers. In practice, it can be used by travel agencies and individual tourists, as well as by all lovers of underground monuments of nature and culture.*

Keywords: *expedition, survey, caves, cave plan, church, tourism, photo-documentation, cave map.*

Samvel Shahinyan*

E-mail: sshahinyan@nuaca.am

Received: 14.02.2023

Revised: 03.03.2023

Accepted: 18.03.2023

Introduction

The present-day Republic of Armenia lies geographically in the South Caucasus, between the Black Sea and the Caspian Sea. The most ancient of the countries and nationalities of the Caucasus, the indigenous Armenian people have a legacy stretching back 3.000 years. Eastern Turkey, southern Georgia, western Azerbaijan, and a northern portion of Iran are all part of historical Armenia. The Republic of Armenia is a rugged, mountainous land, with an average elevation of approximately 1.500 meters, and a population of just over three million (due to Armenia's tumultuous and tragic history, there are presently more Armenians residing outside Armenia – the Diaspora). Armenia holds the distinction of being the first nation to declare Christianity as its state religion in 301 A.D. Ancient churches in Armenia (among the oldest in the world), many still standing and in use, pre-date those of Europe by centuries. Some of these churches were hewn out of rock, thus cave churches.

Prior to 2007, available information and literature on natural and man-made caves in Armenia was sparse. After researching this topic and contacting local Armenians in Armenia, first United States (NSS) caving

[1] A previous version of this paper was presented at the 17th International Congress of Speleology (Speleo 2017) in Sydney, Australia, on July 23 – 29, 2017.

expedition to Armenia was organized. The expedition was a success, as we explored and photo-documented four of Armenia's significant caves in the province of Vayots Dzor in south central Armenia. Participating in this first expedition were Steven Johnson, James Wilson, Greg Chavdarian, Seda Chavdarian, and Charles Chavdarian of the United States, and Vrezh Nazarian and Samvel Shahinyan of Armenia, who also acted as our guides (Fig.1).

Fig. 1. *Members of the first U.S. caving expedition in 2007. James Wilson, Greg Chavdarian, Charles Chavdarian, Seda Chavdarian, and Steven Johnson (Left to Right) – Republic of Armenia. Photo by V. Nazaryan*

This was followed by expeditions in 2010, 2011, and 2013. As a result, further exploration occurred not only in Vayots Dzor province, but also in the northern provinces of Tavush and Lori, and the eastern province of Syunik. In addition, we also traveled to the neighboring independent Armenian republic of Nagorno-Karabagh. Both natural and man-made caves have been explored and are discussed in this paper. The following cavers participated in some or all of these subsequent trips: Lara Chavdarian and Charles Chavdarian of the United States, and Vrezh Nazaryan, Smbat Davtyan, Pegor Papazian, and Nyree Abrahamian of Armenia.

Materials and Methods

Vayots Dzor Province, Republic of Armenia

For the 2007 expedition, we maintained a base camp near the village of Mozrov, at an elevation of about 1.700 meters. For subsequent expeditions in Vayots Dzor province in 2010 and 2011, we stayed in bed and breakfast homes in the town of Yeghegnadzor, the provincial capital. We explored and photo-documented several caves.

Mozrov Cave: Mozrov Cave, primarily a limestone cave, was first discovered about 40 years ago [1] during road construction, when a collapse occurred resulting in the creation of a large entrance to the cave (which is also the only known entrance to the cave). The cave sits at an elevation of approximately 1.550 meters adjacent to a mountain road. Due to its accessible location, the cave is vulnerable to visitation by non-cavers and tourists and has sustained some damage. Over the course of the four expeditions, we have explored the cave five times, and have taken a number of photographs. There is substantial decoration in this cave – stalactites, stalagmites, columns, moon milk, flowstone, coral, popcorn, crystalline spars, soda straws, helictites, etc. The cave decoration is also noteworthy for its myriad of colors – red, caramel, yellow, and white. We were to soon find that Mozrov Cave is not unique in this regard. The cave has over 300 meters of known passage. The cave consists primarily of an undulating large and long main chamber, with a separate large chamber that can be entered through a low and difficult to find passage at the back of the main chamber [2]. This second chamber is noteworthy for its extensive multi-colored decoration (and has been aptly named as "Decoration Hall").

Due to the ongoing damage that has been occurring within the cave, Mozrov Cave was recommended for tourism. As such, the cave would be gated and protected, and only controlled access would be allowed. Also, conservation of the cave would be instilled in the visitors. A management plan was created and provided to the foundation. To date, there has been no further action on this cave. It is our hope that Mozrov Cave will eventually be protected [3]. In 2010, at our request, our local Armenian caving colleagues, headed by Smbat Davtyan, returned and surveyed the cave and provided the first cave map of it (Figs. 2,3).

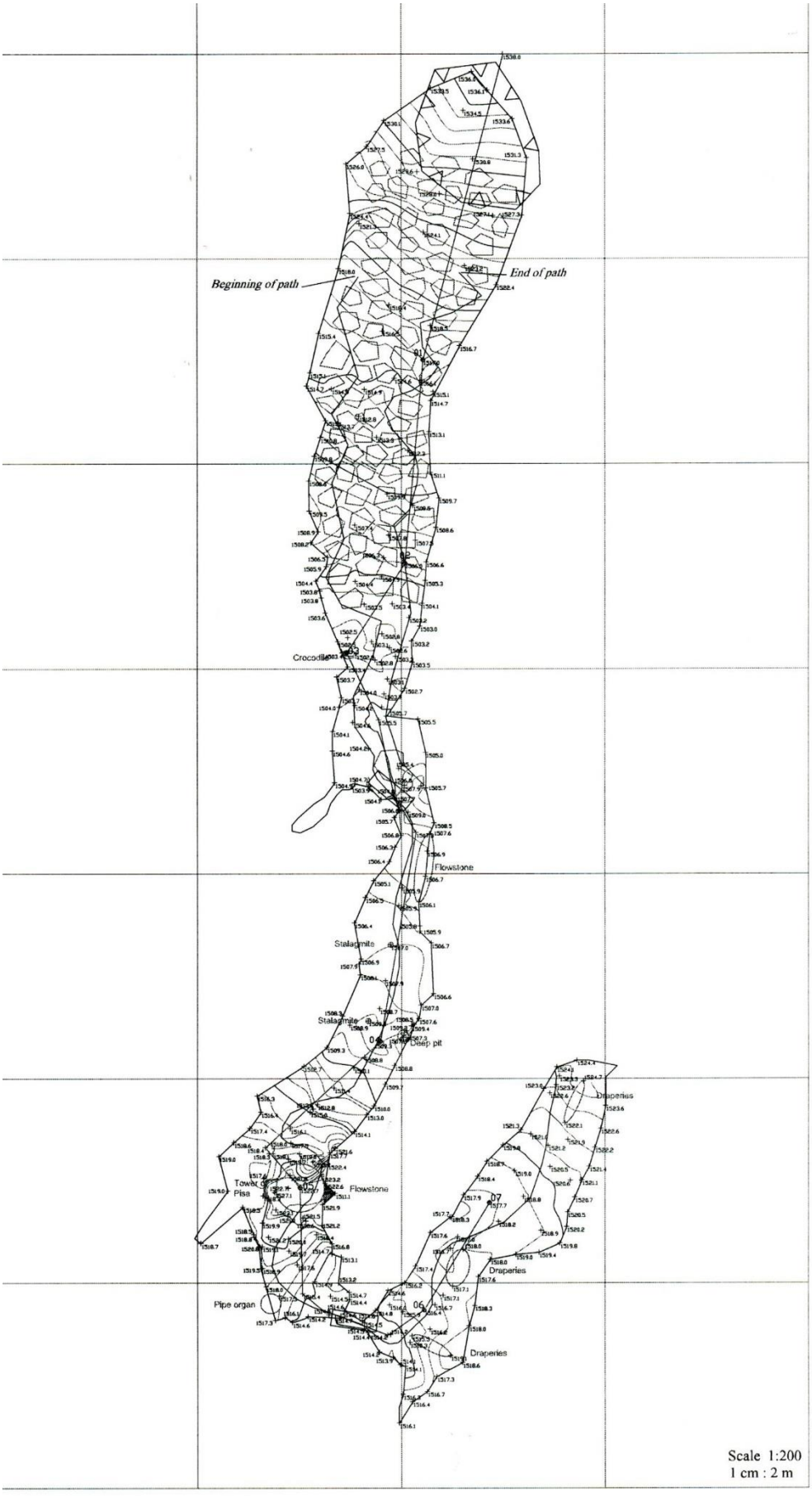

Fig. 2. *Mozrov Cave Map – Survey 2010 – Smbat Davtyan*

Arjeri Cave (Cave of the Bears): Arjeri Cave, at an elevation of nearly 1.700 meters, is Armenia's largest known cave, with currently about 4 kilometers (2.5 miles) of passage. Our only map was a rudimentary overview of the cave which was created by Russian cavers nearly 30 years ago [4]. The cave does require an updated and detailed cave survey and map. A total of four trips were made into this cave in 2007 and 2011. Arjeri Cave, a limestone cave, is the most highly decorated cave in Armenia, and one of the most highly decorated caves we have ever seen. To reach the only known cave entrance, one must leave their 4WD vehicle off-road, and at an elevation of 1.500 meters, and undertake the final steep hike to the cave. Just inside the Entrance Hall, explorers are immediately greeted with the sight of huge flowstone columns (Figs. 4,5,6).After passing through this first large chamber, one enters a slope requiring a steep belly crawl upward over slick flowstone. Along the way, this area is decorated with various formations. This leads into a large chamber known as Photographer's Hall, and the name is certainly appropriate as the room is rife with colorful formations – stalactites, stalagmites, columns, draperies, bacon, coral, and popcorn. The sheer quantity and density of the decoration in this large chamber is overwhelming. From here one continues on into Bear's Hall, which contains the bones of a bear [2]. This, in fact, is the reason for the name of the cave. On the way to Vayk Hall, there is a deep pit, which is estimated to be at least 18 meters deep. This pit has not been explored by us (and may possibly lead to more passage). On entering Vayk Hall, one is actually standing near the top of the hall. The hall descends about 10 meters, and contains large, colorful columns, massive flowstone, and a myriad of formations. Overhead is voluminous white calcite coral – almost cloud-like in appearance. Continuing beyond Vayk Hall, there is a nearly 10 meter climbdown that can be negotiated with a handline.

Fig. 3. *Mozrov Cave – Smbat Davtyan and Nyree Abrahamian in Decoration Hall - Republic of Armenia. Photo by C. Chavdarian*

Fig. 4. *Arjeri Cave Map – Russian Survey – app. 1985*

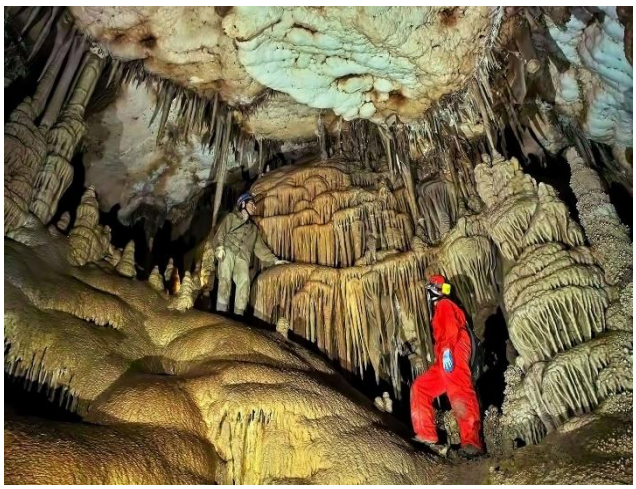

Fig. 5. *Arjeri Cave – Vrezh Nazaryan and Lara Chavdarian in Vayk Hall - Republic of Armenia. Photo by C. Chavdarian*

Fig. 6. *Arjeri Cave – Lara Chavdarian in the Hall of Giants - Republic of Armenia. Photo by C. Chavdarian*

This then leads into a broad swath of massive columns, which we have appropriately labeled as the Hall of Giants. Continuing from this point leads one through a variety of colorful formations along the way, including nearly blood-red speleothems. Continuing on, the passage gradually slopes downward, and eventually leads to the "Lake" near the end of the cave's known passage. On other trips into Arjeri Cave, we also explored some areas that were not present on the Russian map. There is much more exploration and detailed survey required of this cave, and it will surely extend the length of all known passages well beyond 4 kilometers.

Karmir (Red) Cave: In 2007, from our base camp, we did a very steep hike of over 400 meters up the mountainside to Karmir Cave, located at an elevation of over 2.100 meters (Fig.7). The hike took over two hours and required careful negotiating of brush, loose talus, and some exposure along the way. Reaching the entrance requires care due to the final short exposed climb. Nearby is another cave – called Kiklop Cave – but the final 30 meter climb to reach it has significant exposure and is also more challenging [4]. Time also prevented us from exploring this other cave. Karmir Cave has a large entrance chamber, allowing a group of cavers to congregate and also change in and out of caving attire. It is a conglomerate cave consisting of limestone and other mineralization, which provides the amazingly intense red color of much of the interior of the cave [5]. From the entrance chamber, there are several passages leading into the cave interior. The passages tend to intersect and loop back around. Well inside the cave we walked, crawled, climbed, and even traversed. The cave was wet and muddy, and permeated throughout with that remarkable red coloration. Although not highly decorated, there was some flowstone, stalactites, and red coralloids. We even observed some white (not red) moonmilk along the walls. There is also a 90 meter or so side passage in the cave, but neither our leader nor the rest of us could find it on this trip. The cave is well worth further exploration and is quite unique.

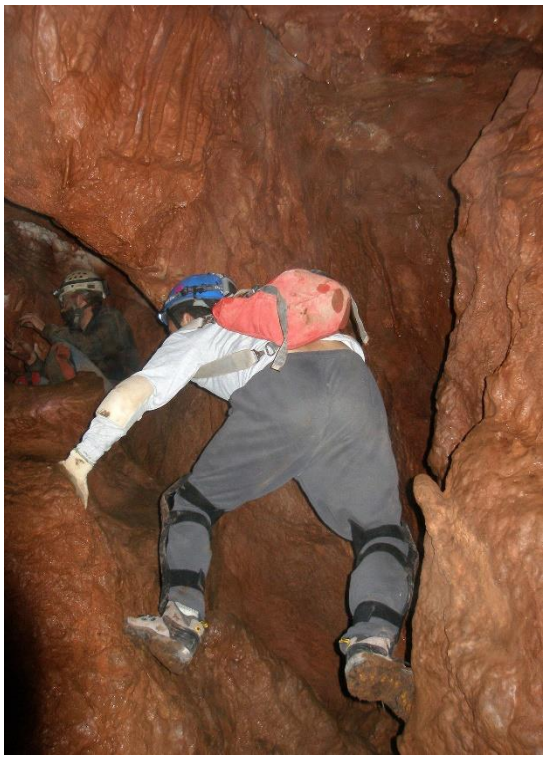

Fig. 7. *Karmir (Red) Cave – Greg Chavdarian climbing in a red passage - Republic of Armenia. Photo by C. Chavdarian*

Mageli Cave: Mageli Cave [4] is located along a gorge near the town of Areni, in Armenia's wine country (Figs. 8,9,10). It sits at an elevation of nearly 1.100 meters and has over 2 km (1.3 miles) of passages. Mageli Cave is a classic example of a conglomerate cave, as it is a mixture of limestone and other minerals [6]. There is a map for the cave, but it is basically an overview, not a detailed representation of the cave. During our expeditions, this cave was explored on two different occasions – in 2007 and 2010. After entering the cave by crawling on hands and knees through the borehole entrance, one can resume walking through parts of the cave. Immediately, on entering the cave, the conglomerate nature of it is obvious, as the walls of the cave resemble coarse, pebbled or gravelly concrete. Some flowstone is observed, but, for the most part, the cave is devoid of decoration (and this is primarily due to the conglomerate composition of the cave). Not far inside the entrance, there exists a bat colony. Fortunately, because of the various passages, one can avoid passing near the bats. Exploring further into the cave, there are tall, narrow passages, boreholes, and a steep, slippery climbdown to a lower level (handline recommended). Well-inside the cave there is also a 3-meter long belly-crawl squeeze with an incredibly intense, cold wind blowing through it (similar to a venturi). We negotiated this squeeze and then ended up in a chamber that allowed us to stand. However, in examining the chamber, we were unable to locate any sizable opening or passage related to the heavy wind. After passing back out of the squeeze the way we came, and gradually working our way towards the cave entrance by a different route, we encountered long, booming passages and came upon an impressive, massive conglomerate block hanging down from above, one of the signature features of the cave. After exploring additional side passages, we exited the cave. In a subsequent trip to this cave in 2010, we entered through the main entrance and then proceeded to negotiate our way through passages, including boreholes, to the upper level of the cave (above the entrance). As we worked our way along this level, we encountered a 12 meter pit (but with no vertical gear, we did not drop the pit for further exploration). However, by passing through another nearby passage, the pit can be avoided, and one can, actually, exit the cave onto a narrow ledge above the main entrance (thus, an upper entrance). On this ledge, one has a spectacular view of the gorge below. A more detailed survey and subsequent map of this cave is certainly warranted.

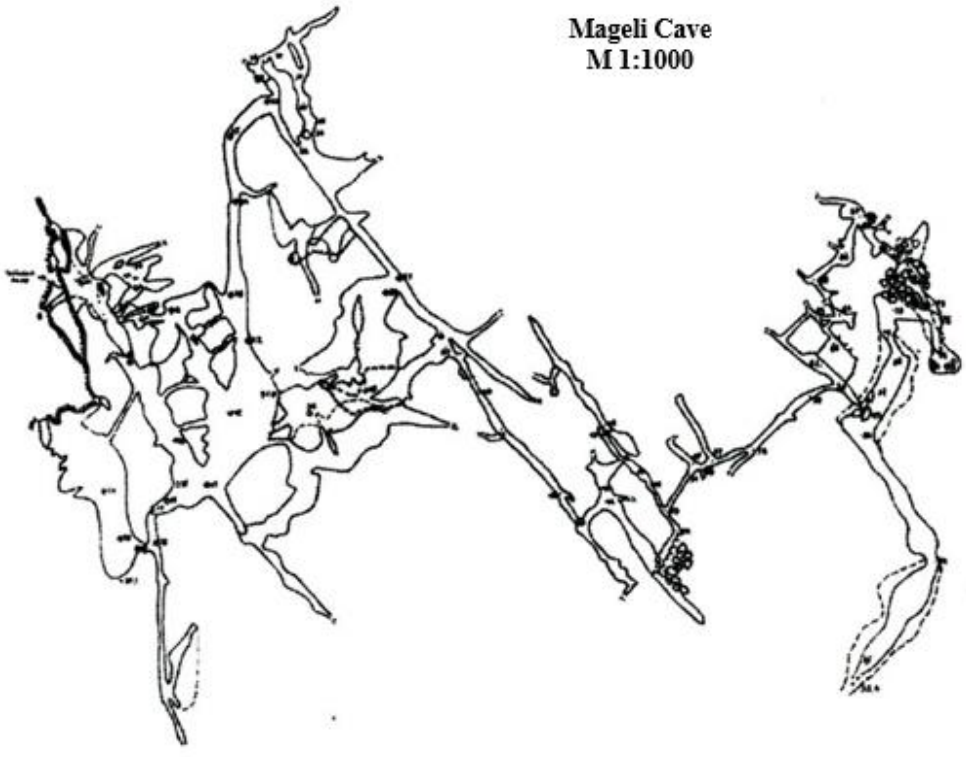

Fig. 8. *Mageli Cave Map – Survey – Smbat Davtyan*

Fig. 9. *Mageli Cave – Smbat Davtyan and Nyree Abrahamian in borehole passages - Republic of Armenia. Photo by C. Chavdarian*

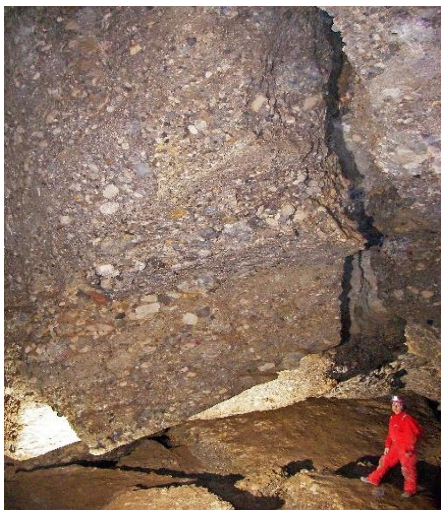

Fig. 10. *Mageli Cave – The massive conglomerate block with Seda Chavdarian - Republic of Armenia. Photo by S. Johnson*

Trchuneri Cave (Cave of the Birds): In 2007, we briefly explored Trchuneri Cave near the town of Areni. This cave is of particular note, as we observed evidence of an archeological excavation at the entrance of the cave [4]. Subsequently, in 2010 and 2011, significant archeological discoveries were reported at this dig, with artifacts dating back 6,000 years. Excavations continue to this day.

Jerovank (Water Cave Church): From the base camp in 2007, we traveled lower in elevation to a gorge with a path, which lead to a very unique cave, known as Jerovank. After hiking through the gorge, we reached the small limestone cave, next to a running stream. The locals make a religious pilgrimage to this cave each year. A church altar was built inside the cave. Some of the nearby water actually permeates into the church, and the water can be seen along the back of the main chamber, and also in an alcove next to the church altar. Along one side of the church chamber a brick wall was built, further enclosing the cave and church from the outside. We observed flowstone along the natural walls of the cave. Due to centuries of turbulence in Armenia, church caves like this existed to provide protection for the congregation.

Syunik Province, Republic of Armenia

In 2011, we traveled to Syunik Province to photo-document the man-made caves of Khndzoresk and the man-made caves of Old Goris near the eastern border of the Armenia.

Caves of Khndzoresk (Deep Gorge): The man-made caves of Khndzoresk are in an isolated and lightly populated mountainous rural region [7]. We hiked into this site. In centuries past, this was a thriving village, with man-made caves (homes) carved into the sandstone cliffs scattered all around (Fig.11). This even included a small church. It was inhabited up until the 1950s. The caves housed people, food supplies, and even livestock. All that now remains are the empty caves and the vacated church. Centuries ago, if one wanted a cave shelter or home, the local mason would fashion or carve a cave out of the soft rock. Over time, this resulted in a large, thriving cave village. The location of the caves rest on high ground, thus providing shelter in a strategic location – especially, important considering the enemies that had invaded Armenia over the ages.

Fig. 11. *The man-made caves of Khndzoresk - Republic of Armenia. Photo by C. Chavdarian*

Caves of Old Goris: In the hills above the thriving Armenian town of Goris lie a series of rock spires (which look similar to "hoodoos"). The spires actually consist of many man-made caves, similar to those in Khndzoresk (Fig.12) [8]. This was the centuries-old village of Old Goris and it is extensive. The present town of Goris lies in a valley below Old Goris. One can access Old Goris, walk through it, and enter some of the carved sandstone caves. In some cases, where sandstone rock shelters may have already been present, the shelters were likely enlarged by local masons. The area is no longer inhabited. Once again it is important to note that Old Goris strategically sits on high ground, having provided protection to its former inhabitants.

Fig. 12. *The man-made caves of Old Goris - Republic of Armenia. Photo by C. Chavdarian*

Tavush Province – Republic of Armenia

In 2013, the focus was on the caves in the northeast section of Armenia, specifically in Tavush Province. We stayed in the town of Ijevan during our explorations in this province.

Lastiver Cave (aka Anapat Cave): Lastiver Cave is perched near a cliff, in a mountainous region of Tavush Province, west of the town of Ijevan [9]. After driving up the mountainous terrain with our 4WD vehicle to a parking area, we then hiked about 4 km to the cave. The cave lies at an elevation just below 1.200 meters. This natural cave is limestone-based. The cave has had some frequent visitation, and, as a result, is fairly devoid of decoration. The chambers in the cave range from about 10 to 100 meters deep to about 15 meters wide. In the past, one of the chambers was used as a crude church, dating back to the 12th century. In this chamber, and opposite the centuries-old altar, are a series of nearly two-meter tall, human wall carvings that appear to be just as old. However, it turns out that these carvings were actually created only about 80 years ago[2], as explained by Smbat Davtyan. Why this was done is not clear. But it certainly has added to the mystique of the cave. In the largest room to the right of the church chamber, there is some actual flowstone remaining along the walls. However, there is breakage of the flowstone, and they are covered in dust and silt. This is now a fairly dry cave. In one of the other chambers we did observe two bats. However, there was no evidence that the cave houses a major bat roost. We explored various large and small chambers. Lastiver Cave is a natural cave that was also used as a church (Fig.13).

Fig. 13. *Lastiver Cave – Smbat Davtyan and Vrezh Nazaryan in a large chamber with aged flowstone - Republic of Armenia. Photo by C. Chavdarian*

Large Grotto Cave, Pool Cave, and Crystal Cave: Hiking beyond Lastiver Cave, we gradually came upon a huge wall or cliff of karst at an elevation of about 1.200 meters, where we came upon a large cave shelter [10]. We named it "Large Grotto Cave", as it consisted of a large entrance estimated to be approximately 45 meters in width. The cave extended back about 15 meters. There was breakdown at the

[2] Speleological Center of Armenia

back of this large cave shelter. We looked for additional passage at the back of the cave but did not locate any. It is possible that there may be passage beyond the breakdown.

We then hiked on along the karst wall and encountered another cave high up in the karst cliff. The way to this cave required some vertical rock climbing with exposure. We found a handline which had been placed there by others who had been to the cave. One member of our team – Vrezh Nazaryan – did the climb and went into the cave entrance. This cave measured about 7 meters in width at the entrance, and 10 meters deep. Further inside this cave (shelter), the width expanded to 35 meters. Inside the cave, someone had actually constructed a circular pool containing water.

Hovk 5 and Hovk 1 Caves: The Hovk caves are high in elevation in a remote area of the mountains west of Ijevan. There had been archeological excavations conducted 10 years earlier [4]. From our base in the town of Ijevan, we drove our 4 WD vehicle high up into that area. After parking off-road, we hiked up a very steep slope to the base of karst cliffs. We found Hovk 5 Cave at an elevation of approximately 2.380 meters. The cave is actually a rock shelter with dimensions of about 9 meters wide and 2 meters deep. We found evidence of an archeological dig. We then continued the hike near the karst cliff toward Hovk 1 Cave (Fig.14) [8]. During the hike, we noted limestone outcroppings scattered all along the way. Even more noteworthy was the lay of the land, which revealed an undulating landscape with sinks. As a result, there is great potential in this region for a potential cave system, or systems, waiting to be discovered. Once we reached the cave, we hiked up a slope and entered the elevated entrance, which sits at an elevation of over 2.050 meters. The first section of the entrance is about 0.5 meter wide and 3 meters long. This is followed by two large steps cut into the entrance – presumably by archeologists who excavated the cave entrance – which then lead into the main part of the cave which is approximately 3 meters wide and over 21 meters in length. The main passage has a high ceiling which eventually pinches down to a marrow slot at the back of the cave. There is little decoration. This was clearly a very habitable cave, and strategically favorable as it sits up into the side of the karst cliff .

Fig. 14. *Hovk 1 Cave – Vrezh Nazaryan in the high entrance - Republic of Armenia. Photo by C. Chavdarian*

Zrngan Cave (or Zerngan Cave): For our next destination, we traveled east of our base - the town of Ijevan - and up into the mountains towering above the town. The goal was to reach Zrngan Cave (Fig.15). at an elevation of approximately 1.850 meters [4]. The last part of our trip was off-road with our 4WD vehicle. This cave has a deep vertical entrance drop thought to be at least 45 meters in length. At the time of this trip, our colleague Smbat Davtyan told us that he knew of only one attempt at dropping down the entrance pit. This occurred about 30 years earlier. A group of non-cavers had lowered one of their people down to the bottom of the pit. This person actually explored some passage, but became frightened, and was hauled out of the

Fig. 15. *Zrngan Cave - C. Chavdarian on rope at the entrance drop. - Republic of Armenia. Photo by V. Nazaryan*

cave. No one knows the true extent of the cave. Unfortunately, on the day we were there, **C. Chavdarian** was the only caver with extensive experience at single-rope technique. Although very tempting, the correct decision was made to not drop the pit – that is, not to do any solo caving for obvious safety reasons. Instead, he did a demonstration for the caving colleagues by rigging the entrance drop, gearing up, and only rappelling down a short distance, followed by a changeover and ascent out of the cave. An actual cave trip into Zrngan Cave may be planned for in a future expedition.

Lori Province – Republic of Armenia

After leaving Tavush Province, our final caving destination of the 2013 expedition was to a lava cave in the neighboring province of Lori, to the west. This is also a rugged mountainous area of Armenia that also has caves.

Sanahin Lava Cave: Sanahin Lava Cave is the second largest lava cave (aka lava tube) in the Republic of Armenia (Fig.16), as noted by my colleague Smbat Davtyan [11]. The cave is located near the town of Alaverdi and is just off a main mountain road and on the side of a cliff, at an elevation of nearly 1.000 meters. The cave looks out over the town of Alaverdi and the Debed River in the spectacular and scenic gorge below [9]. This lava cave has about 80 meters of passage. There are three entrances to the cave, but only one is negotiable - and that is the main entrance nearest the road. To the left of the main entrance is a very small, squeeze entrance, which is not negotiable as a crawl, and farther to the left is a large, wide cliff entrance. The cliff entrance has an approximate 30 meter vertical drop outside, and thus, very dangerous if one is near this drop when standing inside the cave and looking out this entrance. Over the years, people and livestock have inhabited the cave,but we saw no one there during our trip. The cave appeared to be abandoned. Inside, there is mostly walking passage. However, there is a wet passage of about 9 meters in length which required kneeling and crawling. We did observe some small secondary formations overhead in the cave inside this wet passage – small stalactites of about 2.5 to 5 cm in length, generated from solution deposition. Inside the main entrance and to the left is the main trunk passage. This passage curves and eventually ends at the wide cliff entrance with the sheer vertical drop. This cave is well worth exploring.

Fig. 16. *Sanahin Lava Cave – Vrezh Nazaryan and Smbat Davtyan at the impressive cliff entrance, with a spectacular view of the town of Alaverdi in the gorge below - Republic of Armenia. Photo by C. Chavdarian*

Kotayk Province – Republic of Armenia

In Kotayk Province sits the medieval monastery of Geghard. This church is noteworthy as it was originally created by boring by hand into a rocky mountainside. It is now a UNESCO World Heritage Site. The majority of the church sits inside the mountainside, thus, the interior walls and massive columns of the main chapel, built in 1215 A.D., are entirely carved out of rock. It is, in essence, Armenia's most famous man-made cave church. Our team spent a day inside the church, marveling at it.

The Nagorno-Karabakh Republic

East of the Republic of Armenia lies the Nagorno-Karabagh Republic (NKR), home to an estimated 150,000 Armenians. This present-day independent Armenian republic is actually part of historical Armenia

(and contains Armenian churches dating back centuries) but was tragically partitioned away and placed under the jurisdiction of Azerbaijan by the Soviet Union. Following the break-up of the Soviet Union in 1991, the Armenians of NKR fought for and regained their independence. This war with Azerbaijan ended in a cease-fire in 1994. Presently, one can travel through most areas of the Republic. Thus, in 2011, Vrezh Nazaryan, Smbat Davtyan, and Charles Chavdarian journeyed to NKR to explore a specific cave.

The Caves of Tegh: On our way to NKR, we initially passed through the border village of Tegh (Fig.17), located just inside the Republic of Armenia, and east of the town of Goris. As we drove through, we looked off to our left, and there along a ridge, just below the main plain of the present-day village, we saw a number of large holes running along it. These were indeed caves, but it was not clear if they were all man-made. ome may have been natural caves that may have been enlarged to house families, and some may have been totally man-made. We did not stop there, but we did capture some photos.

Fig. 17. *The Caves of Tegh - Caves below the village - Republic of Armenia. Photo by C. Chavdarian*

Azokh Cave: Azokh Cave, located in the southern region of NKR, was the goal of our trip. Lying on a hillside in NKR's Hadrut province, and overlooking the village of Azokh, is Azokh Cave (Fig.18). This cave is of archeological significance, as a Pleistocene, pre-Neanderthal mandible fragment was discovered there in 1968 [12]. This led to a series of subsequent excavations up to the present. A number of artifacts have been found, but the excavations are essentially all at the three entrances (not deep inside the cave), with most of the excavations at the large main entrance (which is a high and wide vertical slot entrance). It is known that the cave consists of roughly three chambers, and three cave entrances, and has roughly 180 meters of cave passages. In researching this cave prior to the expedition, we found very little information regarding the actual interior of the cave (beyond the main entrance), and hardly any photographs. There is only a very rudimentary hand-drawn outline map of the cave [5]. It appeared that very few individuals ventured beyond the main entrance and deep into the cave. Once we passed through the main entrance chamber and into the next chamber, we discovered why there was so little information. In the second chamber and beyond, one is subjected to massive amounts of flying bats, flies,and guano (and its odor), which can be overwhelming. This was a shock, but it also answered the riddle of this cave, as to why so little was known of it. A non-caver would not have lasted longer than 10 minutes inside the cave. However, we cavers were determined to explore and photo-document the cave. We managed to remain in the cave for about 1.5 hours. We gingerly moved through the narrow passages connecting the chambers, either upright or by crouching, and were careful not to fall into the slippery,

Fig. 18. *Azokh Cave - Smbat Davtyan with a column and decoration - Nagorno-Karabakh Republic. Photo by C. Chavdarian*

deep guano. The cave is mostly devoid of decoration however, we were pleased to find two large limestone columns – one of which was rather impressive with surrounding flowstone. We also discovered an incredibly large mound of guano taller than us – reminiscent of the guano mound in the Planet Earth television series. As tough as this trip was, all caves deserve to be explored, regardless of the conditions one may encounter. We accomplished the objective, and now have a clear understanding of the nature of this cave.

Discussion

Inside one of the caves, someone had actually constructed a circular pool containing water. Stones lined the pool. As a result, we named the cave "Pool Cave". It is not clear the purpose of the pool. It may have provided a water source for the more contemporary inhabitants, or possibly a source for bathing.

We then continued our hike along the bottom of the karst wall and soon came to another cave at an elevation of approximately 1.200 meters. The walk-in entrance was approximately 2.5 meters high and 2 meters wide. The cave extended back over 20 meters, and we could walk upright through the entire length of it. There was no noticeable decoration, and a fair amount of breakdown. It is possible that there had been an excavation inside this cave. The notable feature was that there was a pile of crystalline calcite near the entrance, which had been partially scavenged by others. Because of this, we simply named the cave "Crystal Cave".

The medieval monastery of Geghard in Kotayk province is, in essence, Armenia's most famous man-made cave church. The original name of the monastery was Ayrivank, which means "The Cave Monastery" or "The Monastery of the Cave". It was later called Geghard, which refers to the spear which wounded Christ during the crucifixion, and was subsequently alleged to have been brought to this church for storage (the spear currently resides in the Holy See of Echmiadzin, near the capital of Yerevan, Armenia). In any event, Geghard is a must-see for any visitor to Armenia, including cavers.

Conclusion

Over a period of six years, with four expeditions to Armenia in 2007, 2010, 2011, and 2013, we explored and photo-documented a number of natural and man-made caves – limestone, conglomerate, sandstone, and lava. We experienced the color and beauty of Armenia's natural caves, the intriguing man-made cave villages, and the reverent use of caves as chapels and churches. Caves have been an integral part of the landscape and culture of Armenia and the Armenians. Through these expeditions, one cannot help but gain a greater and enduring respect for this ancient land and its people.

References

[1]. S. Shahinyan, S. Balyan, S. Davtyan, Caves of Artashat, Ararat and Yeghegnadzor Regions of Armenia. SSR, Report of the Speleological Detachment, Expedition of the GS of RA AS, 1985.

[2]. S. Shaginyan, G. Ogannisyan, Osobennosti podzemnogo landshafta Yekhegnadzorskogo i Idzhevanskogo karstovykh massivov izvestnyakov, vyyavlennyye v rezul'tate issledovaniy 2013–2014. Speleology and Spelestology, Proceedings of the VI International Scientific Conference, Naberezhnye Chelny, 2015, 77–79 (in Russian).

[3]. R. Ruggieri, S. Davtyan, A. Ugujyan, Armenia Karst Project. Proceedings of the UIS 17th International Congress of Speleology, Australia, 2017, 82–85.

[4]. S. Shahinyan, Hayastani karandzavnery, Zangak, Yerevan, 2005 (in Armenian).

[5]. S.P. Balyan, Strukturnaya geomorfologiya Armyanskogo nagor'ya i okaymlyayushchikh oblastey. Yerevan University Press, Yerevan, 1969 (in Russian).

[6]. R. Ruggieri, S. Davtyan, S. Shaihinyan, A. Ugujyan, R. Orsini, A. Ingallinera, G. Agosta, Armenian Karst Project. Carbonates Evaporites, 37 (1), 2022. Doi: https://doi.org/10.1007/s13146-021-00755-0

[7]. A.T. Aslanyan, Regional Geology of Armenia. Haypethrat, Yerevan, 1958 (in Russian).

[8]. R.A. Mandalyan, O razvitii karbonatnogo karsta v Tavushskoy i Syunikskoy oblastyakh Armenii. Proceedings of the NAS RA, Earth Sciences, 56(2), 2003, 44–46 (in Russian).
[9]. R. Ruggieri, S. Davtyan, R. Orsini, Armenian Karst Project 2nd Phase: Karst Surveys in the Region of Ijevan and Lori (North-Eastern Armenia). International Scientific Conference "Man and Karst 2019", Ragusa, June 24–26, 2019.
[10]. S. Shahinyan, A. Gevorgyan, Karstogenic Peculiarities of the Karst Structures in the Lime Massive of the Region of Walk of the Armenian S.S.R. Proceedings-communications-v2, International Congress on Speleology -10, Budapest, Hungary, August 13–20, 1989.
[11]. S.R. Davtyan, Opyt speleologicheskogo rayonirovaniya Respubliki Armeniya. Speleology and Spelestology, Proceedings of the IV International Scientific Correspondence Conference, Naberezhnye Chelny, 2013, 39-41(in Russian).
[12]. V.N. Dublyanskiy, Peshchery i moya zhizn. Ukrainian Institute of Speleology and Karstology, Simferopol, 2010 (in Russian).

Charles G. Chavdarian, Doctor of Philosophy (PhD) in Chemistry *(United Kingdom,Cambridge) - AstraZeneca, Cambridge, United Kingdom, caver3d@comcast.net*

Smbat Davtyan, Doctor of Philosophy (PhD) in Geodesy, Cartography and Cadastre *(RA, Yerevan) - Brusov State University, Lecturer at the Chair of Tourism and Service, srdavtyan@mail.ru*

Samvel Shahinyan, Doctor of Science (Architecture) *(RA, Yerevan) - National University of Architecture and Construction of Armenia, Head of the Chair of Geoecology and Biosafety, sshahinyan@nuaca.am*

INVESTIGATING THE OPTIMUM TILT ANGLE OF PV MODULES IN AL-SHEROUK CITY, CAIRO

Mohamed Atef[1], Wahbi Albasyouni[2]*

[1]The British University in Egypt, Al-Sherouk, Cairo, Egypt

[2]Newcastle University, Newcastle upon Tyne, United Kingdom

Abstract: *Energy is a crucial element that can ensure the quality of life for citizens. The consumption of energy by citizens is increasing rapidly, and future existence also became reliant on the sufficient availability of energy and its sources. Nevertheless, energy consumption is becoming a major concern due to the increase in usage rates and the lack of sufficient renewable sources of energy. Nowadays, the technological advancement that lies in the use of photovoltaic panels (PV panels) can help in generating energy and take the advantage of the sun especially in Egypt. The usage of PV's relies on multiple factors that can ensure the highest potential generation of energy. Therefore, several studies investigated these factors including the optimum titling angle that can be different according to the location and orientation of the panel. Modifying the titling angle can play a significant role in generating high rates of power depending on the measurements and calculations. The aim of this paper was to investigate the efficient titling angle that can be used for PV panels that are installed in Al-Sherouk City in Egypt. The methodology involved the implementation of an experimental investigation that is based on position 2 similar PV panels to estimate the power generation over a period of 2 days from 9 am to 4 pm. The findings have shown that the theoretical and experimental results were similar, and the optimum tilting angle was determined to range between 54.7 degrees and 8.16 degrees. The study demonstrated the differences between an adjusted and a fixed angle, and the variable titled angle can generate more energy than the fixed one. This paper contributes to the body of knowledge by presenting the significance of a variable tilting angle to generate more power than relying on a fixed angle as demonstrated by many previous studies.*

Keywords: *solar energy, photovoltaic panels, renewable energy, solar energy in Egypt, optimum tilt angle*

Wahbi Albasyouni*

E-mail: Wahbi_mah@hotmail.com

Received: 16.02.2023

Revised: 10.03.2023

Accepted: 25.03.2023

Introduction

People should pay more attention to renewable energy due to the lack of sufficient energy sources and the positive impact of using a renewable source of energy. It is important for developing and developed countries to consider finding new solutions to increase in prices of oil, increase in electricity demands, high rate of greenhouse gas emissions, and even global warming [4]. Solar energy is categories as a renewable source of energy which has been developing to an extent scale due to limitations in energy transmission [2]. Normally, there are multiple benefits of solar energy over the use of fossil fuels such as reduced carbon emissions, cleaner air, and can generate power over a long period of time. Hence, due to the huge increase in electricity consumption, researchers are more concerned about developing solar energy developments with excellent efficiency, less environmental pollution, and with proper investments cost [2].

The overall global energy consumption in 2014 was recorded to be around 160310 million MWh, and it was estimated that this value is expected to keep on increasing to reach around 240318 million MWh by 2040 [6]. It was recorded in 2010 that the electrical generation systems that are based on renewable energy increased by 20% from the overall electricity generation, and this value will keep on increasing until it reaches 31% by 2035 [3]. The use of renewable energy can help in generating around 57% of global electricity supply by 2025 [3]. Eventually, the dependency on solar energy for electricity production is growing around the globe. Hence, solar energy production should be developed and promoted due to the negative impact of conventional energy production [1]. During the past few years, a huge amount of investment was focused on the improvement in

solar energy production which helped countries to reach better technological advancement and cost-effective production of energy [1].

Shu et al [5] investigated the optimum tilt angle for solar panels in Kitakyushu City. There are multiple variables that were considered in the experiment including the sensitivity of optimum tilting angle, radiation rates, reflection rates, and declination of solar. The results demonstrated that the 35 degrees tilting angle had the most intensity of radiation between December to November of the following year. Another important factor to be considered is that if the latitude gets higher than the optimal angle might increase.

Tlijani et al [7] conducted a study regarding the optimization of tilt angle of solar panels that are located in Tunisia. The research focused on the comparison between the experimental and theoretical results using Matlab simulation analysis. The angles used in the study were 0, 30, 45, 60, and 90 degrees and the panel was positioned once in the west, then changed to south and east. The first panel had dimensions of 370*295*15 mm and was placed at a temperature of 25 degrees Celsius. The second one had a dimension of 215*225*18 mm and was located in the same way as the first one. The findings of this study demonstrated that climate conditions and the location of the solar panel might impact the total power generated by the system. This paper discussed the potential optimum tilt angle for PV to generate optimum power and energy.

Materials and Methods

Procedure of Calculations (Table 1)

1. The first step taken in the calculations was determining the deflection angle as shown in the equation below:

Deflection angle equation

$$\delta = 23.45 \sin\left(360 \cdot \frac{284+n}{365}\right) \quad (1)$$

2. B is then calculated using the following equation

$$B = n - 1\frac{360}{365}$$

3. True solar time is then measured using this equation

$$E = 229.2 \cdot 0.000075 + 0.001868 \cdot \cos B - 0.032077 \cdot \sin B - 0.014615 \cdot cos2B - 0.04089 \cdot \sin 2B)$$

4. After calculating the B, the solar time (ST) is then calculated, ST is the time where the measurements are taken (14:00pm). This time was basically chosen because the radiations from the sun were considered the highest during the entire day time. I_{st} is the standard longitude of time zone, and I l_{oc} is the longitude of the location. l_{oc} of the chosen location "Al-Sherouk City" is taken as 31.610584.

$$Solartime - ST = 4 \cdot (l_{st} - l_{loc}) + E$$

5. Hour angle is then measured using the following equation, where the t_s is known as the solar time.

Hour angle

$$\omega = 15(t_s - 12) \quad (2)$$

6. Zenith angle is then measured as follows, where Φ is the latitude and taken as 30.1187 according to Al-Sherouk City location.

Zero angle

$$\cos\theta_z = \cos\delta \cdot cos\emptyset \cdot cos\omega + sin\delta \cdot sin\emptyset \quad (3)$$

7. The solar elevation angle is then measured using this equation.

Calculating the zero elevation angle

$$\alpha = 90 - \theta_z \quad (4)$$

8. Solar Azimuth angle is the next to be calculated.

Solar azimuth angle $$\gamma_s = cos^{-1}[(\sin(\alpha) \cdot \sin(\emptyset) - \sin(\delta)/\cos(\alpha) \cdot \cos(\emptyset) \quad (5)$$

9. Incidence angle is then measured using the following equation.

Incidence angle $$\theta = cos^{-1}[\cos(\delta) \cdot \cos(\emptyset) \cdot \cos(\omega) + \sin(\delta) \cdot \sin(\emptyset) \quad (6)$$

10. Then the tilt angle is measured as follows.

Calculation for the tilt angle $$\beta = |\emptyset - \delta| \quad (7)$$

Table 1. Measured calculation of all above parameters

Days / parameters	δ	B	E	Solar time	W	Cos zenith angle	Zenith angle	Solar elevation angle (α)	Without (cos) inverse	Solar azimuth angle (ϒs)	β
1	-23.01	0.00	-2.90	14.16	32.34	0.46	62.37	27.63	0.61	52.45	54.62
2	-22.93	0.99	-3.35	14.16	32.45	0.46	62.35	27.65	0.61	52.53	54.54
3	-22.84	1.97	-3.39	14.17	32.56	0.46	62.33	27.67	0.61	52.60	54.45

Calculating the solar irradiance

The theoretical calculations are based on previously obtained results of using solar panels in the same locations investigated in the experimental part of this study. The below are the data collected from specific dates in 2017 (Table 2).

Table 2. Calculation of Solar Irradiance of tilted angle "S"

Date	A	B	C	Zenith angle	Tilt angle	Gbn	Gd	G	rb	F	Ground reflectivity	Gt
17/1/2017	1232.46	0.1416	0.057	61.31	52.23	917.46	52.93	493.38	1.02	0.988	0.2	523.4
16/2/2017	1216.58	0.1436	0.059	55.19	44.57	945.87	56.44	596.44	1.01	0.991	0.2	622.8
16/3/2017	1190.18	0.1538	0.009	45.99	34.03	953.76	52.04	714.69	1.00	0.994	0.2	733.2
15/4/2017	1144.68	0.1753	0.091	35.69	22.2	922.41	84.83	834.1	0.99	0.989	0.2	844.60
15/5/2017	1109.4	0.1928	0.116	28.87	12.82	890.17	103.43	882.97	0.98	0.986	0.2	884.13
11/6/2017	1092.84	0.2020	0.129	27.28	8.52	870.56	113	886.74	0.98	0.983	0.2	884.09
17/7/2017	1085.4	0.2067	0.135	29.76	10.43	855.39	116.10	858.68	0.98	0.981	0.2	859.78
16/8/2017	1103.45	0.1967	0.124	33.9	18.16	865.15	107.50	825.59	0.99	0.983	0.2	834.43
15/9/2017	1142.48	0.1816	0.097	40.06	29.39	901.11	88.13	777.82	0.99	0.987	0.2	795.64
15/10/2017	1183.8	0.1634	0.076	48.3	41.21	925.98	71.11	687.10	1.00	0.989	0.2	713.75
14/11/2017	1213.68	0.1514	0.052	56.51	50.52	922.30	60.18	569.10	1.01	0.988	0.2	601.07
10/12/2017	1228.23	0.1445	0.059	61.24	54.66	909.47	53.84	491.42	1.02	0.987	0.2	524.11

Table 3 represents the average day for each month in order to measure the solar irradiance in this specific day.

Table 3. Average day for each month

Month	N for ith day of month	For average day of month		
		Date	n	δ
January	i	17	17	-20.9
February	31 + i	16	47	-13
March	59 + i	16	75	-2.4
April	90 + i	15	105	9.4
May	120 + i	15	135	18.8
June	151 + i	11	162	23.1
July	181 + i	17	198	21.2
August	212 + i	16	228	13.5
September	243 + i	15	258	2.2
October	273 + i	15	288	-9.6
November	304 + i	14	318	-18.9
December	334 + i	10	344	-23

Calculating Power Output and Efficiency of Panel:

The total power output had to be measured for the panel during the experiment for the whole month according to the data obtained from the British University in Egypt as shown in Table 4.

Table 4. Measurements of power for each month

		Jan	Feb	Mar	Apr	May	Jun	Jul	Aug	Sep	Oct	Nov	Dec
Power (KWH/month)	Optimum	57.5	53.1	58.4	55	56.4	54.6	56.0	55.5	53.9	55.9	53.7	55.6
Power (KWH/month)	Tilt 30	52.4	50.9	58.2	54.3	53.2	50.0	52.1	54.0	53.9	54.6	49.6	49.6

Maximum efficiency equation

$$\eta_{max}(maximum\ efficiency) = \frac{P_{max}\,(maximum\ power\ output)}{(E(incident\ radition\ flux)\cdot A_c(area\ of\ collector)} \quad (8)$$

Experimental Procedure

The experimental procedure that was followed in this research focused on comparing the generated results between the theoretical analysis and experimental results and indicate any variations in the generated results (Fig.1). The experiment included the use of 2 identical panels that are directed to the south direction using multiple tilt angels that ranged from 0 degrees, 15, 30, and until 45 degrees. These panels were positioned on the top of the British University in Egypt.

Fig. 1. *Used PV panels in the experiment*

The main objective was to indicate the solar radiation and generated power from the panels during an annual measurement where the size of the PV module used was 1.65 · 0.953 meters and the overall area is 1.57 m^2. In addition, the maximum power within the panel was 280W. The type of the used PV panel is Monocrystalline Silicon Module. The field observations were decided to be undertaken during 2 various days which are 24/5/2018, and 26/5/2018. The PV panel was installed and kept on recording starting from 9 am until 4 pm, while the readings are taken each half an hour. The field procedure consisted of the following steps:

1. The first step was to properly clean the panels in order to remove any sand particles, dust, or any objects that might affect the collection of solar radiation by the panel.
2. Then, the panels were adjusted into 2 different angles at which to determine the optimum angle that could generate the highest solar radiation.
3. PV system analyzer was adjusted to include the data and specifications of the panel used.

Experimental Results

The results demonstrated that 15 degrees tilt angle generated the highest potential power output from the panel as shown in Fig.2.

Fig. 2 shows the experimental readings that were taken during the 2 days of field observations starting from 9am until 4pm. Certain radiations were chosen after the experiment in order to estimate the power energy while the most optimum angle will usually yield the highest power. In the theoretical results the optimum angle was estimated to be from 10 to 11 degrees as shown in Fig. 3. The highest angles that provided most power were recorded in 0, 15, 30, 45 degrees respectively. Therefore, the experimental and theoretical results were quite close according to the generated optimum tilt angle (Fig.3).

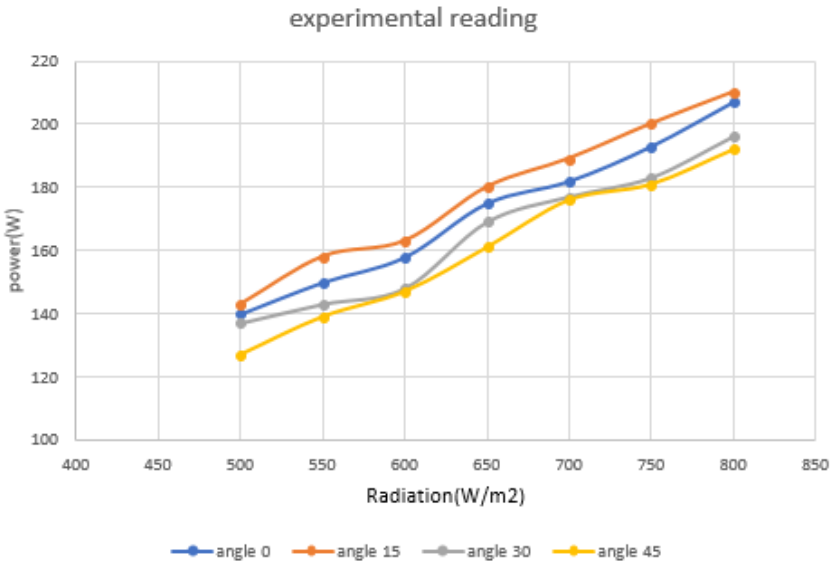

Fig. 2. *Experimental readings for the different tilt angles and power outputs*

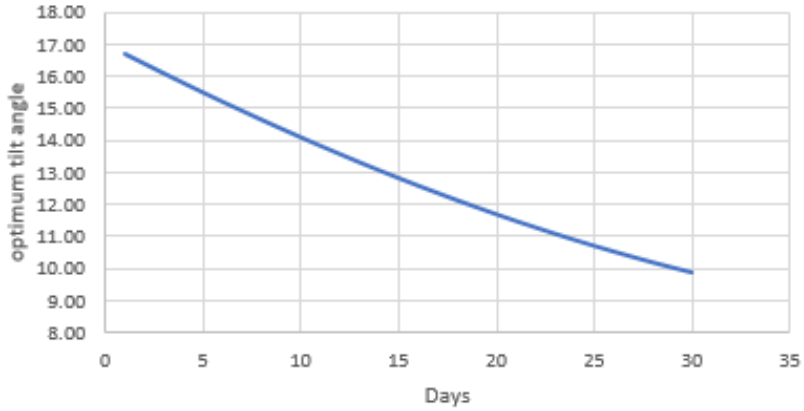

Fig. 3. *Tilt angle for May (theoretical observations)*

Difference between Theoretical and Experimental Results

Radiation Results

The rate of radiation was measured for all angles and compared with the theoretical values as shown in Figs. 4,5,6 and 7.

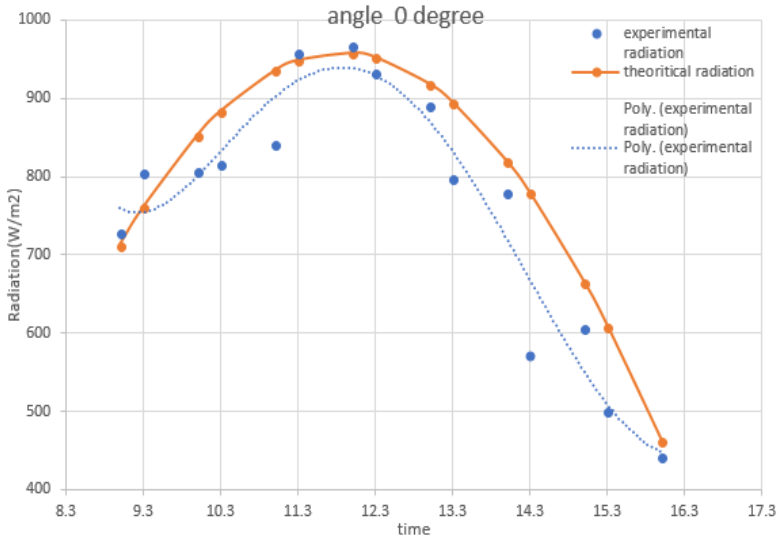

Fig. 4. *Difference between experimental and theoretical radiation at 0 degrees tilt angle*

The theoretical radiation was optimum during the mid-day and kept on reducing by time. The experimental line was also similar but with less solar radiation during most of the day except during mid-day.

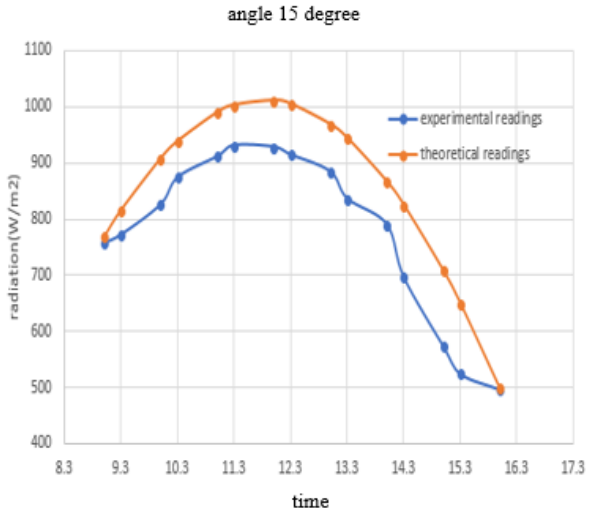

Fig. 5. *Difference between experimental and theoretical radiation at 15 degrees tilt angle*

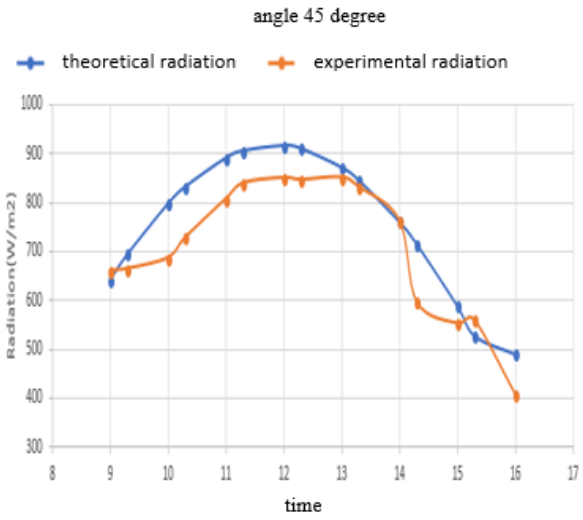

Fig. 6. *difference between experimental and theoretical radiation at 45 degrees tilt angle*

If the tilting angle was rotated to 15 degrees, the theoretical readings were quite similar to the experimental ones as shown in Fig. 5, and the 30 degrees tilt angle also yielded similar results to this one.

The 45 degrees tilting angle scored different values than the theoretical numbers as indicated in Fig. 7. According to the previous figures, the results were quite close and identical in terms of solar radiation which proves the credibility and validity of the generated results. However, it was observed that most of the experimental readings suffered from potential weather conditions such as dust. The highest solar radiation was estimated to occur at the solar time which is around 12 pm mid-day. Another measurement that was considered in the experiment was the power generated by the panel. The highest variation that was observed between the theoretical and experimental results was estimated to occur at 11 am. The differences between the generated power between the experimental and theoretical results was around 73 Watt. The following are the results of each tilt angle and the generated power:

- In 30 degrees angle the power variation was 66 Watt at 11 Am.
- In 15 degrees angle the power variation was 73 Watt at 12 Pm.
- In 45 degrees angle the power variation was 41 Watt at 10 Am.

The results have shown that the major variations between theoretical and experimental results were observed between 10 am and 12 pm due to the efficiency of the panel. It must be taken into account that the theoretical observations are taken with the optimum panel efficiency, while the experimental ones might vary according to the properties and conditions of the solar panel.

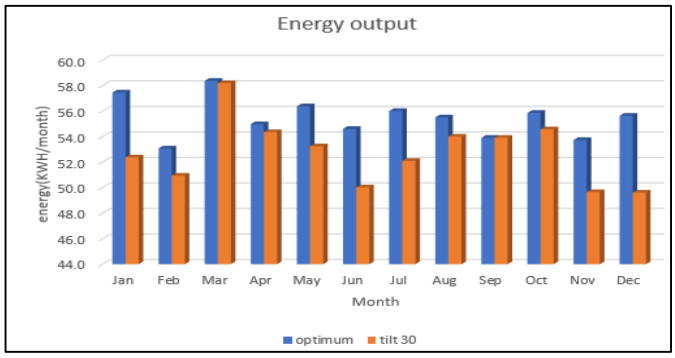

Fig. 7. *Power vs months output*

Fig. 7 demonstrates the generated power by solar panels for each month. It helps in understanding the generated power from the optimum tilt angle during the entire year. The blue bar shows the optimum energy output which keeps on changing during the year. The orange bars indicate the energy output for the solar panel if the tilt angle is set at 30 degrees. The used tilt angles for these solar panels were 50,45,34,23,13,9,11,18,30,41,50,55 respectively. The results indicated that this program can be used to determine the critical tilt angle, solar radiation, and most possible power through changing the latitude and longitude of certain points any location.

Parameters that Affect Theoretical and Experimental Results

There are multiple factors at which play a major role in introducing variations between the theoretical and experimental results such as the following:

1. Weather conditions due to the presence of clouds that covers the sun most of the day.
2. The radiation sensor is not accurately fixed in the system at which can influence the final readings.
3. The ground reflectivity factor is not quite accurate at which can generate the highest power possible.
4. Calculating the A, B, and C factors is not quite effective as it might contain any errors especially during any calculations.
5. Assuming that the rb ratio is zero when the incidence angle is higher than 90 degrees is not quite effective and can generate multiple errors.
6. The efficiency depends mainly on the solar radiation and generated power which ranged from 7.9% until 12.85% in the experimental results, while in the theoretical calculations the efficiency kept on the same value of 17.8% which is the highest efficiency possible.

Conclusion

Renewable energy is the source of electricity generation in the future and consistent research and development is required to enhance the current knowledge and understanding. One of the most common sources of renewable energy is solar panels and further studies are essential to better understand the design and efficiency of this system. Future researchers that are looking to apply the same conducted theory must take into account the results obtained in this research. It is important to take solar radiation results and measurements over a long run as it can be affected by the weather conditions or any other external factors that would prevent the generation of accurate results. Designing the solar panel to have a fixed inclined angle might help in generating more energy, and studies also recommended developing panels that can flexibly rotate during the day to generate optimum energies. The study investigated the theoretical and experimental results of power generation of solar panels in Al-Sherouk City in Egypt. The findings have shown that the theoretical and experimental results were similar, and the optimum tilting angle was determined to range between 54.7 degrees and 8.16 degrees. The study helped in providing the significance of the tilt angle for power and energy generation of solar panels. Future studies are expected to investigate similar properties in other regions and in different climate conditions.

Recommendations

There are various factors to be considered by future studies in order to develop on the findings that were reached in this study including the below:

1. Changing the tilt angle can generate the highest possible solar radiation and power, thus it must be properly applied and taken into account, but at the same time the location of the panel and weather conditions might play a major role in finding the optimum angle.
2. Ensure the consistent change of tilt angle monthly to generate the highest energy possible. These angles are 50,45,34,23,13,9,11,18,30,41,50,55 respectively in El-Sherouk City.

References

[1]. S. Abolhosseini, A. Heshmati, J. Altmann, A Review of Renewable Energy Supply and Energy Efficiency Technologies. SSRN Electronic Journal, 2021. Doi: https://doi.org/10.2139/ssrn.2432429

[2]. U. Arachchige, S. Weliwaththage, Solar Energy Technology. Journal of Research Technology and Engineering, 1 (3), 2020, 67-75. https://www.researchgate.net/publication/342610877_Solar_Energy_Technology

[3]. M. Islam, M. Hasanuzzaman, N. Rahim, A. Nahar, M. Hosenuzzaman, Global Renewable Energy-Based Electricity Generation and Smart Grid System for Energy Security. Scientific World Journal, 2014. Doi: https://doi.org/10.1155/2014/197136

[4]. O. Peter, C. Mbohwa, Renewable Energy Technologies in Brief. International Journal of Scientific and Technology Research, 8 (10), 2019, 1283–1289.

[5]. N. Shu, N. Kameda, Y. Kishida, H. Sonoda, Experimental and Theoretical Study on the Optimal Tilt Angle of Photovoltaic Panels. Journal of Asian Architecture and Building Engineering, 5 (2), 2006, 399–405. Doi: https://doi.org/10.3130/jaabe.5.399

[6]. S. Thomas, L. Brischke, J. Thema, L. Leuser, M. Kopatz, Energy Sufficiency Policy: How to Limit Energy Consumption and Per Capita Dwelling Size in a Decent Way. ECEEE Summer Study Proceedings, 2017, 103–112. https://nbn-resolving.org/urn:nbn:de:bsz:wup4-opus-67156

[7]. T. Tlijani, A. Aissaoui, R. Younes, Optimization of Tilt Angle for Solar Panel: Case Study Tunisia. Indonesian Journal of Electrical Engineering and Computer Science, 8 (3), 2017, 762–769. Doi: https://doi.org/10.11591/ijeecs.v8.i3.pp762-769

***Mohamed Atef**, **BSc in Mechanical Engineering** (Egypt, Cairo) - The British University in Egypt, Mohamedalameldin@outlook.com*

***Wahbi Albasyouni, Doctor of Philosophy (PhD) in Architecture, Planning, and Landscape** (Newcastle, United Kingdom) - Newcastle University, Wahbi_mah@hotmail.com*

RUPESTRIAN WORKS AND ARTIFICIAL CAVITIES: CATEGORIES OF CONSTRUCTION TECHNIQUES

Bixio Roberto[(1)] *, **De Pascale Andrea**[(2)], **Galeazzi Carla**[(1-3-5)], **Parise Mario**[(1-4)]

[(1)] *Union International de Spéléologie, Artificial Cavities Commission, Postojna, Slovenia*

[(2)] *Civic Museums of Genoa, Educational Services and Cultural Mediation, Genoa, Italy*

[(3)] *Egeria Underground Research Centre, Rome, Italy*

[(4)] *Department of Earth and Geo-Environmental Sciences, University Aldo Moro, Bari, Italy*

[(5)] *National Commission on Artificial Cavities - Italian Speleological Society, Bologna, Italy*

Abstract: *Artificial cavities, i.e. man-made structures excavated within rock masses in the mountains, below the ground, or in the subsoil of urban areas, are typically distinguished based upon the epoch of realization and the function for which they were originally used. They can be ranked into the following types, in turn divided in sub-classes: hydraulic works, dwelling works, worship works, war works, mining works, transit way works and others. The above criteria are essential for establishing a general common line aimed at providing optimal elements for cataloguing and comparing subterranean features, which may favor the creation of databases functional to knowledge, protection and enhancement of the hypogean works. In addition, there is another useful aspect for studying the origin and evolution of underground structures that takes into account their implementation modalities. The National Commission on Artificial Cavities of the Italian Speleological Society has identified, according to its experience in the field and in function of the construction techniques, six general categories of underground works: cavities dug in the subsoil, cavities built in the subsoil, cavities obtained by re-cover, anomalous artificial cavities, mixed artificial cavities and natural caves modified by men (anthropized caves). In this contribution we will discuss the specific details of each category, thus extending the concept of rupestrian heritage, usually confined to temples or dwellings carved in the rock, to a culture of building in "negative" that finds larger and more diversified evidences.*

Keywords: *Rupestrian Works, Artificial Cavities, Categories, Typologies, Underground, Construction Techniques.*

Bixio Roberto*

E-mail: roberto_bixio@yahoo.it

Received: 14.03.2023
Revised: 04.04.2023
Accepted: 20.04.2023

Introduction

And nowadays, man-made structures excavated within rock masses in the mountains, below the ground, or in the subsoil of urban areas (artificial grottos, cavities), do not cease to attract the researchers' attention, although they are sufficiently studied and classified based on the epoch of realization and the function for which they were originally used.

For those who study the origin and evolution of underground structures, accurate records of the ways of their implementation become very important in order to correctly understand the scientific problem, its significance and direct the study to certain results. As such, six general categories of underground work defined by the National Commission on Artificial Cavities of the Italian Speleological Society, according to its experience in the field and in function of the construction techniques are considered, which, in their important details, expand the hitherto existing conception of the rupestrian heritage.

Materials and Methods

During the preliminary research, data in the scientific literature was examined. Materials about the cavities located in Armenia were developed from publications in international conferences. The necessary sections of geological, stratigraphic, geomorphological, hydrogeological, and geophysical maps were collected and

developed. During the fieldwork of the scientific expeditions, a comparative analysis of these maps was carried out using data gathered from each site.Then the main works began, such as identifying the artificial caves, determining their location in the rock mass, comparing the conformation of the cavity elements with appropriate topographical surveys, and drawing the relevant conclusions.

From "rupestrian works" to "artificial cavities"

Usually, when the "rupestrian works" topic is dealt with, one thinks immediately to structures dug by men in the rock-faces in order to obtain underground spaces to inhabit, with related sites for productive activities (warehouses, stables, mills, dovecotes, etc.), or to spaces used for worship, both for liturgical purposes (temples, churches, etc.) and for the burial (tombs of various types), according to a functional types subdivision [1-4].

We find striking examples in various parts of the world, as the rupestrian settlements in southern Italy, the most famous of which are the Sassi of Matera, consisting of thousands of dwelling units. However, not less important are the many sites excavated in the gorges (locally named *gravine* [5]) of the Apulian-Lucan area, counting almost 600 churches, nearly the same number estimated for the hundreds of rupestrian settlements of Cappadocia, in central Turkey, and others in Armenia. Equally well known are the Dogon cliff villages of Mali, the Buddhist "caves" of China and India, the rupestrian city of Petra, in Jordan, the Pueblo villages in Colorado, and many others in different parts of the world.

The use of exploration techniques derived from the experiences of cave progression has allowed, since the 1960s, the finding of underground man-made works, less visible than those mentioned above, more dangerous to explore, and more difficult to be documented. This approach has produced a quantitative increase in knowledge of underground structures and, especially, has extended the investigations to issues not much considered before about the use by man of underground structures. This union, which began in prehistoric times with occupation of the caves by man, later evolved over the millennia with surprising and ingenious works. These are not limited to the already mentioned cavities intended for dwelling or worship, but include structures for transit, hydraulic engineering, mining, war, and related sub-classes (see Table at the end of the article).

Furthermore, the research field has expanded from the works excavated by man in the rocky outcrops or below the countryside level to those in the subsoil of urban areas.

It was therefore necessary to go beyond the idea of "rupestrian work", as defined above, replacing it with the most extensive "artificial cavity," or "anthropic cavity", in its turn complementary to that of a natural cavity, or cave. We can define artificial cavity as a space created by man in the subsoil, in broad sense, which implies an idea of a "negative" construction culture, as an alternative to the outer buildings at the surface, but also to the hypogean environment produced by meteoric agents and geological phenomena.

This approach completely defines the relationship between man and the underground world, taking into account not only the many variable purposes - identified in the types above described – but also the different construction ways according to morphological, lithological and urban characteristics of the environment in which the structures have been made over time, also including those structures which were not excavated, but share many similarities with hypogean places.

Categories of construction techniques

The *Commissione Nazionale Cavità Artificiali (CNCA), i.e.* National Commission on Artificial Cavities of the *Società Speleologica Italiana* (Italian Speleological Society), according to the exploration experience of its researchers, has developed a catalogue of artificial cavities based upon the construction techniques, identifying six categories, according to their intended purpose [6]. In the Register of Artificial Cavities, compiled by the Commission [2,7-9], not only the strictly rupestrian works are therefore included, but all those structures built or dug by man in the subsoil and, sometime, in the above ground, according to the following criteria.

Cavities dug in the subsoil

These are obtained exclusively by removal of stone materials (rocks), and can be divided into two groups [10].

a) Rupestrian (or rock-cut) structures, strictly speaking. They consist of spaces (rooms, tunnels, shafts) dug by man above the ground surface, in the outermost portion of rocky towers, pinnacles, cliffs, canyons, slopes. These are also defined "cliff cavities" [11].

Generally they can have very long horizontal development, even kilometres, on a single level (linear cavities/settlements), or on a series of stepped levels (terraced cavities/settlements), or on levels superimposed over the same vertical wall (wall cavities/settlements). When dug inside individual pinnacles they are called "cone cavities" (Fig. 1,2).

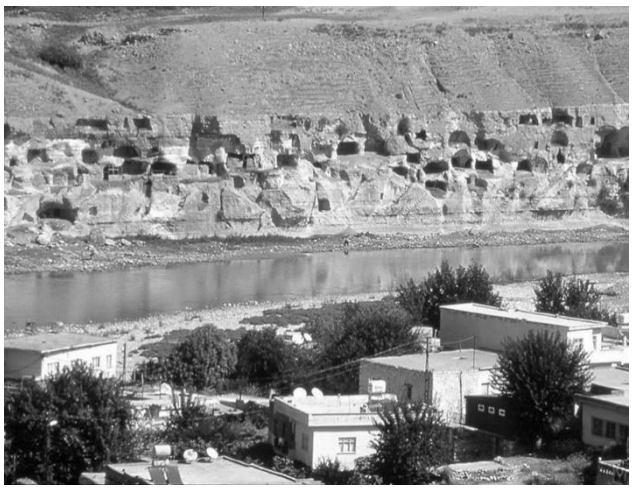

Fig. 1. *Cliff rock-cut village of Hasankeyf on the Tigris River, in southeasternTurkey (photo M. Traverso)*

b) Underground structures, dug in depth (deep layer), under the ground level (mesas or plateau areas) or in the inner part of rock mountains (butte and other ridges). In this case, too, we can have networks extending on a single horizontal level (Figs. 3,4), or networks descending in the subsoil for tens of meters on superimposed levels (Figs. 5,6).

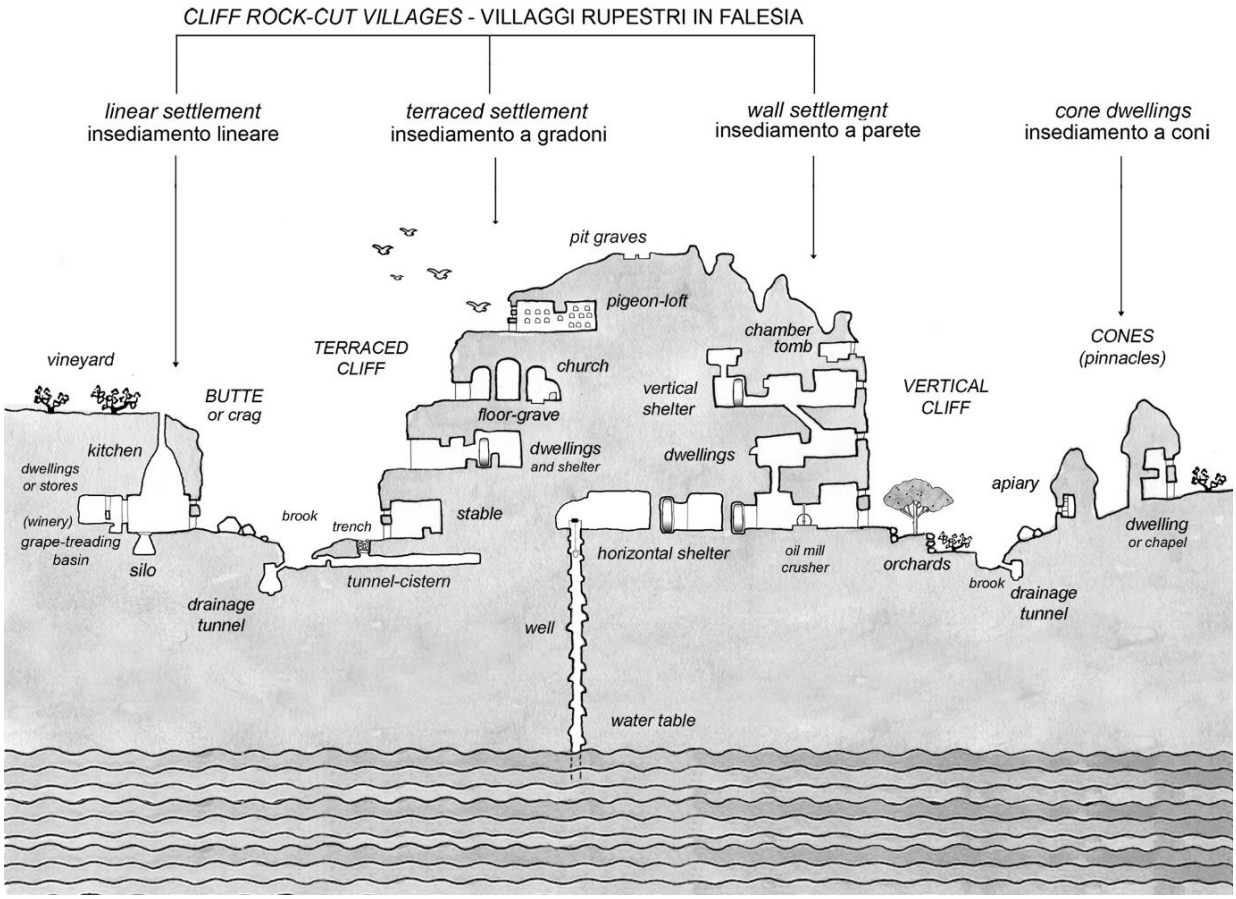

Fig. 2. *Exemplification of different cliff rock-cut village models in Cappadocia, central Turkey (drawing R. Bixio)*

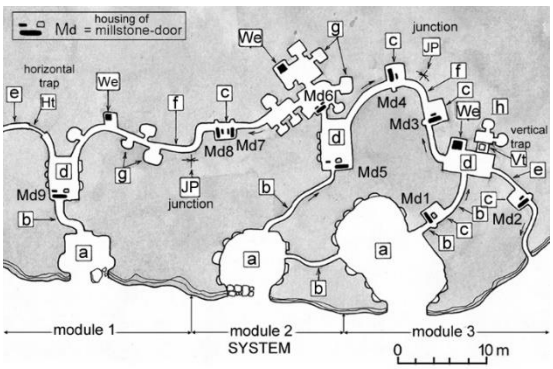

Fig. 3. *Scheme of the "horizontal" underground shelter of Filiktepe in Cappadocia, central Turkey (drawing R. Bixio)*

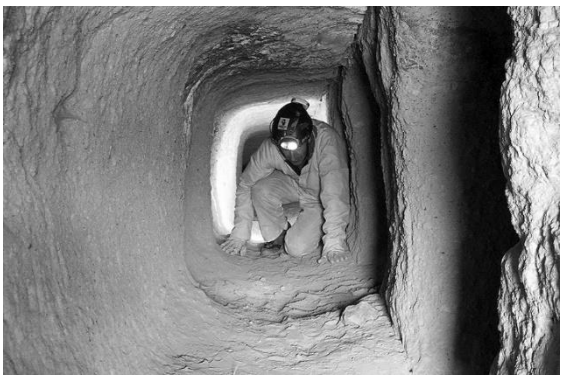

Fig. 4. *Artificial tunnel under the site of Ani, ancient capital of Armenian kingdom, now in - eastern Turkey (photo R. Bixio)*

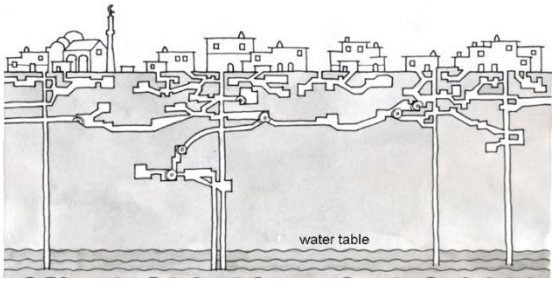

Fig. 5. *Scheme of the "vertical" underground settlement of Derinkuyu, in Cappadocia, central Turkey (drawing R. Bixio)*

Fig. 6. *Underground settlement of Derinkuyu in Cappadocia. Well at depth of about 40 m (photo G. Bologna)*

Note: the distinction between rock-cut cavities and underground cavities is not always clear, so that often the terms can be used interchangeably.

Cavities constructed in the subsoil

The underground spaces belonging to this category are those obtained with masonry works created to define volumes produced as a result of excavation of the subsoil, through two techniques.

c) Tunnel excavation technique (tunnelling). Removal of the rock is carried out entirely underground. The rooms are then coated with different masonry techniques. Coating can interest only part of the excavation.

d) Trench excavation technique. It is realized with a open air excavation, followed by total or partial coating of the walls, building of the vault, and finally re-covering (Fig. 7). It is a technique very useful at not great depths: generally, it is simpler, faster, and cheaper than the tunnel excavation technique. It can also be used in clayey soils.

In some cases, the walls are not coated, and the only built part is the cover, which can be with flat ceiling, obtained by laying stone slabs or concrete slabs, or barrel-like ceiling, obtained using various materials such as ashlars, bricks, or concrete.

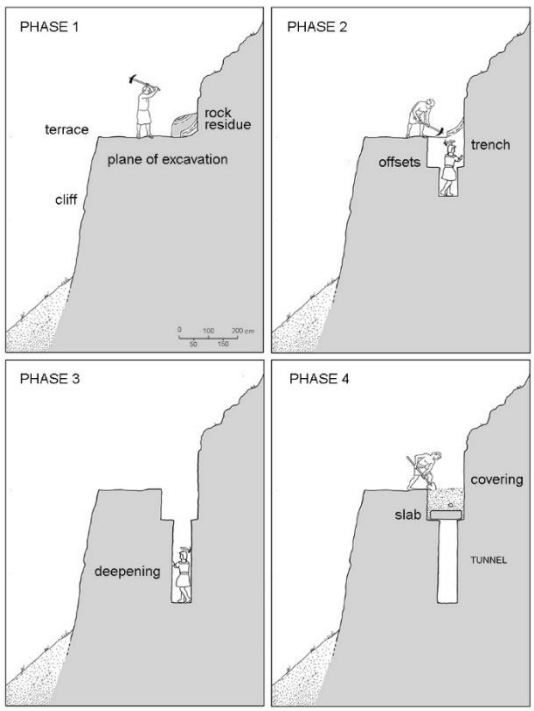

Fig .7. *Reconstruction of the excavation technique of the trench of Ahlat, lake Van, eastern Turkey (drawing R. Bixio)*

The underground aqueduct of Gravina in Puglia (Southern Italy), for example, has been realized with both the tunnelling technique, without any coating, and the trench excavation technique, with partial coating and barrel covering by tuff blocks (Fig. 8) [12,13].

Mixed artificial cavities

These are works dug to reach, extend or modify substantially a natural cave. The artificial part can be carried out with one of the methods described above.

We found a significant example of mixed cavity in the archaeological site of Troy (Turkey). This is a work for the low city's water supply, attributed to the 3rd millennium BC and used until the Byzantine period [14]. The initial part, accessible from the outside, is a natural tunnel. The artificial part consists of a long tunnel, almost straight, led from an internal point of the cave to the base of some ascending shafts/wells, dug into the body of the rock. The excavation of the tunnel was made using the opposite fronts technique, that is, by two teams digging one towards the other, most likely simultaneously: this is evidenced at the junction point, typically identified because of the change in direction and the related blind appendix due to a slight alignment error (Fig. 9).

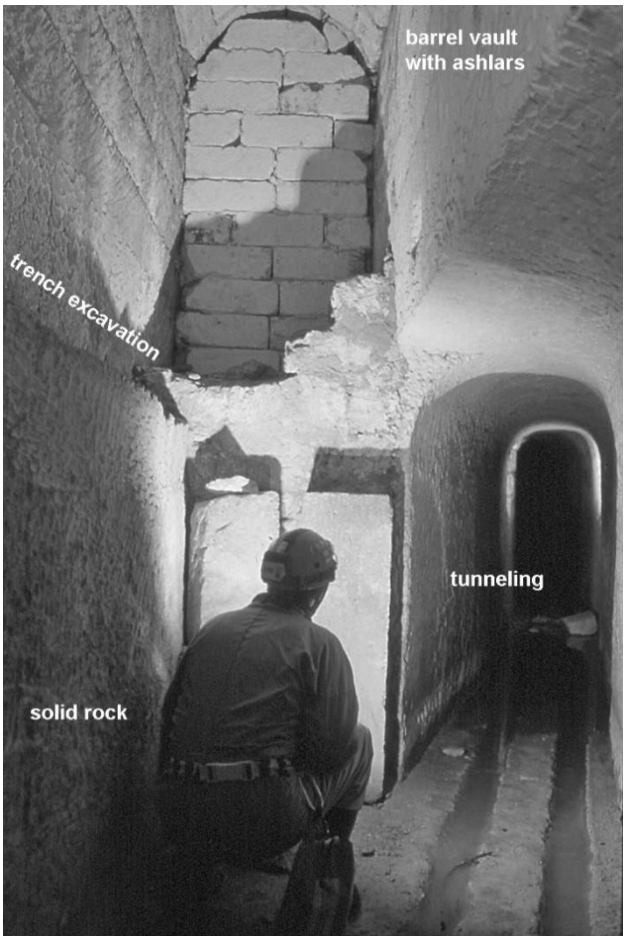

Fig. 8. *Underground aqueduct of Gravina in Puglia (southern Italy). Mixed excavation technique in solid rock: tunnel and trench, with partial coating and cover in stone ashlars (photo M. Traverso)*

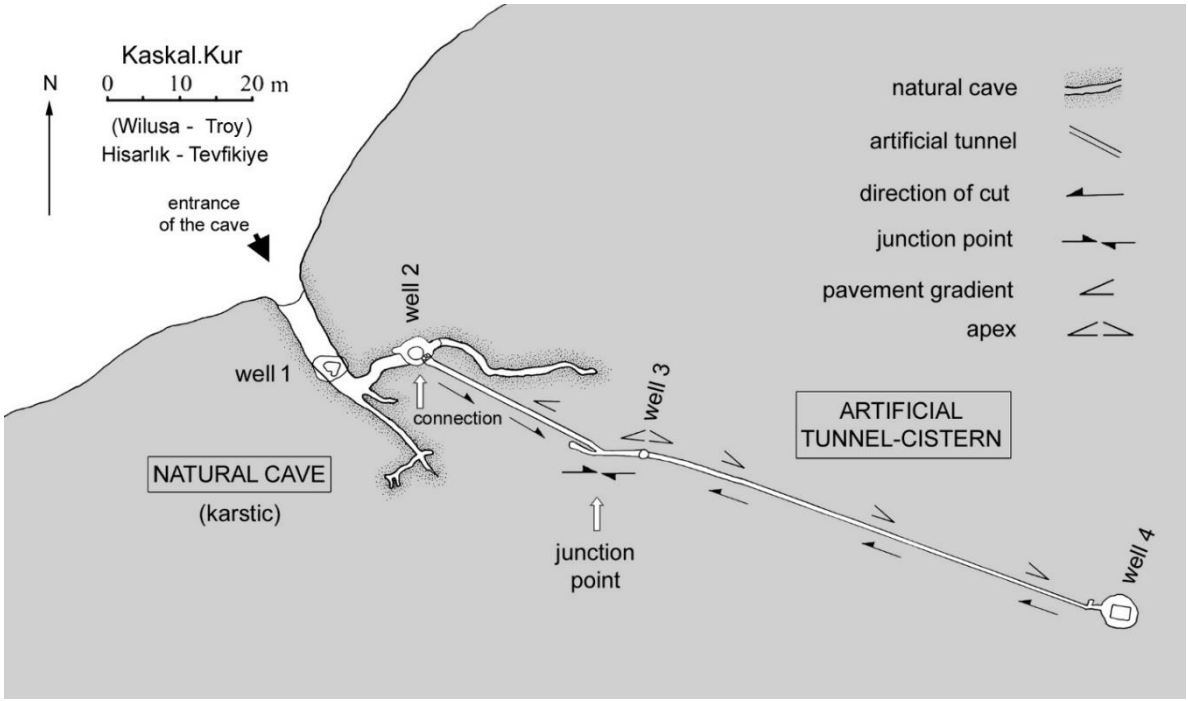

Fig. 9. *Plan of Troia water supplying tunnel, mixed cavity (R. Bixio, elaboration after M. Korfman 2003)*

Anthropized caves

We define "anthropized caves" the natural caves that have undergone limited human interventions. They represent the boundary line between the natural cavities, produced by weathering and geological phenomena, and the artificial or anthropic cavities, entirely man-made in the subsoil.

In general, these are wide but not very extensive caverns, in which man has built masonry structures, for dwelling and/or for worship, sometimes supplemented by small digging actions.

The best known examples are, for the first type, the "Pueblo" villages built by American Indians in Arizona, Colorado and New Mexico between the 12th and 14th centuries (Fig. 10).

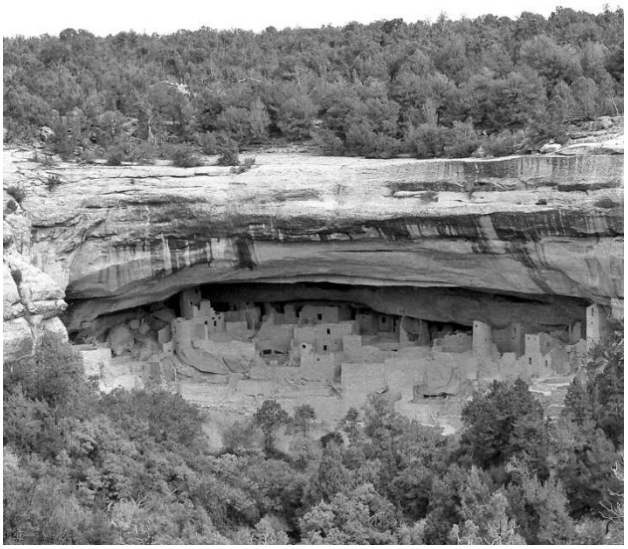

Fig. 10. *Antrophized cave: Pueblo at Mesa Verde in Colorado, USA (photo G. Stalteri)*

The second type is represented by the sanctuary-caves. We have examples in Italy (Santa Lucia, Toirano), France (La Saint Baume, near Var), Turkey (Sumela, near Trabzon), to cite a few, and in many other places in the Mediterranean basin, where there are churches and monasteries from the early centuries of Christianity, built inside karst caves.

Non-excavated artificial cavities

Finally, we describe the "re-covered cavities" and the "anomalous cavities" that are quite different from the rupestrian works, as previously defined, because they do not contemplate digging works to obtain spaces within the rock mass. However, they are included in the classification of the *Commissione Nazionale Cavità Artificiali* and inserted in the related register, as there is no doubt that, by their nature, they fall within the categories of anthropic cavities.

Cavities obtained by re-covering

Often the human activity on surface, particularly in urban areas, has produced the overlap, the burial and the embedding of natural or artificial spaces originally not located in underground spaces.

For example, the fifty-two streams crossing the city of Genoa (Italy), in medieval times flowed in sub-aerial beds [15,16]. The need, with urban growth, to obtain new spaces for the city, has caused over the centuries their progressive coverage (Fig. 11), almost always coincident with road axis, producing the incorporation of existing structures (bridges, dikes, masonry banks, remains of buildings, etc.).

Fig. 11. *Rio Groppo, Liguria, Italy. Tunnel obtained with the cover of the river bed (photo M. Traverso)*

For the sake of completeness, we would like to remind that there are also natural underground waterways (karst rivers) throughout the world. In this case, they are considered as natural caves, and therefore included in the Register of the Natural Cavities of the Italian Speleological Society.

Anomalous cavities, constructed above the surface

These are works built in elevation, or as part of buildings at the surface, but with characteristics similar to real underground spaces.

The best known example is documented inside the pyramid of Cheops at Giza (Cairo, Egypt), dating from the fourth dynasty, about 2500 BC [17]. The "Great Pyramid", a massive structure composed of gigantic blocks of stone, is crossed by a series of tunnels and rooms where it is possible to transit for a total extent of about 400 metres. The oldest tunnels were dug under the basement, directly into the solid rock. They fall into the category of "underground cavities". Other passages are placed in the body itself of the structure, above the natural level of the plateau. They were realized simultaneously to the laying of the blocks, and are therefore classified as "anomalous cavitie" (Fig. 12).

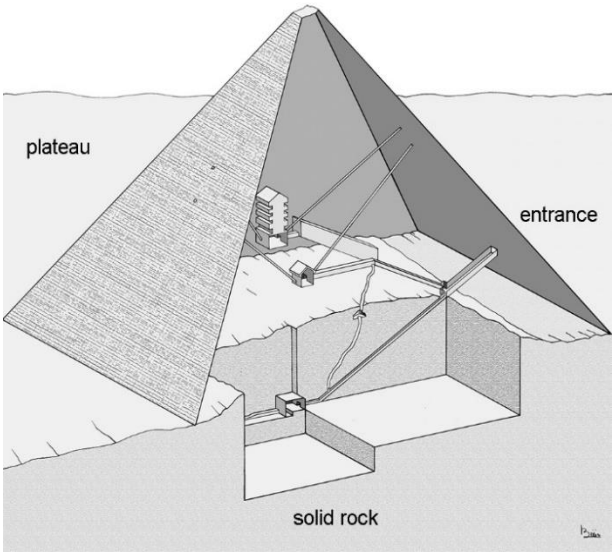

Fig. 12. *Section of Cheops' pyramid with tunnels and sepulchral chambers representation (drawing R. Bixio)*

Another striking example is the "Ponte Monumentale" (Monumental Bridge) at Genoa (Italy). It is a viaduct that crosses a road below, therefore suspended at 20 m from the ground (Fig. 14). The internal structure is hollow, supported by transversal wings (wall sections) in exposed stone with sub-circular arches that appear concentric due to the curvature of the extrados (Fig. 13). Access and investigation inside the bridge are faced as real speleological explorations [18].

Fig. 13. *Genoa (Italy). Interior of Ponte Monumentale (photo C. Leoni)*

Results and Discussion

The results of the study and the indicated classification (Table) will enable builders, engineers, and urban planners to take appropriate measures to ensure the safety and stability of their designs already at the planning stage, to reduce possible risks while designing roads and hydro-engineering structures in places where underground structures are numerous. These investigations particularly refer to the central and southeastern part of Turkey, including Cappadocia, Akhlat, Ani, and Armenia's Syunik, Shirak, and Aragatsotn regions.

Fig. 14. *Genoa (Italy). Exterior of Ponte Monumentale (photo A. Bixio)*

Conclusion

Definition of the different categories of artificial cavities according to the construction techniques, here illustrated, started up - as mentioned - in CNCA after decades of explorations conducted with a multidisciplinary approach, in various underground works all over the world, and from the need to establish clear and shared criteria useful to their study and classification.

The formalized categories allow, together with the functional investigation of artificial cavities and the relating typological cataloguing, to have a reading-key for a basic scientific analysis, from which to develop – case by case - the specific research on each underground structure, aimed at better understanding the fundamental elements such as age, original purpose, modification, and reuse over time.

For each artificial cavity the survey and the study of the construction techniques are fundamental, inextricably linked to that of the work signs left during the construction of the work itself, such as marks produced by pickaxes, hammers and chisels on the rock walls, from which one can also infer the digging direction. These observations and surveys can provide crucial elements of interpretation and understanding about the underground setting, borrowing and adapting to artificial cavities those systems and approaches improved in the last thirty years by the Archaeology of the Architecture [19-22]. They allow to read properly, according to stratigraphic principles, the peculiar characteristics of the "masonry evidences" shaped by subtraction of the raw material, following the excavation of rock masses whose modelling of empty spaces create the hypogean structure: from the general structures (floors, wall covering, pillars and roofs), to the specific elements (frames, capitals, scaffolding holes and plasters) forming the artificial cavity.

In many cases it is possible to distinguish different "stratigraphic masonry unit" useful for relative dating of the structure, and often in connection with various construction techniques. The measurement of recurring elements in artificial cavities, such as niches and footholds, in addition to the possible presence of structural components also characteristic of the elevated architecture, such as brick and stone ashlars, can be used to recognize these elements as possible chronological indicators, as developed again by the Mensiochronology [23].

In summary, the study about the origin and the evolution of underground structures through the analysis of their way of execution and the use of the six general categories developed by the CNCA, based on the construction techniques above described (summarized in the Table together with the "type tree"), is a basic survey instrument designed to achieve a thorough historical understanding of the hypogean architectural heritage.

Table. Categories and Types of artificial cavities classified by Commissione Nazionale Cavità Artificiali of Società Speleologica Italiana (R. Bixio, elaboration after Bixio and Galeazzi 2009: //document.speleo.it/)

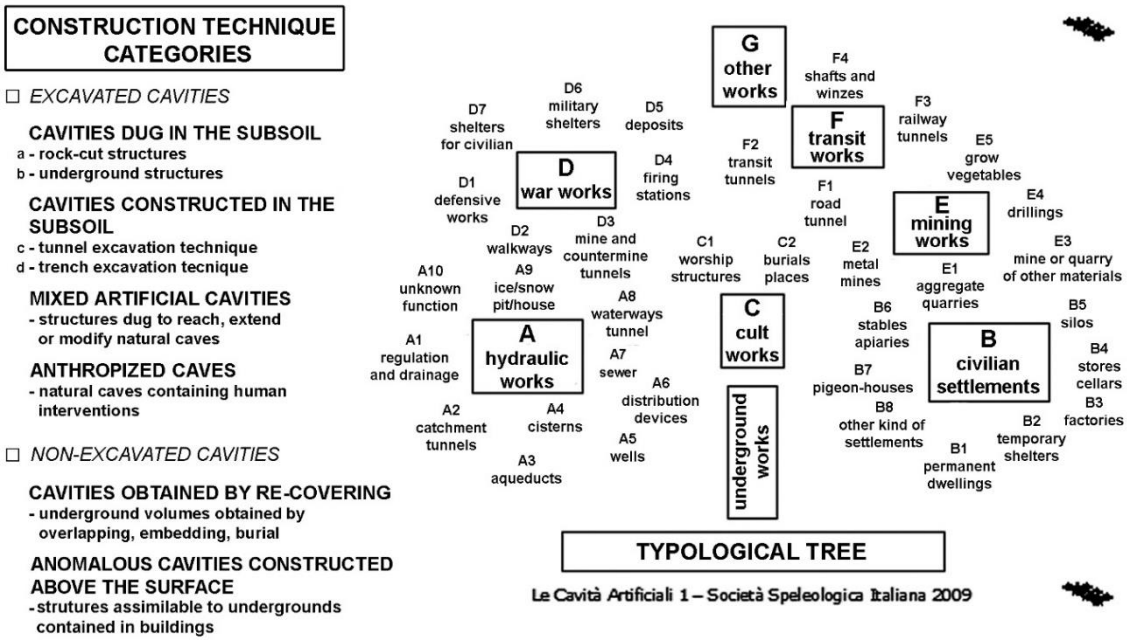

References

[1]. G. Cappa, Procedure per l'accatastamento di Cavità Artificiali. Società Speleologica Italiana, Bologna, 1999 (in Italian).

[2]. E. Di Labio, I dati sintetici. L'albero delle tipologie. Dati catastali, in: E. Di Labio (ed.), Il Catasto Nazionale delle Cavità Artificiali. Opera Ipogea, anno VI (2/3), 2004, 9-79 (in Italian).

[3]. P. Guglia, Il Catasto Nazionale delle Cavità Artificiali, in: E. Di Labio (ed.). Il Catasto Nazionale delle Cavità Artificiali. Opera Ipogea, anno VI (2/3), 2004, 5-8 (in Italian).

[4]. C. Galeazzi, The typological tree of artificial cavities: a contribution by the Commission of the Italian Speleological Society. Opera Ipogea, 1, 2013, 9-18 (in Italian).

[5]. M. Parise, A. Federico, M. Delle Rose, M. Sammarco,. Karst terminology in Apulia (southern Italy). Acta Carsologica, 32 (2), 2003, 65-82.

[6]. R. Bixio, C. Galeazzi, Le cavità artificiali 1: categorie e tipologie, in: Progetto Power Point 'Risorse Didattiche per la Speleologia e il Carsismo', no. 41, Società Speleologica Italiana, 2009 (in Italian).

[7]. E. Di Labio, Catasto Nazionale delle Cavità Artificiali. Aggiornamenti: Abruzzo, Lazio, Piemonte, Toscana, Trentino Alto Adige. Opera Ipogea, anno VIII (1/2), 2006, 89-94 (in Italian).

[8]. M. Meneghini, Situazione aggiornata del Catasto Nazionale delle Cavità Artificiali della Società Speleologica Italiana. Atti VI Convegno Nazionale di Speleologia in cavità artificiali (30 maggio-2 giugno 2008, Napoli). Opera Ipogea, anno X (1/2, 2008, 235-260 (in Italian).

[9]. M. Meneghini, Aggiornamento dei dati del Catasto Nazionale delle Cavità Artificiali. Atti VII Convegno Nazionale di Speleologia in cavità artificiali (2010, Urbino). Opera Ipogea, anno XIII (1/2), 2011, 229-244 (in Italian).

[10]. R. Bixio, Cappadocia: records of the underground sites. British Archaeological Report (BAR), International Series, 2413. Archaeopress, Oxford, 2012, 10-20.

[11]. G. Golany, Chineseearth-sheltered dwellings. University of Hawaii Press, 1992.

[12]. R. Bixio, V. Castellani, P. Maifredi, S. Saj, L'acquedotto sotterraneo di Gravina in Puglia "Sant'Angelo-Fontane della Stella", in: Il Parco della Pietra e dell'Acqua, Consorzio Sidin/UNESCO, Gravina in Puglia, 2000, 215-253 (in Italian).

[13]. R. Bixio, M. Parise, S. Saj, M. Traverso, L'acquedotto sotterraneo di Gravina in Puglia "Sant'Angelo-Fontane della Stella". Opera Ipogea, anno IX (1), 2007, 105-112 (in Italian).

[14]. M. Korfmann, Troia in light of new research. Reden an der Universität (Dies academicus 2003), English edition, Universität Trier, 2003, 38-39.

[15]. P. Melli, R. Bixio, L. Ferrando, S. Saj, M. Traverso, Genova sotterranea. Erga edizioni, Genova, 2006, 64-65 (in Italian).

[16]. R. Bixio, F. Faccini, A. Maifredi, L. Perasso, S. Saj, M. Traverso, The culverted streams in the historical amphitheatre of Genoa city (Italy): flood risk or geoheritage protection?. Proceedings of the International Congress in Artificial Cavities 'Hypogea 2017', Cappadocia (Turkey), March 6-8, 2017, 165-176.

[17]. J. Baynes, J. Malek, Atlante dell'Antico Egitto. Istituto Geografico De Agostani, Novara, 1985, 156-161 (in Italian).

[18]. R. Bixio, M. Traverso, S. Saj, Un sotterraneo sospeso nel vuoto: il Ponte Monumentale di Genova - La Casana 3, anno LIII, 2011, 16-19. Banca Carige editore, Genova (in Italian).

[19]. G.P. Brogiolo, Archeologia dell'edilizia storica. Como, 1988 (in Italian).

[20]. A. Cagnana, Archeologia dei materiali da costruzione. Mantova, 2000 (in Italian).

[21]. A. Azkarate Garai-Olaun, L. Caballero Zoreda, J.A. Quirós Castillo, Editorial: Arqueología de la arquitectura: definición disciplinar y nuevas perspectivas. Arqueología de la Arquitectura, 1, 2002, 7-10 (in Spanish).

[22]. T. Mannoni, Archeologia della produzione architettonica. Le tecniche costruttive. Arqueología de la Arquitectura, 4, 2005, 11-19 (in Italian).

[23]. T. Mannoni, M. Milanese, 1988. Mensiocronologia, in: R. Francovich, R. Parenti (eds.), Archeologia e restauro dei monumenti. Firenze, 383-402 (in Italian).

Bixio Roberto, *Union International de Spéléologie, Artificial Cavities Commission (Slovenia, Postojna), roberto.bixio@gmail.com*

De Pascale Andrea, *Civic Museums of Genoa, Educational Services and Cultural Mediation (Italy, Genoa), adepascale@comune.genova.it*

Galeazzi Carla, *Union International de Spéléologie, Artificial Cavities Commission (Slovenia, Postojna); Egeria Underground Research Centre (Italy, Rome); National Commission on Artificial Cavities - Italian Speleological Society (Italy, Bologna), carla.galeazzi123@gmail.com*

Parise Mario, *Union International de Spéléologie, Artificial Cavities Commission (Slovenia, Postojna); Department of Earth and Geo-Environmental Sciences, University Aldo Moro (Italy, Bari), mario.parise@uniba.it*

POSSIBLE PROSPECTS FOR HEAT SUPPLY OF MULTI-APARTMENT BUILDINGS IN ARMENIA

Anna Karamyan [1]*, Artur Avetisyan[1], Stefan Noack[2]

[1] *National University of Architecture and Construction of Armenia, Yerevan, RA*

[2] *University of Applied Sciences Zwickau, Germany*

Abstract: *The research was carried out for the selection of optimal options for the heat supply of multi-apartment buildings, taking as an example several new buildings in Yerevan. The purpose of the study is to confirm the choice of the best method of providing heat in apartment complexes. It was used to calculate and analyze the energy-economic and operational-technical indicators of individual heating boilers, small centralized systems, and hybrid systems to solve this problem. The calculations considered both natural gas tariffs and fluctuations in the value of the Armenian dram against the US dollar. The value of 1 kWh of thermal energy or specific heat capacity has been determined as an important criterion for choosing the most efficient method of heat supply, considering the careful analysis of almost all variable factors.*

Keywords: *multi-apartment, individual or centralized heat supply, specific heat capacity.*

Anna Karamyan *

E-mail: a.qaramyan@nuaca.am

Received: 18.03.2023
Revised: 10.04.2023
Accepted: 26.04.2023

Introduction

The best solutions for heat supply have been the subject of numerous studies in the past, but the relevance of this research has increased due to contemporary social and political circumstances [1,2].

Since the RA and many other nations import fuel, their economies strongly depend on the stability of its price and supply, making efficient methods for heating apartment complexes a crucial concern.

Central boiler houses and thermal power plants (TPPs), were the primary source of heat for the cities of the former Soviet Union and many other Eastern European nations [3]. The heat was transferred through heating networks. After the energy crisis of the early 1990s, when gas supplies to the country fully ceased, Armenia's district heating systems essentially stopped functioning. New issues with the heating of residential areas emerged once the gas supply was resumed in the early 2000s [4].

Using cutting-edge cogeneration technology at the time, some regions of the RA made an effort to rehabilitate central heating systems [5,6]. Due to the outdoor heating network's prolonged idleness, it deteriorated, and the heating systems of apartment buildings were either fully or partially disassembled. Since the beginning of the certificate of property rights to real estate, it has been technically impossible to restore the unified heat supply system for buildings because it would require large investments. It became common to install individual gas boilers to heat each apartment in multi-unit residential buildings as well as individual homes [7].

It is necessary to compare and assess the viability of individual and centralized heat supply options in apartment buildings that are currently under construction, taking into account the proportion of thermal energy consumed by residential buildings in the Republic of Armenia's overall energy balance as well as a noticeable increase in newly built residential buildings. The probability of gas equipment mishaps and water leaks in the heating systems is extremely high, despite the fact that individual heating systems are not supervised by the building operator. Due to the fact that the heating boiler, heating appliances, as well as the acquisition, installation, and ongoing maintenance of the system, are typically handled in this situation, the majority of developers continue to prefer the individual-apartment version of building heating and hot water supply [6].

The theoretical value of the generated thermal energy should be utilized as the main criterion for orientation, however, considering the regulatory framework of the republic and the socioeconomic position of the population [8,9].

Based on the peculiarities of settlement development, individual gas boilers with a capacity of 24-32 kW are now used in the Republic of Armenia to heat apartments. The typical heat load of apartments or small private homes under "Yerevan parameters" throughout the heating season calculation period is 4–12 kW.

According to our past research:

- 8–12 kW in January,
- 6–8 kW in December,
- 8–12 kW in February,
- 4-6 kW around in November and March.

So, an apartment or private home's gas boiler, therefore, runs at 35 to 55 percent load [5]. The "Yerevan parameters" do not only apply to the city of Yerevan, it should be mentioned, based on the Republic of Armenia's territory's climate zoning, which takes into account climate, degree-days, the length of the heating season, and a seasonal benchmark for energy production[1] (Fig.1). The trends found by the study can be applied to other communities in the third zone, which composes around 20% of the republic's land area and is also the most densely populated in Armenia (56 percent of the total population) [9].

Fig. 1. *RA Climatic Zones*
1 - Cold Dry, 2 - Temperate, 3 - Hot dry, 4 - Cold humid, 5 - Average cold, 6 - Hot medium humid

The choice of heat source is not necessarily ideal in a traditional district heating system with huge district heating boilers or TPPs because of the network's high heat loss, particularly in the case of TPPs.

Since investments for medium and small businesses are mainly made through banks, attracting private capital is counterproductive. As a result, local residents are often forced to use individual heating systems for their homes.

The main focus is on the use of individual heating and hot water systems, with the expanded use of renewable energy sources, in accordance with the regulation on heat supply of the program ensuring the growth of the energy sector of the RA until 2040[2,3].

Materials and Methods

Various new building projects were surveyed in Yerevan's administrative districts of Shengavit, Kanaker-Zeytun, Malatia-Sebastia, Ajapnyak, and Kentron. They were contrasted in terms of how they delivered heat. To compare the economic viability of two systems, centralized and individual heat supply, it is crucial to calculate the precise values of thermal energy generated. In this study, the boiler rooms designed for multi-apartment buildings' own needs are considered central heating systems.

[1] RACN II-7.01-2011**,** Construction Norms, Construction climatology, Yerevan, 2013.
[2] Energy Law of the Republic of Armenia, March 7, 2001.
[3] Government of RA. Resolution No. 48-L. To adopt the Republic of Armenia's strategic plan for the development of the energy sector (until 2040), the plan-time-table assuring the implementation of the strategic plan for the development of the energy sector (until 2040), and a number of government decisions on repeal; 14.01.2021.

Table 1 presents the geometric and thermal characteristics of apartment buildings designed for several districts of Yerevan, RA in 2020-2022. The Table shows the number of stories of buildings, the number of apartments, the estimated number of residents, the heated volume, the calculated heating and ventilation load, and the specific heat and power characteristics of heating and ventilation [1]. Calculations were carried out for the difference in air temperatures in the room and outside ($\Delta T = 39K$). The thermal protection characteristics of building envelopes designed after 2016 practically do not differ from each other and comply with the requirements of RASN 24-01-2016. When calculating the thermal and ventilation loads of buildings, the materials of the external structures of buildings and their design features were considered[4].

Table 1. Geometric and thermal characteristics of apartment buildings designed for several districts of Yerevan, RA in 2020-2022

N	District	Number of floors	Living area (m^2)	Heated volume (m^3)	Number of apartments	Number of inhabitants	Heating and ventilation loads (*kW*)	Hot waterheat load (*kW*)	Specific thermal energy characteristics ($W / (m^3 K)$)
1.	Shengavit	10	5300	15900	110	330	259.2	627	0.418
2.	Kanaker-Zeytun	14	6048	18144	84	252	358.2	377.0	0.506
3.	Malatia-Sebastia	18	8586	25758	72	216	447.2	471.0	0.445
4.	Achapnyak	17	6562	19686	102	306	447.7	667.1	0.583
5.	Kentron	16	11376	34128	128	384	513.4	729.6	0.386

Let's assume that the lower combustion heat of natural gas imported to Armenia has an average value of 8000–8200 kcal/m^3. Assuming that natural gas's average lower combustion heat is 8000 kcal/m^3, it turns out that burning 1 m^3 of gas results in the production of 9.3 kWh of heat.

The studies were conducted between May 2021 and June 2022. The calculations were made taking into account the natural gas tariffs that were valid until 04/01/2022[5], and set after 01/04/2022[6]. In the first case, with the consumption of up to 10.000 m^3 of natural gas, the monthly tariff for 1.000 m^3 of natural gas was 139.000 drams including value added tax, in the second case – 143.

700 drams including value added tax. For consumers with a monthly consumption of 10.000 m^3 or more, the price of each 1.000 m^3 of natural gas sold is $255.91 and $265.81, respectively, including value-added tax. The tariff has increased by 3-4 percent.

During this time, the cost of natural gas sold to consumers has fluctuated significantly, as has the exchange rate of the US dollar against the Armenian dram (the US currency has depreciated by more than 27 percent, see Fig. 2, line 1). Since RA is a fuel-importing country, changes in the exchange rate have a large impact on the economy, especially in the gas and heat supply sectors. Taking into account exceptional fluctuations in the exchange rate of the US dollar (USD) against the Armenian dram (AMD) (see Fig. 2, line 2). The average exchange rate index for the period from May 2021 to June 2022[7,8] was also determined [10].

[4] RACN 24-01-2016, Construction Norms, Thermal Protection of Buildings, Yerevan, 2016.
[5] Tigran Gnuni. 2018. Energy Balance of the Republic of Armenia. Development of Armenia's Fourth National Communication and Second Biennial Update Report to the UNFCCC.
[6] RACN II-7.02-1995, Construction Norms, Building Thermophysics of Fencing constructions, Yerevan, 1995.
[7] Central Bank of the Republic of Armenia, https://www.cba.am/am/SitePages/ExchangeArchive.aspx-URL 26.05.2022
[8] RA Public Services Regulatory Commission. Decision No. 83-N.

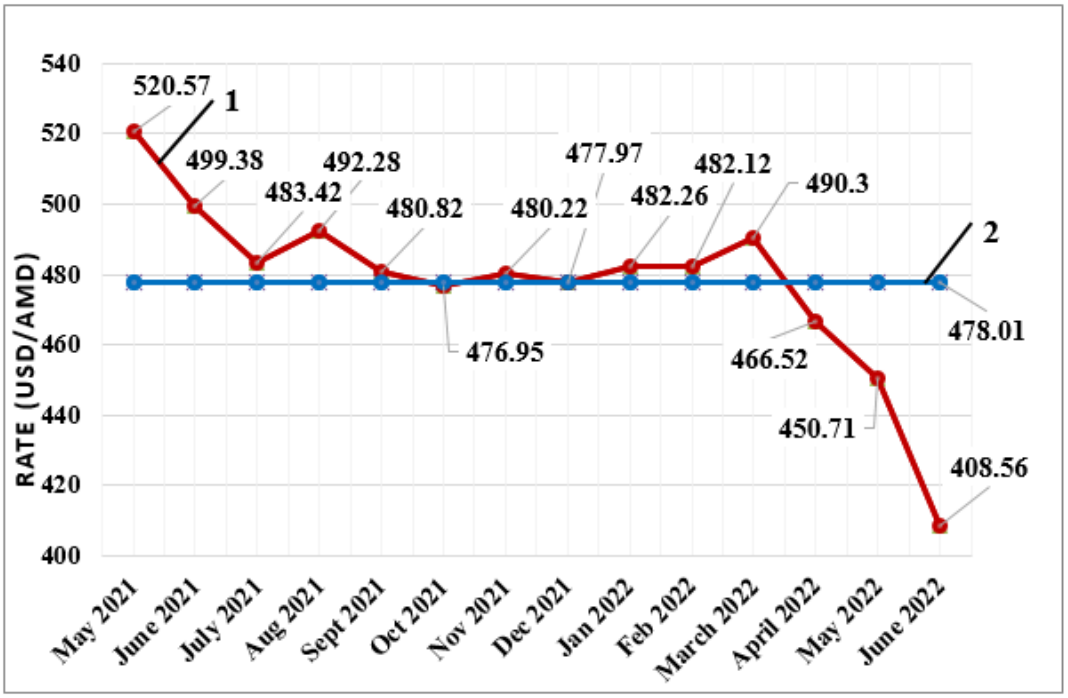

Fig. 2. *May 2021 to June 2022 fluctuations in the USD/AMD exchange rate*

Natural gas usage for residential needs (heating, domestic hot water, cooking) is limited to 10.000 m^3, while power plants, production facilities, boiler houses, and other facilities all use 10.000 m^3 or more.

To ensure that the calculations were practical, they were also performed using the following formula for determining the unit cost of the product, which is currently widely used [8,9]:

$$C_i = \frac{K_i + E_i + M_i + H_i}{Q_i},$$

K_i is the annual component of capital investments (*AMD/USD),*

E_i is the system operation annual cost (*AMD/USD),*

M_i are mandatory costs regardless of production processes (such as salaries and benefits), *(AMD/USD),*

H_i are taxes and fees (*AMD / USD),*

Q_i is the annual amount of heat received (*kWh/year*).

For clients with a monthly usage of up to 10.000 m^3 of natural gas, the price per 1000 m^3 was 255.91 USD in 2021 and 265.85 USD in 2022[9]. Production facilities, massive boilers, thermal power plants, etc. use more than 10.000 m^3 [10].

For the observed apartment buildings, the specific value of thermal energy was calculated in 2 variants: in one case with a centralized heating system, in the other case with individual boilers. Table 2 shows the calculation results. According to studies, a medium-capacity boiler's average seasonal efficiency is about 0.85. The specific average cost of heat energy with centralized heat supply was around 0.042 USD/kWh (before 01/04/2022) and around 0.044 USD/kWh (after 01/04/2022), while with decentralized heat supply, the average value was around 0.113 USD/kWh (until 04/01/2022) and 0.126 USD/kWh (after 04/01/2022).

[9] RA Public Services Regulatory Commission. Decision N95 and, Natural Gas Supply and Use Rules, 08.07.2005.

[10] RA Public Services Regulatory Commission. Decision № 221-N. - On repealing the decision 333 of November 25, 2016 of the Public Services Regulatory Commission of the Republic of Armenia to set the tariffs for natural gas sold to consumers by "Gazprom Armenia" Closed Joint-Stock Company. 19.06.2020.

Table 2. Value of the product or specific heat capacity (SHC), *(USD/ kWh)*

Value	Centralized heating					Individual heating
	№ 1	№ 2	№ 3	№ 4	№ 5	
Value of the product (SHC), (*USD/ kWh)*	Up to 01.04.2022					
	0.046	0.037	0.04	0.043	0.042	0.1
	After 01.04.2022					
	0.048	0.039	0.042	0.046	0.045	0.13

The estimates take inflation into account in addition to variations in the dram's value relative to the US dollar and natural gas tariffs. In particular, the 12-month average inflation rate in Armenia (June 2022 compared to June 2021) was 10.3 percent based on data released by the RA Statistical Committee. According to a thorough review of all indications, the cost of 1 *kWh* of thermal energy increased by approximately 5% with centralized heat supply and by approximately 12% with individual heat supply[11].

Result and Discussion

Based on the study, an attempt was made to justify the choice of an effective method of heat supply. In this paper, the authors did not consider all aspects of energy saving in buildings, which will help reduce the energy consumption of buildings and dependence on imported fuel and energy resources. However, having assessed the danger of the method of providing heat supply by individual boilers, which is widely used in multi-apartment buildings being designed and newly built today, attention was also paid to the energy-economic side of this important issue. The study carried out in the article can serve as a basis for further correction of the vision of heat supply in the Republic of Armenia, quickly overcoming the problems associated with the import of fuel resources, in particular natural gas, to create prerequisites for effective and sustainable harmonious development.

Conclusion

Thus, along with the growth of modern construction in the Republic of Armenia, important issues that contribute to increasing the energy independence of the country and protecting the environment are ignored. In the Republic of Armenia, the regulatory and technical base of approaches to the design of apartment buildings is far behind the requirements of the time. Not only normative documents on heat supply of multi-apartment buildings and new residential areas are subject to revision, but also the attitude of residents to receive more affordable and safe heat supply.

References

[1]. V.L. Granovskiy, Individual Metering of Heating Energy in Apartment Buildings: Specifics, Opportunities, Problems. ABOK, 2, 2020, 58-64.
[2]. Marco Siddi, Theorising Conflict and Cooperation in EU-Russia Energy Relations: Ideas, Identities and Material Factors in the Nord Stream 2 Debate. East European Politics, 36(2) (2019), 544-563. Doi: https://doi.org/10.1080/21599165.2019.1700955
[3]. A. Bloess, W-P. Schill, A. Zerrahn, Power-to-Heat for Renewable Energy Integration: A Review of Technologies, Modeling Approaches, and Flexibility Potentials. Applied Energy, 212, 2018, 1611-1626.
[4]. Sonny Myrefelt, Functional Availability of HVAC Systems. International Journal of Ventilation, 2016, 89-98. Doi: https://doi.org/10.1080/14733315.2008.11683802
[5]. A.G. Avetisyan, Analysis of Power and Economic Indicators of Heat and Cold Supply Systems and Development of New Technological Scheme. Bulletin of the National University of Architecture and Construction of Armenia, 1 (58), 2018, 109-116 (in Armenian).

[11] Statistical Committee of the Republic of Armenia. https://www.armstat.am/ - URL - 07.07.2022.

[6]. A.G. Avetisyan, The Application of Seasonal Energy Efficiency Ratio of the Residential Houses Heating System for the Energetic Zoning of the RA Territory. Bulletin of the National University of Architecture and Construction of Armenia, 2 (51), 2016, 67-73 (in Armenian).
[7]. A.L. Petrosyan, A.G Avetisyan, HH klimayakan paymanneri verlutsut'yuny tarber jermaghbyurneri energetik bnutagreri voroshman u hamematman hamar. Bulletin of Builders' Union of Armenia, 7-8 (179-180), 2012, 54-64 (in Armenian).
[8]. A.G. Avetisyan, Jermagazamatakararman yev odapokhutyan hamakargeri ekonomika yev energatntesakan ardyunavetutyan bardzratsman metodabanutyun. Printing and Information Center of National University of Architecture and Construction of Armenia, Yerevan, 2018 (in Armenian).
[9]. A.G. Avetisyan, A.L. Petrosyan, The Ways of Improving the Energy Efficiency in Heat and Cold Supply Systems of Buildings. The 5th International Renewable and Clean Energy Conference "The Prospects of Low Carbon Development in Armenia", Yerevan, Armenia, October 24 - 25, 2013, 147-152 (in Armenian).
[10]. A.K. Karamyan, Weather Control Management of Heating Systems as a Means of Increasing Energy Efficiency. Scientific Papers of National University of Architecture and Construction of Armenia, 4, 2012, 174-180.

Anna Karamyan, Doctor of Philosophy (PhD) in Engineering, Associated professor *(RA, Yerevan) - National University of Architecture and Construction of Armenia, Head of the Chair of Heat and Gas Supply and Ventilation, a.qaramyan@nuaca.am*

Artur Avetisyan, Doctor of Philosophy (PhD) in Engineering (*RA, Yerevan*) - *National University of Architecture and Construction of Armenia, Associate Professor at the Chair of Heat and Gas Supply and Ventilation, art.avetisyan@gazpromarmenia.am*

Stefan Noack, Master of Arts *(Zwickau, Germany) - University of Applied Sciences Zwickau, PhD student in a cooperative PhD program between Kazakh-American Free University, Ust-Kamenogorsk, Kazakhstan, and University of Applied Sciences Zwickau, Germany, stefan.noack.cyp@fh-zwickau.de*

PLANE-PARALLEL LAMINAR FLOW OF VISCOUS FLUID IN THE TRANSITION ZONE OF THE INLET SECTION

Arestak Sarukhanyan [1]*, Garnik Vermishyan [1], Hovhannes Kelejyan[1]

[1] *National University of Architecture and Construction of Armenia, Yerevan, RA*

Abstract: *A study was conducted to analyze how hydrodynamic parameters change in the entrance region of plane-parallel flow under stationary flow conditions, with an initial arbitrary distribution of velocities in the entrance section. This study was based on boundary layer equations, and a boundary problem was formed under the conditions of plane-parallel flow. The boundary conditions were chosen to reflect the pattern of arbitrary velocity distribution in the entrance section. A general solution of the approximating Navier-Stokes equations is provided, which depends on the initial conditions and the Reynolds number. The boundary conditions are established based on the nature of the motion, and the boundary value problem is described. A method for integrating the boundary value problem has been developed, and regularities for the change in velocities along the length of the inlet section have been obtained for both constant and parabolic velocity distributions in the entrance sections. Analytical solutions have been derived to obtain patterns of velocity and pressure changes in any given flow direction. Through computer analysis, velocity change patterns in various sections along the inlet transition area have been constructed, allowing for the determination of fluid velocity at any point on the section and an estimation of the length of the transition area. These proposed solutions provide a framework for accurately constructing individual units of hydromechanical equipment.*

Keywords: *viscous fluid, inlet section, velocity, velocity distribution, pressure, length.*

Arestak Sarukhanyan *

E-mail: asarukhanyan51@mail.ru

Received: 20.03.2023
Revised: 12.04.2023
Accepted: 28.04.2023

Introduction

Studies of velocity distribution patterns after the inlet section in closed beds show that the particles near the static walls perform a decelerated motion, and the particles near the axis experience an acceleration and perform an accelerated motion. These two tendencies result in a rearrangement of the velocity field at a certain point of the movement, causing a change in the distribution pattern of velocities in the inlet section. Within the transition zone, the distribution of the inlet section velocities is rearranged to match the velocity distribution pattern of the stabilized zone in closed beds. The accuracy of the research for the transition zone of the inlet section is determined by the challenges associated with the precise construction of the fluid channels of the machinery. It is necessary to ensure clear and stable operation of the control and regulation systems.

Therefore, the problem discussed is both relevant and of significant practical importance. The vital problem of fluid flow research is the mathematical model construction of the given physical phenomenon, which determines the applicability limits of the selected calculation method. It is vital that the built model more accurately describe the ongoing hydromechanical phenomena and, meanwhile provide the possibility of obtaining analytical solutions.

Literature review and problem statement

Research on the flow patterns of viscous fluid in transition areas of liquid channels, such as inlet and outlet sections, sudden expansion and narrowing, etc., is an applied problem that provides solutions for designing various machine tools. Due to their urgent and applied importance, the investigation of these problems remains highly relevant.

The starting equation for the study is the system of Navier-Stokes equations in a non-deformable medium. For each problem, boundary conditions are defined and the basic equations are simplified. However, obtaining analytical solutions to the problem is often not feasible. In such cases, modern computing techniques can provide an opportunity to obtain approximate solutions, which ensure accuracy in practice.

Many theoretical and approximate calculation methods have been developed for studying the hydrodynamic phenomena in the transition area of the inlet section.

Each calculation method is based on conclusions about the nature of the flow, which are used to conduct theoretical research and summarize the results. These conclusions often refer to certain ranges of motion, due to which the applicability of the obtained results is limited. A method for calculating the entrance transition area of plane-parallel motion was proposed in work [2], in which the author numerically implemented the integration of the boundary layer equations, which makes it possible to calculate the image of the distribution of velocities in any section of the transition area of the entrance section. Similar solutions were also implemented in [1]. In that study, solutions were obtained for velocity distribution and pressure change in the transition zone of the inlet section of the plane-parallel motion. These solutions were obtained using the parabolic law of velocity distribution in the boundary layer and the condition of their constancy at the core. Studies have been conducted to identify patterns of changes in the hydrodynamic parameters of the flow in the transition zone of the inlet section of the plane-parallel motion based on the approximation of the Navier-Stokes equations [3,4]. In these studies, a boundary problem was developed and analytical solutions were obtained to determine the patterns of changes in velocities and pressure. The results of the analytical solutions were compared with those obtained from experimental research, and the comparative analysis confirmed the reliability of the obtained results.

Similar research was conducted in [9], where approximate solutions were obtained for a cylindrical and plane-parallel isothermal laminar motion, providing results with sufficient accuracy. The study also investigated the laws of the velocity field and pressure change under conditions of a four-step change of velocities in the boundary layer of the entrance region [14].

In [11], the viscous fluid flow in the inlet transition zone under the conditions of changing pressure gradient in axisymmetric pipes is considered. The proposed solutions are also applicable to Newtonian fluids.

Under the conditions of varying the kinematic coefficient of viscosity according to an arbitrary law, the proposed solutions to the momentum equation [12] are represented by the Fourier series and the Bessel and Kelvin functions. Reference [13] analyzed flow stability based on the flow rate ratio to the steady-state laminar flow rate. This analysis led to the establishment of stability conditions for unsteady flow in a pipe. In [8], the authors developed a mathematical model to determine the velocity field and pressure distribution in the laminar motion of a viscous incompressible fluid in a two-dimensional change environment. However, the proposed solutions do not apply to determining the hydrodynamic parameters of the flow in areas of sudden expansion.

The studies mentioned mainly focus on the interpretation of phenomena occurring at the entrance of the pipe. However, hydrodynamic parameter rearrangement phenomena also occur at other transition sites in the pipe, for which research is scarce. For instance, at the site of sudden expansion of the cut (D/d = 4), numerical integration was utilized to construct current lines using the equations of plastic fluid current movement. This allowed for the determination of velocity and pressure changes in the axial direction [15].

Extensive experimental studies on the area of sudden expansion have been conducted [16]. The authors utilized the magnetic-resonance tomographic method to obtain quantitative estimates of the change in velocities in the transition area. Under conditions of sudden, symmetric and asymmetric expansion of the section, quantitative estimates of the Navier-Stokes equations' members were obtained, and the resulting nonlinear inhomogeneous differential equations were numerically integrated [18]. The integration results were compared with the results of experiments. Remarkable experimental studies on the region of sudden expansion were conducted in [19]. To that end, test equipment was constructed, and the areas of sudden expansion were

tested for the cases d/D = 0.22; 0.5 and 0.85. The investigations were carried out under both Newtonian and non-Newtonian fluid conditions.

The study [7] examined the patterns of changes in the hydrodynamic parameters of laminar motion in a viscous fluid at the transition zone of the entrance section of a cylindrical pipe with a radius R under the conditions of an initially arbitrary distribution of velocities.

Under these conditions, an axisymmetric, isothermal viscous fluid flow occurs. At the pipe inlet section, the velocity of the fluid $u = \varphi(r)$, which is moving with the velocity profile on the pipe wall, becomes zero. It leads to a deformation of the velocity profile, which extends over a certain distance along the length of the pipe. A boundary layer is formed near the pipe walls, where the velocity gradient $\frac{du}{dn}$ becomes very large. It causes friction forces to take on high values regardless of the viscosity coefficient μ. The boundary layer gradually spreads from near the pipe walls until it covers the entire pipe. Therefore, studies should be conducted in the transition area using boundary layer equations.

The aim and objectives of the study

The theoretical aim of studying the transition zone is to obtain patterns of variation in hydrodynamic parameters along the length of the pipe and to develop methods for calculating energy losses.

The study aims to find patterns in the hydrodynamic parameters of a viscous fluid while flowing through a round pipe, depending on the Reynolds number.

To achieve this goal, the following tasks must be accomplished:

- to develop a boundary value problem and determine the initial and boundary conditions,
- to develop a method for solving the boundary value problem and identifying patterns of changes in hydrodynamic parameters of the viscous flow at the entrance section of the plane-parallel pressure movement,
- to construct graphs of changes in axial velocities in length and Reynolds numbers,
- to identify conditions for determining the length of the entrance section.

Materials and Methods

Choosing a Calculation Scheme

The study observes the plane-parallel laminar flow of the viscous fluid at the transition zone of the entrance section. The origin of the Z-axis is the center of the entrance section (as shown in Fig. 1) and is directed infinitely long in the direction of motion.

Plane-parallel motion in a round pipe will be considered in Cartesian coordinates, starting from the zero point (Fig. 1).

The study assumes that the velocities change according to an arbitrary law at z=1 in the entrance section. It is necessary to find patterns of change in the hydrodynamic parameters of a viscous fluid in the transition zone, considering them to be axisymmetric and non-stationary. Mass forces are neglected.

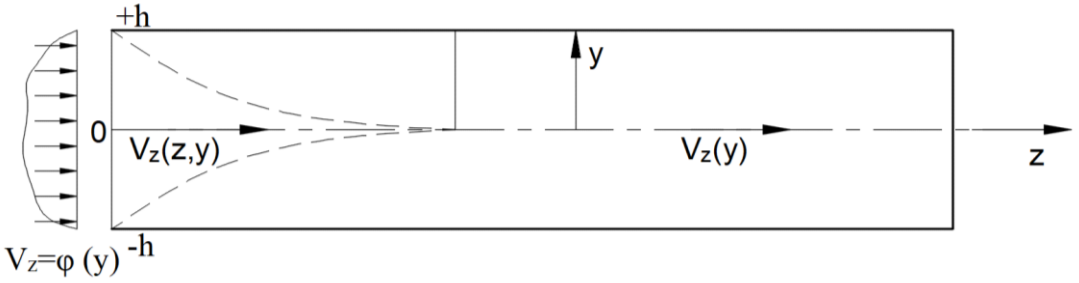

Fig. 1. *On the study of a viscous incompressible fluid at the inlet plane-parallel motion*

Statement of the problem and formulation of the system of differential equations for the study

Let's assume we have two stationary walls placed at a distance of 2 h from each other, between which there is a laminar, static viscous fluid flow. The pattern of the distribution of forces in the entrance section is given in the form of an arbitrary function $V_z = \varphi(y)$.

Under these conditions, an axisymmetric, isothermal movement of a viscous fluid flow occurs. Fluid velocity at the pipe inlet is $u = \varphi(y)$, and a deformation of the velocity profile occurs over a certain distance. A boundary layer occurs near the tube walls, where the velocity gradient $\frac{du}{dn}$ becomes very large, due to which the friction forces assume very high values regardless of the viscosity coefficient μ. The boundary layer gradually spreads from near the stationary walls and covers the entire pipe. Therefore, it is necessary to conduct studies in the transition zone using boundary layer equations.

Prandtl suggested using the Nave-Stokes equations [1] for the boundary layer, which can be simplified to obtain the boundary layer equations. Since the main influencing forces in the boundary layer are the viscous forces, Prandtl simplifies the Nave-Stokes equations by ignoring terms that are very small compared to the viscous forces. These results in simplified equations for the boundary layer.

Let's take the midpoint of the entrance section as the origin of the coordinates and point the oz axis in the direction of movement (as shown in Fig. 1). In this case, the boundary layer equations proposed by L. Prandtl [2] will take the following form:

$$V_y \frac{\partial V_z}{\partial z} + V_z \frac{\partial V_z}{\partial y} = -\frac{1}{\rho} \cdot \frac{\partial P}{\partial z} + \nu \frac{\partial^2 V_z}{\partial y^2}, \quad (1)$$

$$\frac{\partial V_z}{\partial z} + \frac{\partial V_z}{\partial y} = 0. \quad (2)$$

By linearizing this system of equations according to [3,4], we will have:

$$U_0 \frac{\partial V_z}{\partial z} = -\frac{1}{\rho} \frac{\partial P}{\partial z} + \nu \frac{\partial^2 V_z}{\partial y^2}, \quad (3)$$

$$\frac{\partial V_z}{\partial z} + \frac{\partial V_y}{\partial y} = 0 \quad (4),$$

where U_0 is the characteristic velocity of the entrance section, which is equal to the average velocity of the entrance section:

$$U_0 = \frac{1}{2h} \int_{-h}^{+h} \varphi(y) dy. \quad (5)$$

Accepting that the pressures at each point of the hydraulic section have the same values, we will have: $P = P(z)$.

To integrate equations (3) and (4), the boundary conditions of the problem are defined:

$$V_z = 0, \quad V_y = 0, \quad \text{when} \quad y = \pm h, \quad (6)$$

$$V_z = \varphi(y), \quad \text{when} \quad z = 0, \quad -h < y < +h, \quad (7)$$

$$V_z \to V', \quad \text{when} \quad z \to \infty, \quad -h < y < +h, \quad (8)$$

where V' is the velocity at the stabilized area, which is determined by the following equation:

$$\frac{1}{\rho} \frac{\partial P}{\partial z} = \nu \frac{\partial^2 V'}{\partial y^2}. \quad (9)$$

The study assumes that the boundary layers forming near the stationary walls in the stabilized section merge to form a symmetric parabolic velocity profile. The solution to equation (9) will be:

$$V'(y)=\frac{3}{2}U_0\left(1-\frac{y^2}{h^2}\right). \tag{10}$$

This corresponds to the uniform distribution of velocities in the case of plane-parallel motion [1].

To obtain appropriate solutions for the changes in hydrodynamic parameters in the transition zone of the entrance section, let's introduce dimensionless variables:

$$\bar{V}_z=\frac{V_z}{U_0},\ x=\frac{y}{h},\ \sigma=\frac{z}{h},\ \bar{p}(\sigma)=\frac{p(z)}{p_0}. \tag{11}$$

Under these conditions, equation (3) will take the following form:

$$\frac{\partial\bar{V}_z(x,\sigma)}{\partial\sigma}=-\frac{p_0}{\rho U_0^2}\frac{\partial\bar{p}(\sigma)}{\partial\sigma}+\frac{1}{\mathrm{Re}}\frac{\partial^2\bar{V}_z}{\partial x^2}, \tag{12}$$

where $\mathrm{Re}=\frac{U_0h}{\nu}$ - is the Reynolds number.

The boundary conditions for integrating equations (12) will be:

$$\bar{V}_z(1,\sigma)=0,\ \bar{V}_z(x,0)=\psi(x),\ \frac{\partial\bar{V}_z(x,\sigma)}{\partial\sigma}\to 0,\ \text{when } \sigma\to\infty,\ \bar{V}_z=0,\ \bar{V}_z(x,\infty)\to\bar{V}'(x). \tag{13}$$

Results of research to identify patterns of changes in hydrodynamic parameters

The solution of the inhomogeneous equation (12) under the boundary conditions (13), let's look for a solution in the form of a sum [5]:

$$\bar{V}(x,\sigma)_z=U(x,\sigma)+\psi(\sigma), \tag{14}$$

where $U(x,\sigma)$ represents the general solution of the homogeneous equation for inhomogeneous boundary conditions, while $\psi(\sigma)$ is the particular solution of the inhomogeneous equation (12) for zero boundary conditions.

Let's look for the general solution of the homogeneous equation $\frac{\partial U(x,\sigma)}{\partial\sigma}=\frac{1}{\mathrm{Re}}\frac{\partial^2U(x,\sigma)}{\partial x^2}$ in the form of a sum:

$$U(x,\sigma)=\sum_{k=1}^{\infty}C_k(\sigma)\cos(\gamma_k x). \tag{15}$$

If the function $U(x,\sigma)$ satisfies the equation (15), then the coefficients $C_k(\sigma)$ must satisfy the following equation:

$$C_k'(\sigma)=-\frac{1}{\mathrm{Re}}C_k(\sigma), \tag{16}$$

from where

$$C_k(\sigma)=C_k\cdot\exp\left(-\frac{\gamma_k^2}{\mathrm{Re}}\sigma\right), \tag{17}$$

where C_k is the arbitrary constant coefficient.

By inserting the value of function $C_k(\sigma)$ into equation (15) and taking into account equation (14), we obtain the following expression:

$$\bar{V}_z(x,\sigma)=\sum_{k=1}^{\infty}C_k\cos(\gamma_k x)\cdot\exp\left(-\frac{\gamma_k^2}{\mathrm{Re}}\sigma\right)+\psi(\sigma). \tag{18}$$

To determine the value of the unknown function $\psi(\sigma)$, we multiply both sides of equation (4) by bdx and integrate x over the interval $-1\le x\le+1$. Taking into account that the viscous liquid on the static wall has zero velocity, we obtain the following expression:

$$\int_{-1}^{+1}\frac{\partial\bar{V}_z(x,\sigma)}{\partial\sigma}dx=0. \tag{19}$$

By substituting the value of velocity $\bar{V}_Z(x,\sigma)$ from equation (18) into equation (19) for determining the function $\psi(\sigma)$, we obtain the following expression:

$$2\psi'(\sigma)=\frac{2}{\mathrm{Re}}\sum_{k=1}^{\infty}\gamma_k C_k\sin\gamma_k\cdot\exp\left(-\frac{\gamma_k^2}{\mathrm{Re}}\sigma\right). \tag{20}$$

Integrating the last equation according to σ, we will have:

$$\psi(\sigma)=-\sum_{k=1}^{\infty}\frac{C_k}{\gamma_k}\sin\gamma_k\cdot\exp\left(-\frac{\gamma_k^2}{\mathrm{Re}}\sigma\right)+C(x), \tag{21}$$

where $C(x)$ is the integration constant.

By substituting the value of function $\psi(\sigma)$ into equation (14), we obtain the following equation for the velocity $\bar{V}_Z(x,\sigma)$:

$$\bar{V}_z(x,\sigma)=\sum_{k=1}^{\infty}C_k\left[\cos(\gamma_k x)-\frac{\sin\gamma_k}{\gamma_k}\right]\cdot\exp\left(-\frac{\gamma_k^2}{\mathrm{Re}}\sigma\right)+C(x). \tag{22}$$

We determine the value of the constant $C(x)$ from the boundary condition of the problem when $\sigma\to\infty$ $\bar{V}_z(x,\sigma)\to\frac{3}{2}\left(1-\frac{y^2}{h^2}\right)$. The value of the constant $C(x)$ will correspond to this boundary condition:

$$C(x)=\frac{3}{2}\left(1-x^2\right). \tag{23}$$

Thus, the final solution to the problem will be:

$$\bar{V}_z(x,\sigma)=\frac{3}{2}\left(1-x^2\right)+\sum_{k=1}^{\infty}C_k\left[\cos(\gamma_k x)-\frac{\sin\gamma_k}{\gamma_k}\right]\cdot\exp\left(-\frac{\gamma_k^2}{\mathrm{Re}}\sigma\right). \tag{24}$$

This velocity distribution equation must satisfy the boundary condition of the problem (13), according to which $\bar{V}_z(x,0)=\psi(\sigma)$. Taking into account the equation (24) and the boundary condition, we will have:

$$\psi(\sigma)=\frac{3}{2}\left(1-x^2\right)+\sum_{k=1}^{\infty}C_k\left[\cos(\gamma_k x)-\frac{\sin\gamma_k}{\gamma_k}\right]. \tag{25}$$

To determine the values of the C_k coefficients, we must multiply both parts of the equation (25) by given expression $\left(\cos(\gamma_k x)-\frac{\sin\gamma_k}{\gamma_k}\right)$ and integrate it over the range of (-1,+1) and we will have:

$$\int_{-1}^{1}\psi(x)\left(\cos(\gamma_n x)-\frac{\sin\gamma_n}{\gamma_n}\right)dx-\frac{3}{2}\int_{-1}^{1}(1-x^2)\left(\cos(\gamma_n x)-\frac{\sin\gamma_n}{\gamma_n}\right)dx=$$
$$\sum_{k=1}^{\infty}C_k\int_{-1}^{1}\left(\cos(\gamma_n x)-\frac{\sin\gamma_n}{\gamma_n}\right)\left[\cos(\gamma_k x)-\frac{\sin\gamma_k}{\gamma_k}\right]dx \qquad (26)$$

As

$$\int_{-1}^{1}\left(\cos(\gamma_n x)-\frac{\sin\gamma_n}{\gamma_n}\right)\left[\cos(\gamma_k x)-\frac{\sin\gamma_k}{\gamma_k}\right]dx=\begin{cases}0, & \gamma_k\neq\gamma_n\\ \sin^2\gamma_k, & \gamma_k=\gamma_n\end{cases}, \qquad (27)$$

we will have:

$$C_k=\frac{L_k^{(1)}}{\sin^2\gamma_k}-\frac{3L_k^{(2)}}{\sin^2\gamma_k}, \qquad (28)$$

where

$$L_k^{(1)}=\int_{-1}^{1}\psi(x)(\cos(\gamma_n x)-\cos(\gamma_n))dx, \qquad (29)$$

$$L_k^{(2)}=\int_{0}^{1}(1-x^2)(\cos(\gamma_n x)-\cos(\gamma_n))dx, \qquad (30)$$

γ_k is the $\cos(\gamma_k)-\frac{\sin\gamma_k}{\gamma_k}=0$, or the positive roots of the equation $tg\gamma_k=\gamma_k$. Taking into account (28-30), we will have the solution to the problem.

$$\bar{V}_z(x,\sigma)=\frac{3}{2}(1-x^2)+\sum_{k=1}^{\infty}\left[\frac{L_k^{(1)}-3L_k^{(2)}}{\sin^2\gamma_k}\right]\left(\cos(\gamma_k x)-\frac{\sin\gamma_k}{\gamma_k}\right)\cdot\exp\left(-\frac{\gamma_k^2}{\mathrm{Re}}\sigma\right). \qquad (31)$$

The resulting equation will satisfy the boundary conditions of the problem.

We get the pattern of pressure change from equations (12) and (31), and we will have:

$$\frac{\partial\bar{p}(\sigma)}{\partial\sigma}=-\frac{\rho U_0^2}{\bar{p}_0\,\mathrm{Re}}\left\{\sum_{k=1}^{\infty}\frac{\gamma_k\left(L_k^{(1)}-3L_k^{(2)}\right)}{\sin\gamma_k}\cdot\exp\left(-\frac{\gamma_k^2}{\mathrm{Re}}\sigma\right)+3\right\}. \qquad (32)$$

By integrating the last equation, we can obtain the pattern of pressure variation in the transition area of the inlet section:

$$\bar{p}(\sigma)=\bar{p}(0)-\frac{\rho U_0^2}{\bar{p}_0}\sum_{k=1}^{\infty}\frac{\gamma_k\left(L_k^{(1)}-3L_k^{(2)}\right)}{\gamma_k\sin\gamma_k}\cdot\left[1-\exp\left(-\frac{\gamma_k^2}{\mathrm{Re}}\sigma\right)\right]-\frac{3\rho U_0^2}{\bar{p}_0\,\mathrm{Re}}. \qquad (33)$$

Let's consider two special cases:

1. The incoming fluid has a uniformly distributed velocity field $V_z(y,z)=\varphi(y)=U_0$. Under these conditions, we will have $\bar{V}_z(x,0)=\psi(x)=1$, corresponding to which we will get:

$$L_k^{(1)}=\int_{-1}^{1}\psi(x)(\cos(\gamma_n x)-\cos(\gamma_n))dx=2\int_{0}^{1}(\cos(\gamma_n x)-\cos(\gamma_n))dx=0,$$

$$L_k^{(2)}=\int_{0}^{1}(1-x^2)(\cos(\gamma_n x)-\cos(\gamma_n))dx=-\frac{2\sin\gamma_k}{3\gamma_k}.$$

Inserting these values into the equation (31):

$$\bar{V}_z(x,\sigma)=\frac{3}{2}\left(1-x^2\right)+\sum_{k=1}^{\infty}\left[\frac{2}{\gamma_k\sin\gamma_k}\right]\left(\cos(\gamma_k x)-\cos(\gamma_k)\right)\cdot\exp\left(-\frac{\gamma_k^2}{\mathrm{Re}}\sigma\right). \quad (34)$$

In this case, the irregularity of pressure distribution according to (33) will be equal to:

$$\bar{p}(\sigma)=\bar{p}(0)-\frac{\rho U_0^2}{\bar{p}_0}\sum_{k=1}^{\infty}\frac{2}{\gamma_k^2}\cdot\left[1-\exp\left(-\frac{\gamma_k^2}{\mathrm{Re}}\sigma\right)\right]-\frac{3\rho U_0^2}{\bar{p}_0\,\mathrm{Re}}\sigma. \quad (35)$$

2. Let's imagine the velocity of the liquid entering the reservoir changes according to the parabolic law $V_z(y,z)=\varphi(y)=A\left(1-y^2\right)$, according to which we will have $\bar{V}_z(x,0)=\psi(x)=\left(1-x^2\right)$,

$$L_k^{(1)}=\int_{-1}^{1}\left(1-x^2\right)\left(\cos(\gamma_n x)-\cos(\gamma_n)\right)dx=-\frac{4\sin\gamma_k}{3\gamma_k}, \quad (36)$$

$$L_k^{(2)}=-\frac{4A\sin\gamma_k}{3\gamma_k}. \quad (37)$$

In this case, the velocity change patterns according to (31), (36) and (37) will be:

$$\bar{V}_z(x,\sigma)=\frac{3}{2}\left(1-x^2\right)+\sum_{k=1}^{\infty}\frac{2(3-A)}{3\gamma_k\sin\gamma_k}\left(\cos(\gamma_k x)-\cos(\gamma_k)\right)\cdot\exp\left(-\frac{\gamma_k^2}{\mathrm{Re}}\sigma\right). \quad (38)$$

Having the velocity distribution patterns, we can get the pressure distribution pattern in the transition zone:

$$\bar{p}(\sigma)=\bar{p}(0)-\frac{\rho U_0^2}{\bar{p}_0}\sum_{k=1}^{\infty}\frac{2(3-A)}{3\gamma_k^2}\cdot\left[1-\exp\left(-\frac{\gamma_k^2}{\mathrm{Re}}\sigma\right)\right]-\frac{3\rho U_0^2}{\bar{p}_0\,\mathrm{Re}}\sigma. \quad (39)$$

The resulting patterns of velocity and pressure changes make it possible to fully reveal the physical nature of the ongoing phenomena and make generalizations.

Results and Discussion

The integration of differential equations of viscous fluid flow yielded patterns of changes in the distribution of axial velocities $\bar{V}_z(x,\sigma)$. To visually represent these patterns of changes in the axial velocity $\bar{V}_z(x,\sigma)$ across the cross-section and along the length of the transition zone, depending on the initial distribution of velocities $\bar{V}_z(x,0)=\psi(x)$ and Reynolds number, their graphs of change were constructed. Figs. 2…5 show the specified calculated graphs for cases $\bar{V}_z(x,0)=1$ and $\bar{V}_z(x,0)=\left(1-x^2\right)$.

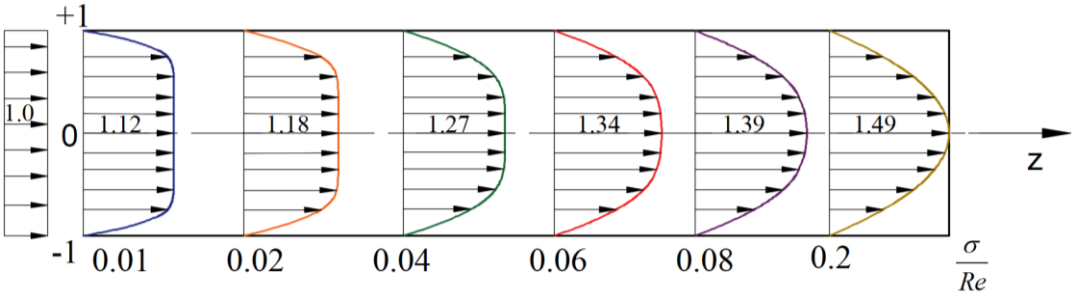

Fig. 2. *Graphs of changes in axial velocities* $\bar{V}_z(x,\sigma)$ *along the cross-section in the transition zone of the entrance section of the plane-parallel pressure flow at* $\bar{V}_z(x,0)=1$ *and*

$1.\frac{\sigma}{Re}=0.01;\ 2.\frac{\sigma}{Re}=0.02;\ 3.\frac{\sigma}{Re}=0.04;\ 4.\frac{\sigma}{Re}=0.06;\ 5.\frac{\sigma}{Re}=0.08;\ 6.\frac{\sigma}{Re}=0.2$

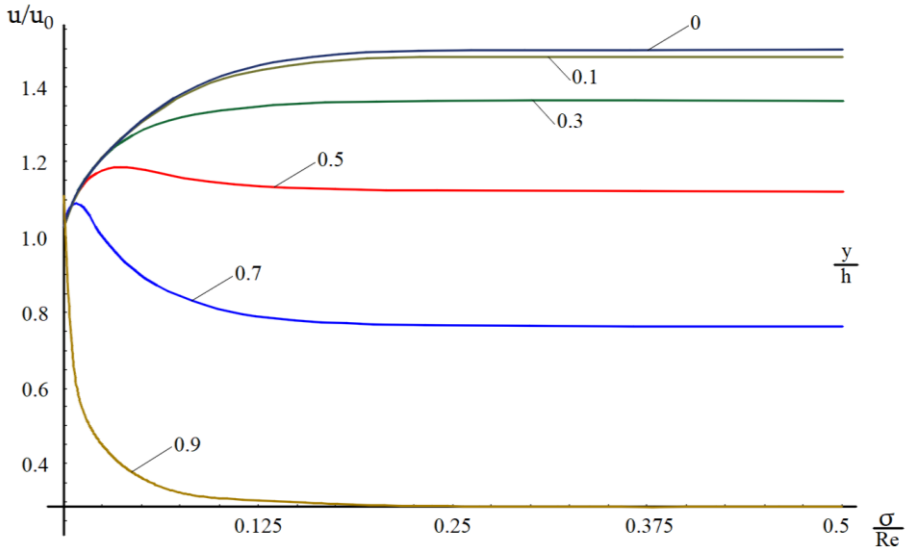

Fig. 3. *Graphs of changes in axial velocities* $\overline{V}_z(x,\sigma)$ *at* $\overline{V}_z(x,0)=1$ *and*

$1.x=0;\ \ 2..x=0.1;\ \ 3.x=0.3;\ \ 4.x=0.5;\ \ 5.x=0.7;\ \ 6.x=0.9$

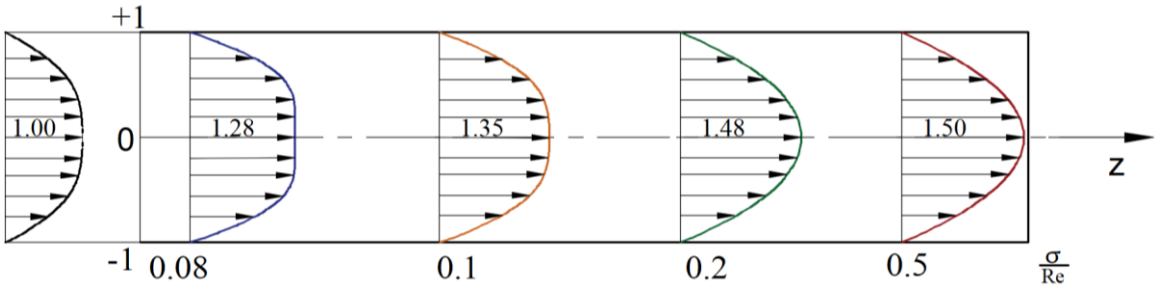

Fig. 4. *Graphs of changes of the axial velocities* $\overline{V}_z(x,\sigma)$ *along the cross-section on the entrance section of the plane-parallel pressure flow at* $\overline{V}_z(x,0)=(1-x^2)$ *and*

$$1.\frac{\sigma}{Pe}=0.08;\ \ 2.\frac{\sigma}{Pe}=0.1;\ \ 3.\frac{\sigma}{Pe}=0.2;\ \ 4.\frac{\sigma}{Pe}=0.5$$

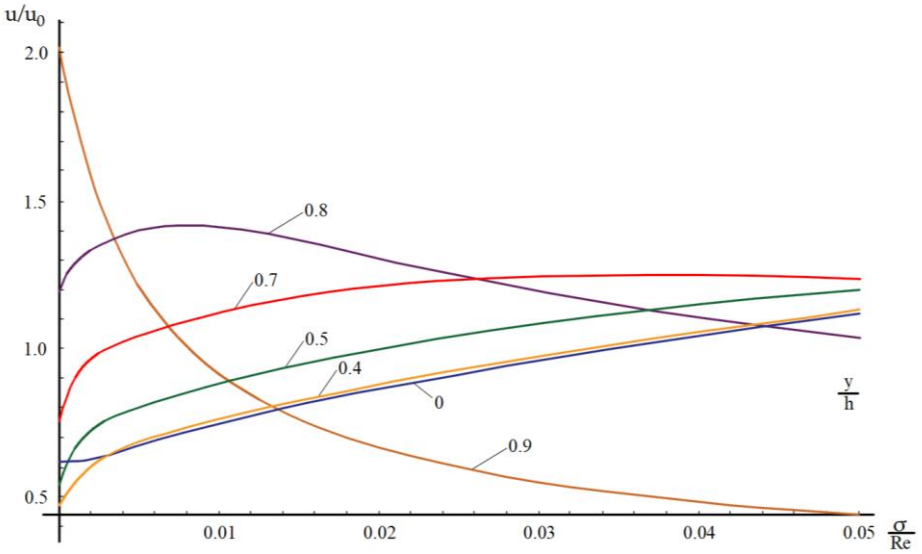

Fig. 5. *Graphs of changes in axial velocities* $\overline{V}_z(x,\sigma)$ *at* $\overline{V}_z(x,0)=(1-x^2)$ *and*

$1.x=0;\ \ 2.x=0.1;\ \ 3.x=0.3;\ \ 4.x=0.5;\ \ 5.x=0.7;\ \ 6.x=0.9.$

The dynamics of the transition zone were determined based on the results of numerical calculations and graphs, using the condition that the ratio of axial velocities between the transitional and stabilized areas is 0.99. From this condition, it was found that $L = \frac{\sigma}{\mathrm{Re}} = 0.147$. The proposed method for calculating velocity rearrangements in the transition area of the entrance section enables the determination of patterns of changes in hydrodynamic parameters of the flow under general boundary conditions. Using the identified relationships, the deformation process of the velocity field at the transition site of the entrance section was determined for both constant and parabolic law distributions of incoming liquid. This enables the calculation of changes in the hydrodynamic parameters of the flow and facilitates generalizations of the results.

The patterns of changes in the velocity field in the transition area of the entrance section of plane-parallel pressure flow, along with the graphs constructed based on these findings, provide valuable information for the accurate design of hydromechanical equipment units.

Conclusion

The study of viscous fluid flow in the transition zone of the entrance area of a plane-parallel pressure flow has revealed the following findings:

- A boundary value problem was formulated to investigate the regularities of changes in hydrodynamic parameters of a viscous incompressible fluid in the transition zone of the entrance section of a plane-parallel pressure flow.
- A method for solving the boundary value problem was developed, and formulas were derived to calculate axial velocities across the cross-section and pressure along the length of the diffuser.
- Graphs were constructed to illustrate the changes in hydrodynamic parameters of the flow across the cross-section and along the length of the transition zone for constant and parabolic distributions of initial velocities at the entrance section.
- A calculation formula was derived to determine the length of the transition zone of the inlet section of a plane-parallel pressure flow.

The solutions derived from the approximating Navier-Stokes equations to identify patterns of changes in hydrodynamic parameters of a plane-parallel pressure flow with constant and parabolic distributions of initial velocities at the entrance section provide a comprehensive understanding of the underlying processes. These results are essential for hydraulic calculations of various systems.

References

[1]. B.T. Yemtsev, Tekhnicheskaya gidromekhanika. Mashinostroyeniye, Moscow, 1978 (in Russian).
[2]. H. Schlichting, K. Gersten, Boundary-Layer Theory, Springer, 2017. https://link.springer.com/book/10.1007/978-3-662-52919-5
[3]. N.A. Slezkin, Dinamika vyazkoy neszhimayemoy zhidkosti. Gosudarstvennoye izdatel'stvo tekhniko-teoreticheskoy literatury, Moscow, 1955 (in Russian).
[4]. S.M. Targ, Osnovnyye zadachi teorii laminarnykh techeniy. Gosudarstvennoye izdatel'stvo tekhniko-teoreticheskoy literatury, Moscow-Leningrad, 1951 (in Russian).
[5]. A.N. Tikhonov, A.G. Samarskiy, Uravneniya matematicheskoy fiziki. Nauka, Moscow, 1999 (in Russian).
[6]. S. M. F. Letelier, H. J. Leutheusser, Unified Approach to the Solution of Problems of Unsteady Laminar Flow in Long Pipes. Journal of Applied Mechanics, 50 (1), 1983, 8-12.
[7]. A.A. Sarukhanyan, Development of a Laminar Unsteady Flow of a Viscous Fluid in the Entrance Region of a Round Cylindrical Pipe. Proceedings of the International Scientific and Technical Conference "Architecture and Construction - Topical Problems", Yerevan - Jerrnuk, Armenia, October 15-18, vol.3, 2008, 242-247 (in Russian).
[8]. L.A. Belyaev, A.S. Zaitsev, A.A. Kondakov, S.A. Shevelev, E.P. Valkov, A.A. Matveeva, Numerical Analysis of Fluid Particles Motion in Curved Ducts. MATEC Web of Conferences, 2015. Doi: https://doi.org/10.1051/matecconf/20153701007

[9]. R.Y. Chen, Flow in the Entrance Region at Low Reynolds Numbers. Journal of Fluid Engineering, 95 (1), 1973, 153-158. Doi: https://doi.org/10.1115/1.3446948
[10]. E.M. Sparrow, S.H. Lin, T.S. Lundgren, Flow Development in the Hydrodynamic Entrance Region of Tubes and Ducts. Physics of Fluids, 7, 1964, 338–347. Doi: https://doi.org/10.1063/1.1711204
[11]. A.E.Vardy, J.M.B. Brown, Laminar Pipe Flow with Time-Dependent Viscosity, Journal of Hydroinformatics, 13 (4), 2011, 729-740.
[12]. I. Dapra, G. Scarpi, Unsteady Flow of Fluids with Arbitrarily Time-Dependent Rheological Behavior, Journal of Fluids Engineering, 139 (5), 2017. Doi: https://doi.org/10.1115/1.4035637
[13]. A. Kannaiyan, N. Sekarapandian, B.R. Vinoth, Stability of a Laminar Pipe Flow Subjected to a Step-Like Increase in the Flow Rate. Physics of Fluids, 34 (6), (2022). Doi: https://doi.org/10.1063/5.0090337
[14]. A.K. Mohanty, S.B.L. Asthana, Laminar Flow in the Entrance Region of a Smooth Pipe. Journal of Fluid Mechanics, 90 (3), 1979, 433-447.
[15]. G.N. Rocha, R.J. Poole, P.J. Oliveira, Bifurcation Phenomena in Viscoelastic Flows Through a Symmetric 1:4 Expansion. Journal of Non-Newtonian Fluid Mechanics, 141 (1), 1-17, 2007. Doi: https://doi.org/10.1016/j.jnnfm.2006.08.008
[16]. T. Mullin, J.R.T. Seddon, M.D. Mantle, A.J. Sederman, Bifurcation Phenomena in the Flow Through a Sudden Expansion in a Circular Pipe. Physics of Fluids, 21 (1), 2009. Doi: https://doi.org/10.1063/1.3065482
[17]. Engin Gücüyen, Recep Tuğrul Erdem, Ümit Gökkuş, Numerical Modelling of Sudden Contraction in Pipe Flow. Sigma Journal of Engineering and Natural Sciences, 37 (3), 2019, 903-916.
[18]. T. Hawa, Z. Rusak, Viscous Flow in a Slightly Asymmetric Channel with a Sudden Expansion. Physics of Fluids, 12 (9), 2000, 2257-2267. Doi: https://doi.org/10.1063/1.1287610
[19]. V. Fester, B. Mbiya, P. Slatter, Energy Losses of Non-Newtonian Fluids in Sudden Pipe Contractions. Chemical Engineering Journal, 145 (1), 2008, 57-63. Doi: https://doi.org/10.1016/j.cej.2008.03.003

Arestak Sarukhanyan, Doctor of Science (Engineering), Professor *(RA, Yerevan) - National University of Architecture and Construction of Armenia, Head of the Chair of Water Systems, Hydraulic Engineering and Hydropower, asarukhanyan51@mail.ru*

Garnik Vermishyan, Doctor of Philosophy (PhD) in Engineering *(RA, Yerevan) - National University of Architecture and Construction of Armenia, Associate Professor at the Chair of Higher Mathematics and Physics, vermishyan.garnik@gmail.com*

Hovhannes Kelejyan, Doctor of Philosophy (PhD) in Engineering *(RA, Yerevan) - National University of Architecture and Construction of Armenia, Associate Professor at the Chair of Water Systems, Hydraulic Engineering and Hydropower, hovo98@mail.ru*

ADSORPTIVE REMOVAL OF COPPER (II) IONS FROM AQUEOUS SOLUTION USING PUMICE

Marine Kalantaryan[1]*, Hovsep Hoveyan[1], Suren Hovsepyan[1], George Abrahamyan[2]

[1] *National University of Architecture and Construction of Armenia, Yerevan, RA*

[2] *Shant Laboratories sa/nv, Brussels, Belgium*

Abstract: *This article presents the use of modified pumice as an environmentally friendly adsorbent for copper (II) removal from wastewater. The water pollution by toxic elements is a major concern for human health and environmental quality. New and cheaper methods of wastewater treatment are increasing the quality of the environment and reducing negative impacts on fauna, flora, and human beings. The sorption technique is considered a cost-effective method for effectively removing heavy metals. In recent years, there have been increasing studies dedicated to using low-cost adsorbents such as pumice. For the study, Kuchak pumice has been used. The modified pumice was prepared by surface modification with polysiloxane, evaluated by studying the effects of pH, contact time, dosage, and initial concentration, and was optimized in batch processing mode. The chemical changes in pumice were fully characterized using FT-IR techniques. Overall, these results suggest that surface-modified pumice is a low-cost adsorbent for the removal of copper (II).*

Keywords: *pumice, modification, polysiloxane, adsorbent, heavy metal removal.*

Marine Kalantaryan*

E-mail: kalantaryanm@mail.ru

Received: 02.04.2023
Revised: 20.04.2023
Accepted: 02.05.2023

Introduction

The rapid development of the industry has resulted in a significant increase in heavy metal contamination, which has become a major environmental issue. The most significant challenge facing humanity today is effectively managing the problem of water pollution caused by heavy metals. The physical and chemical techniques traditionally used for cleanup are associated with high capital costs and can damage already contaminated areas. In today's highly industrialized society, several industrial operations release aqueous effluents containing heavy metals. The presence of heavy metals in aquatic systems can harm numerous living species [1]. Copper (Cu^{2+}) ions are present in many biological systems at low levels but can be toxic at high concentrations. Although copper can exist in different forms, such as Cu (0), Cu (I), and Cu (II), Cu (II) is the primary species of concern in aqueous solutions. Cu^{2+} rapidly binds to organic and inorganic compounds in aqueous solutions, which is pH dependent. It harms aquatic life and makes natural water unsuitable for human use. Ingesting high concentrations of Cu can also be toxic to humans, leading to cancer and promoting oxidation [2,3]. Toxic metals can now be removed from soil and water using various clean-up technologies developed over time. Currently, physical-chemical processes such as filtration, chemical precipitation, ion exchange, adsorption, and electrodeposition, form the foundation of the most extensively utilized remediation technologies [3]. Different types of materials have been used as adsorbents for copper adsorption, such as activated carbons and zeolites [4], alumina - silica [5], molecular sieve powder [6] and different pumices. The current study aims to establish the ideal conditions for the maximum amount of copper to be absorbed by pumice from aqueous solution and to evaluate the effects of various experimental parameters on copper adsorption.

Different treatment strategies, such as physical, chemical, and biological treatments, were discussed based on the past few years. These introduced methods are adsorption, membrane filtration, electrodialysis, and photocatalysis. However, there are some precautions that should be taken seriously as they are influenced by

parameters such as the initial concentration of copper ions, pH values, economic parameters such as operation cost, and the environmental effects and compatibility of each of the various methods conducted.

Currently, many adsorbents are being produced and used for cleaning up wastewater. These adsorbents can be of either natural or artificial origin. Considering the numerous advantages of natural materials, including their availability in large quantities and non-toxicity, it is more appropriate to use adsorbents based on natural materials. Efforts have been made recently to modify the surface of these natural adsorbents to increase their efficiency, and extensive research has been conducted in this direction [1,2].

The aim of the present study is to investigate the influence of various experimental parameters on copper adsorption and determine the optimum conditions for maximum adsorption of copper by pumice from aqueous solution. The influence of temperature, sorbent mass, solution pH and sorbent chemical modification on adsorption process is discussed.

The Republic of Armenia is rich in non-metallic mineral diversity and abundance. The light rocks (tuffs, perlite, pumice stone, zeolite, scoria, etc.) generated because of volcanic activities in the mountains of Armenia are of particular value and significance.

In this article Kuchak pumice deposit is used as an adsorbent for copper removal from aqueous media. The pumice on the territory of the Republic of Armenia according to their petrographic, physical and mechanical characteristics are divided into two types: Ani and lithoidal Kuchak pumice is one of the Ani type pumice varieties. It is located at an altitude of 2050 meters above sea level. On the southern side of the pumice deposit there is a powerful layer of pumice grains with a capacity of 6 ... 7 meters and pumicite with a capacity of 4 ... 6 meters. Studies have shown that the pumice is composed of alumicillicates in which the alkali oxide content varies from 1.5 to 5%, SiO_2 from 71% to 75%, and Al_2O_3 from 12% to 14%. In the Kuchak pumice deposit samples, the content of alkaline oxides varies from 0.03 to 0.1%, SiO_2 from 70% to 73% and Al_2O_3 from 12 to 16% [7].

Materials and Methods

The analysis of the data obtained shows that the Kuchak pumice deposit is environmentally safe and is a chemically neutral silicate rock in water medium. Kuchak pumice has a porosity of 1.64 to 32.70 μm (Fig. 1). The total porosity is about 72.2 - 79.4 % [7].

The presented data show that Kuchak mine pumice is an aluminosilicate rock with well-developed porosity, mechanical strength, high buoyancy. It is chemically inert and eco-friendly.

In this study the following reagents were used: polysiloxane emulsion, copper sulphate ($CuSO_4.5H_2O$), and hydrochloric acid (HCl). All the reagents used were of highly pure grade. The deionized water was used for all reagent solutions.

Polysiloxane has an extensive record of success and is frequently used in medical applications. Elastomers, gels, lubricants, foams, and adhesives are examples of different material types. Polysiloxane is relatively stable and chemically inert. They have minimal moisture uptake and are hydrophobic. They offer excellent electrical insulation qualities. Nearly all polysiloxane is based on polymethylsiloxane (Fig. 2).

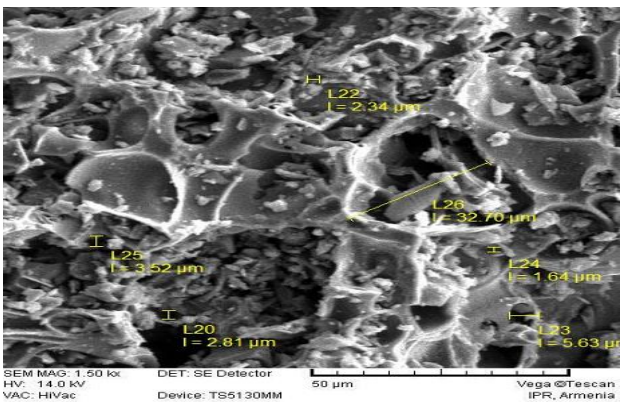

Fig. 1. *Pore sizes of Kuchak pumice deposit [8]*

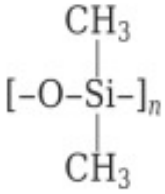

Fig. 2. *Chemical structure of polysiloxanes*

Polysiloxanes (PDMS) or silicones, are a general category of polymers consisting of a silicon-oxygen backbone with organic groups, typically methyl groups, attached to the silicon atoms [9,10,11]. Organic side groups can be used to link two or more chains together. By varying the -Si-O- chain length, side groups, and crosslinking extent, silicones with properties ranging from liquids to hard plastics can be synthesized. Silicone synthesis typically involves the hydrolysis of chlorosilanes into linear or cyclic siloxane oligomers, which are then polymerized into polysiloxanes by polycondensation or polymerization, respectively. Polysiloxanes, characterized by unique material properties combining biocompatibility and biodurability, have found widespread application in healthcare [12,13,14,15].

About 1.0 g of polysiloxane was mixed with 10 g of pumice and 30 mL of distilled water. First, the pumice was washed with water and dried in an oven at 105°C for one hour. Then the polysiloxane emulsion was mixed in 1:30 ratio with distilled water to form a stable mixture. The mixture was then stirred for 5 hours at room temperature. Then it was filtered from the solution, washed, and dried in an oven at 70 °C for 3 hours to allow the emulsion to adhere to the surface. Finally, the modified pumice was washed with water to remove excess emulsion and dried again. Different particle sizes (2.36, 3.54, and 4.87 mm) were collected and used as an adsorbent for the analysis. All pH values were measured with a pH meter (HACH LANGE HQ 14d). Cu^{2+} solutions of different concentrations (5 mg/L, 10 mg/L, 50 mg/L, and 100 mg/L) were prepared in deionized water using $CuSO_4$. Batch adsorption equilibrium studies of Cu were carried out at room temperature in beakers filled with 2.5 g of modified pumice. The contact times were one or two hours. The pH dependence experiment was carried out as a preliminary experiment to establish if the material possesses any affinity for Cu (II) ions. The pH of the solution is a known factor with significant impact on metal ion removal processes. The experiment was conducted in the pH range 2–6.

Fig. 3 shows the effect of pH on copper adsorption onto pumice. The adsorption capacity of pumice samples increased with increasing pH. The highest adsorption value is observed at a pH of four.

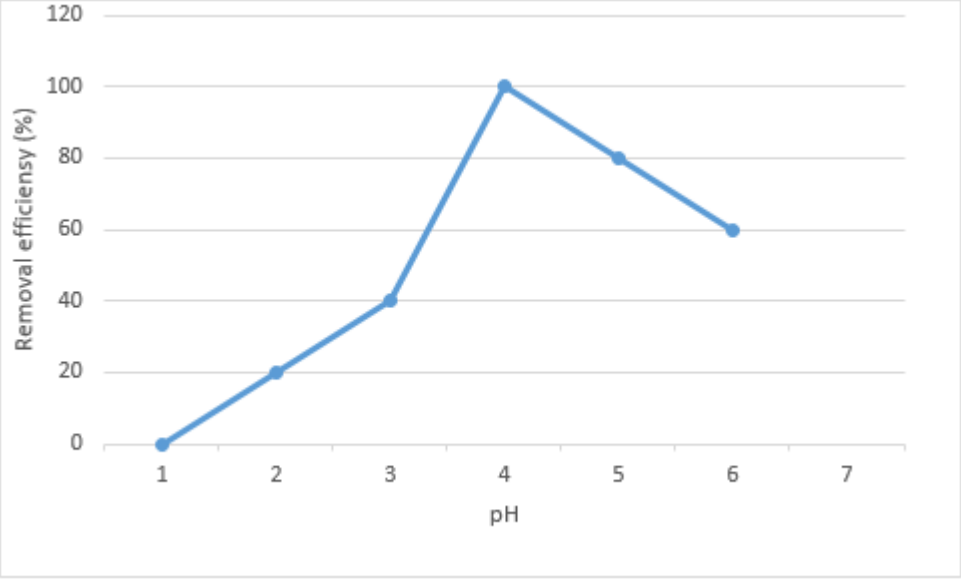

Fig. 3. *Effect of pH on the adsorption of copper by surface-modified pumice*

Results and Discussion

The effect of temperature on the adsorption of copper was studied by conducting a series of experiments at 25, 30, and 40 °C. There is a small effect of temperature on the adsorption of copper by pumice in aqueous solution. Because elevated temperature would be costly in commercial applications, experiments were run at 25 °C. The functional groups were found from the pumice and polysiloxane-modified samples using FT-IR spectrometer. The FT-IR spectrum of pumice is shown in Fig. 4. Compared to that of pumice, $Si-CH_3$ stretching bonds are observed for modified pumice under 1260 cm^{-1} and (Si-O-) bonds under 1100 cm^{-1}.

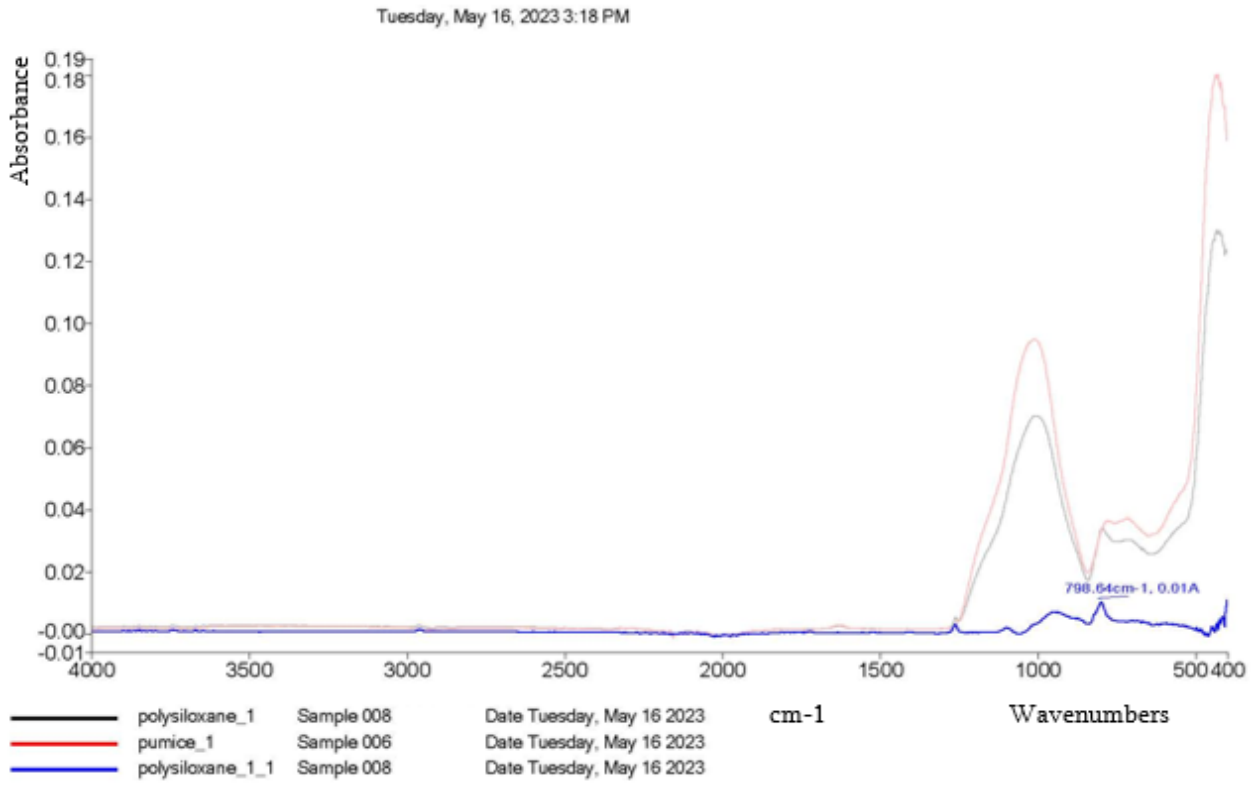

Fig. 4. *FT-IR spectrum of modified and unmodified pumices (PerklinElmer, Spectrum Two)*

The siloxane groups on the modified pumice surface can form coordinate bonds with metal ions such as copper (Cu^{2+}), allowing for effective removal from solution. The adsorption performance of polysiloxane-modified pumice will depend on various factors, including the surface area, pore size, concentration of metal ions, pH, and contact time.

Copper concentrations before and after adsorption were measured using UV-Vis Spectrophotometer (Cary-60). The wavelength of 10.0 nm^{-1} corresponds to the maximum absorbance of the copper on pumice. The spectra show after modification by polysiloxane the copper absorbance increased by 65% compared with unmodified pumice (Fig. 5).

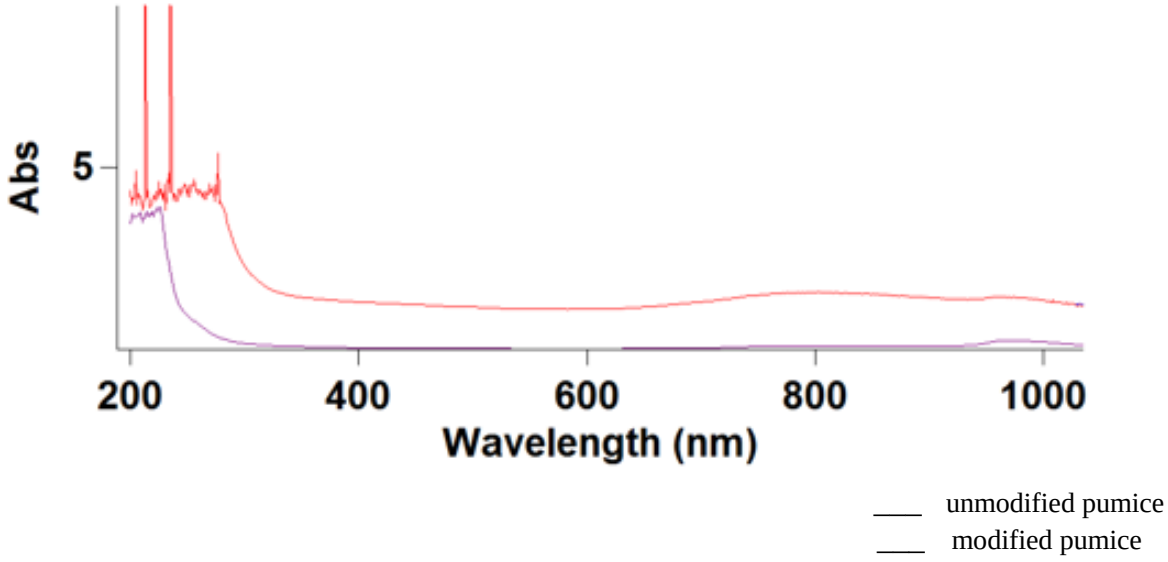

Fig. 5. *UV-Vis Spectrophotometric data (Cary-60)*

Conclusion

The efficiency of the pumice for the adsorption of copper from an aqueous solution was investigated using batch adsorption technique under different experimental conditions. Reported results showed that the adsorption varied strongly by pH. Temperature had a minor effect on the adsorption of copper by pumice. Due to its low cost and ready availability, it can be used as an efficient adsorbent material for the adsorption of copper from contaminated aqueous solutions. The modification of pumice with PDMS introduces siloxane (-Si-O-) functional groups onto the surface of the pumice particles. These siloxane groups can provide adsorption sites for metal ions due to their ability to coordinate with metal cations.

The high surface area and porous nature of pumice, combined with the adsorption properties of PDMS, can enhance the adsorption capacity for metal ions. The siloxane groups on the modified pumice surface can form coordinate bonds with metal ions such as copper (Cu^{2+}), allowing for effective removal from solution. The adsorption performance of polysiloxane modified pumice will depend on various factors, including the surface area, pore size, concentration of metal ions, pH, and contact time. Additionally, the specific synthesis and modification methods of the polysiloxane-modified pumice may influence its adsorption properties.

Overall, polysiloxane-modified pumice has the potential to be an effective adsorbent for copper ions. However, the actual adsorption capacity and efficiency would require experimental evaluation and optimization for specific conditions and metal ion concentrations. In our future research, we aim to develop methods to extract copper ions from polysiloxane-modified adsorbents.

References

[1]. M.W. Wan, I.G. Petrisor, H.T. Lai, D. Kim, T.F. Yen, Copper Adsorption through Chitosan Immobilized on Sand to Demonstrate the Feasibility for In-Situ Decontamination. Carbohydrates Polymers, 55 (3), 2004, 249-254. Doi: https://doi.org/10.1016/j.carbpol.2003.09.009

[2]. J.C.Y. Ng, W.H. Cheung, G. McKay, Equilibrium Studies of the Sorption of Cu(II) Ions onto Chitosan. Journal of Colloid and Interface Science, 255 (1), 2002, 64-74. Doi: https://doi.org/10.1006/jcis.2002.8664

[3]. Y. Sag, Y. Aktay, Kinetic Studies on Sorption of Cr(VI) and CU(II) Ions by Chitin, Chitosan and Rhizopus arrhizus. Biochemical Engineering Journal, 12 (2), 2002, 143-153. Doi: https://doi.org/10.1016/S1369-703X(02)00068-2

[4]. N. Elboughdiri, The use of Natural Zeolite to Remove Heavy Metals Cu (II), Pb (II) and Cd (II), from Industrial Wastewater. Cogent Engineering, 7 (1), 2020. Doi: doi.org/10.1080/23311916.2020.1782623

[5]. A. Chatterjee, J.K. Basu, A.K. Jana. Alumina-Silica Nano-Sorbent from Plant Fly Ash and Scrap Aluminium Foil in Removing Nickel through Adsorption. Powder Technology, 354, 2019, 792-803. Doi: https://doi.org/10.1016/j.powtec.2019.06.035

[6]. Y. Liu, H. Wang, Y. Cui, N. Chen. Removal of Copper Ions from Wastewater: A Review. International Journal of Environmental Research and Public Health, 20 (5), 2023, 3885. Doi: https://doi.org/10.3390/ijerph20053885

[7]. A. Hatsagorcyan, Natural Stone Materials of Armenia. Stroyizdat, Moscow, 1967.

[8]. G.Sh. Hovsepyan, M.A. Kalantaryan, G.R. Babayan, Investigation of Physical and Mechanical Properties of Pumice Stone from the Kuchak Deposit as a Sorbent for Cleaning the Surface of Water from Oil Products. Proceedings of National Polytechnic University of Armenia: Hydrology and Hydraulic Engineering, 1, 2015, 27-35.

[9]. G.S. dos Reis, C.H. Sampaio, E.C. Lima, M. Wilhelm, Preparation of Novel Adsorbents Based on Combinations of Polysiloxanes and Sewage Sludge to Remove Pharmaceuticals Form Aqueous Solutions. Colloids and Surfaces A: Physicochemical and Engineering Aspects, 497, 2016, 304-315. Doi: https://doi.org/10.1016/j.colsurfa.2016.03.021

[10]. A. Colas, J. Curtis, Silicone Biomaterials: History and Chemistry, in: B.D. Ratner, A.S. Hoffman, F.J. Schoen, J.E. Lemons (eds.), Biomaterials Science: An Introduction to Materials in Medicine, 2nd Edition, 2004, 80-85.

[11]. U. Zulfiqar, A.G. Thomas, K. Yearsley, L.W. Bolton, A. Matthews, D.J. Lewis, Renewable Adsorbent for the Separation of Surfactant-Stabilized Oil in Water Emulsions Based on Nanostructured Sawdust. ACS Sustainable Chemistry & Engineering, 7 (23) 2019, 18935-18942. Doi: https://doi.org/10.1021/acssuschemeng.9b04294

Marine Kalantaryan, Doctor of Philosophy (Ph.D) in Chemistry *(RA,Yerevan) -National University of Architecture and Construction of Armenia, Associate professor at the Chair of Production of Construction Materials, Items and Structures, Head of the Research Laboratory "Construction Chemistry", kalantaryanm@mail.ru*

Hovsep Hoveyan, Doctor of Philosophy (PhD) in Engineering *(RA,Yerevan) -National University of Architecture and Construction of Armenia, Chief of the Staff, Assistant at the Chair of Technology and Organization of Construction Production, hoveyan@nuaca.am*

Suren Hovsepyan, Doctor of Philosophy (PhD) in Engineering *(RA,Yerevan) -National University of Architecture and Construction of Armenia, Assistant at the Faculty of Management and Technology, surenhovsepyan@gmail.com*

George Abrahamyan, Doctor of Philosophy (PhD) in Biology *(Belgium, Brussels), CEO & President of Shant Laboratories sa/nv, ag@shantlabs.com*

ADDRESS : Str.Teryan 105, Yerevan
☏: (+37410) 54 74 12
URL : https://www.jaer.nuaca.am/